Synthesis, characterisation and reactions of ferrocene anchored bis(phosphino)palladium(II) and platinum(II) aryldichalcogenide complexes.

By

Letladi Lawrence Maisela

Submitted in partial fulfilment of the requirements for the degree of

Master of Science in the Faculty of Science

in the Department of Chemistry

University of the Western Cape

Private Bag X17

Bellville

7535

Supervisor: Professor James Darkwa

Co-supervisor: Professor Andrew M. Crouch

November 2000

DECLARATION

I declare that *"synthesis, characterisation and reactions of ferrocene anchored bis(phosphino)palladium(II) and platinum(II) aryldichalcogenide complexes"* is my own work, that it has not been submitted for any degree or examination in any other university, and that all the sources I have used or quoted have been indicated and acknowledged by means of complete references.

Full Name: Letladi Lawrence Maisela (Mr) Date: November 2000

Signature: _____

DEDICATION

TO MY LATE GRANDMA RAESETJA MOHUBA AND THE MAESELA FAMILY

TABLE OF CONTENTS

ABSTRACT

Reactions of $M(dppf)Cl_2$ (M = Pd, Pt) and $Pd(dippf)Cl_2$ with equimolar amounts of the aryldichalcogen reagents, 1,2-benzenedithiol (1,2-$(HS)C_6H_4(SH)$ (**a**)), 3,4-toluenedithiol ($(HS)C_6H_3Me(SH)$) (**b**), 3,6-dichloro-1,2-benzenedithiol ($(HS)C_6H_2Cl_2(SH)$) (**c**), 2-mercaptophenol ($(HS)C_6H_4(OH)$) (**d**), thiosalicylic acid ($(HS)C_6H_4(CO_2H)$ (**e**) and thionicotinic acid ($(HS)C_5H_3N(CO_2H)$) (**f**) in the presence of triethylamine afforded complexes of the type $M(dppf)(SC_6H_4E\text{-}o)$ (where dppf = 1,1'-bis(diphenylphosphino)ferrocene and dippf = 1,1'-bis(diisopropylphosphino)ferrrocene). In addition to the above series, $M(dppf)(SC_6H_5)_2$ (M = Pd, Pt) and $Pd(dippf)(SC_6H_5)_2$ were prepared in an attempt to synthesise complexes of the general formula $M(dppf)(SC_6H_4E\text{-}o)$ (M = Pd, Pt; E = Se, Te) *via in situ* generation of $LiSC_6H_4ELi\text{-}o$. All complexes isolated were characterised by a combination of IR, ^1H, $^{31}P\{^1H\}$ NMR, mass spectrometry and elemental analysis. Further characterisation of $Pd(dppf)(SC_6H_4S\text{-}o)$, $Pd(dippf)(SC_6H_4S\text{-}o)$, $Pd(dippf)(SC_6H_3MeS\text{-}o)$, $Pd(dippf)(SC_6H_5)_2$, $Pt(dppf)(SC_6H_4S\text{-}o)$ and $Pt(dppf)(SC_6H_4O\text{-}o)$ by single crystal X-ray diffraction studies confirmed the structures deduced from the spectroscopic data.

Mass spectrometry data suggests that the Pt(II) complexes are more stable than the analogous Pd(II) complexes. Electrochemical data also show that the dippf complexes were easier to oxidise compared to the dppf, as were the Pd complexes compared to the Pt analogues. In complexes containing homoleptic sulfur ligands (**1a-c**, **2a-c** and **3a-c**) the ease of oxidation of the ligand was **b** > **a** > **c** which conforms to either the electron releasing group (**b**) or an electron withdrawing group (**c**) on the ligand. Aryldithiolato

Pd(dppf) and Pd(dippf) complexes reacted with dimethylacetylene dicarboxylate (DMAD) to form hexamethylbenzene hexacarboxylate (HMBC) and tetramethylcyclobuta-1,3-diene tetracarboxylate (TMCTC) as the dominant products. The same series of aryldithiolato complexes that reacted with DMAD reacted reversibly with sulfur dioxide, a process that was monitored by UV-vis and ^{1}H NMR spectroscopy.

LIST OF TABLES

LIST OF FIGURES

ABBREVIATIONS

dppm = bis(diphenylphosphino) methane

dppe = 1,2-bis(diphenylphosphino) ethane

dppp = 1,3-bis(diphenylphosphino) propane

dppf = 1,1'-bis(diphenylphosphino) ferrocene

dippf = 1,1'-bis(diisopropylphosphino) ferrocene

bme-daco = N,N'-bis(mercaptoethyl)-1,5-diazacyclooctane

py = pyridine

bpy = bipyridine

DMAD = dimethylacetylene dicarboxylate

HMBC = hexamethylbenzene hexacarboxylate

TMCTC = tetramethylcyclobuta-1,3-diene tetracarboxylate

triphos = 1,1,1-tris(diphenylphosphinomethyl) ethane

Cp = η^5-C_5H_5

Cp* = η^5-C_5Me_5

ACKNOWLEDGEMENTS

I wish to express my sincere gratitude to my supervisor, Professor James Darkwa, my co-supervisor, Professor Andrew M. Crouch, under whose guidance this research was conducted; their invaluable advice and guidance is highly acknowledged. I also wish to extend my sincere thanks to Mr. Richard M. Mampa (University of the North) for $^{31}P\{^{1}H\}$ NMR analysis, Mr. Tim Lesch (University of the Western Cape) for elemental analysis of the samples, Dr. E.Y. Osei-Twum (King Fahd University of Petroleum and Minerals, Saudi Arabia) for the mass spectral analysis, Dr. John Bacsa (University of Cape Town) and Dr. Ilia A. Guzei (University of Winconsin-Madison, USA) for the X-ray structural analysis of the complexes reported in this thesis. My special thanks are due to my co-researchers Ms. F.A. Nevondo, Ms. A. Ngcai, Mr. M.J. Moloto, Mr. R.M. Moutloali and Dr. K. Li for their helpful suggestions during the project. I am also grateful for the funding provided by the National Research Foundation (NRF) and Eskom for this project. My thanks are also due to the Department of Chemistry, University of the Western Cape, where this research was conducted, its staff members for making my stay there unforgettable. Finally I thank God for helping me work through the difficulties and challenges I experienced throughout my studies.

CHAPTER 1

INTRODUCTION

1.1 Metal thiolato complexes.

Metal thiolates can be loosely classified as metal complexes that contain a metal centre, usually a transition metal, that is bound to a thiolato ligand through the sulfur atom. A complex is not a metal thiolate when the sulfur does not have an organic unit attached to it. An example of a non-metal thiolate is $Ti(\eta^5\text{-}C_5H_5)_2S_5$[1]. Those in which the sulfur atom is attached to an organic group are exemplified by $Ni(PBu_3)(dtc)(SC_6H_4Cl\text{-}4)$[2a] (dtc = diethyldithiocarbamate) and $Pt(PPh_3)_2(SC_2H_4S\text{-}o)$[2b]. Thiolato ligands display a strong propensity for binding to soft metal centres. Those containing ancillary hard donor atoms (e.g. O and N) have attracted interest for their coordination chemistry since the combination of hard and soft donor atoms provides a multitude of bonding opportunities to a wide range of transition metal centres.[3]

Transition metal thiolato complexes can be monomers, dimers and even clusters. Some of the earliest known alkyl thiolato metal complexes are the iridium complexes, $Ir(PPh_3)_2CO(SR)$ (R = Me, Et, ^{i}Pr).[4a] Monomeric coordinately unsaturated thiolates are less common and generally restricted to aryl thiolates of platinum and palladium which are metals that characteristically form 16-electron compounds[2b] although recent studies have shown monomeric complexes of Ru[4b] and Ni[5] thiolates are possible, however some of these tend to be unstable. For example, previous reports on mixed-ligand complexes of Ni(II) with phosphine and thiolato ligands of the type $[NiL_2(SPh)_2]$ (L = PEt_3 or PMe_2Ph) tend to dissociate in solution, whereas $[Ni(dppe)(SPh)_2]$ is reported to be stable.[6]

Rauchfuss and Roundhill[2b] have reported that complexes of Ni, Pd and Pt with ethane-1,2-dithiol, [{M(PPh_3)(SC_2H_4S-o)}$_2$] (M = Ni or Pd) are dimers with bridging sulfur atoms whereas Pt(PPh_3)$_2$(SC_2H_4S-*o*) and Ni(dppe)(SC_2H_4S-*o*) are stable mononuclear complexes. Schmidt and Hoffman[7] have described the synthesis of Ni(dppe)(SCH_2SCH_2S-*o*) and Ni(dppe)(SC_3H_6S-*o*), although the former is unstable at room temperature. Monodentate thiolato complexes such as [M(dppe){$SC_3H_6NMe_2$}$_2$][BPh_4]$_2$[8a] (M = Ni or Pd) have also been reported. Taylor and co-workers[8b] have reported thiolato complexes of Pd(II) and Pt(II) of 4-mercapto-1-methylpiperidine of the types M(dppe)(SR)$_2$ and {M(dppe)(SR)}$_2$$Cl_2$ containing chelating phosphine ligands. The nuclearity of nickel thiolato complexes appears to be highly dependent on the electron density at the nickel centre. Generally, complexes containing alkyl phosphine ancillary ligands form mononuclear compounds of the type $NiL_2(SR)_2$[9] (L = phosphine; R = aryl). The presence of other ligands that influence the electron density on the central metal atoms have been found to greatly affect the eventual structures of these thiolato complexes. For example, thiolato complexes formed from the reactions of Ni(PPh_3)(dtc)Cl and the appropriate thiol invariably leads to the formation of dinuclear compounds, which contain bridging thiolato ligands and the reactions are accompanied by loss of the phosphine.[10] Other examples of sulfur bridged metal thiolates include $Pd_2(PPh_3)_2(SC_2H_4S\text{-}o)_4$[2b] and the one shown in eq. 1.

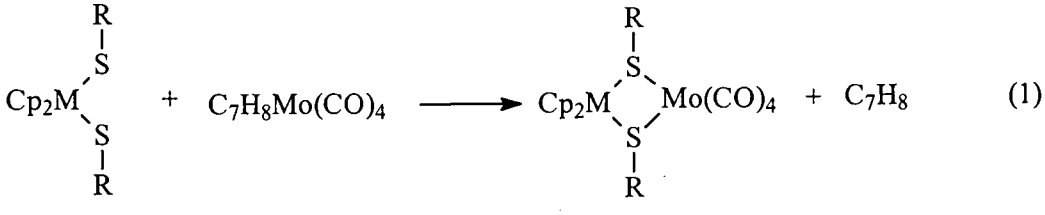

(1)

(M = Ti, Nb; R = Me, Ph)

Although the above discussion seem to relate group 10 metal thiolates structures to the type of thiols and the ancillary ligands, metal thiolates are generally studied for a variety of applications such as (i) nucleophiles for sulfur dioxide reactions, (ii) biological models and also as (iii) catalysts for acetylene reactions. Some of these are reviewed in the subsequent sections.

1.2 Metal thiolates as nucleophiles for sulfur dioxide (SO_2) reactions.

Interest in the transition metal chemistry of sulfur oxides in general and sulfur dioxide (SO_2) in particular, remains high. This is mainly due to environmental concerns as sulfur dioxide is one of the main precursors for the formation of acid rain. Acid rain makes lakes too acidic to support marine life, e.g. fish, and also in corrosion to exposed metals used in railroad construction, vehicles and machinery, and to stone-building materials such as limestone and marble. Studies involving the reactions of metal complexes with sulfur dioxide are directed towards using these compounds to remove sulfur dioxide as a pollutant.[11-13] The bonding of sulfur dioxide with metals is seen to be very crucial in the metal's ability to remove this gas. Two main types of sulfur dioxide reactions with metals are known, namely: reactions where the sulfur dioxide molecule is bound to a metal centre[11d,14-15] and those where the sulfur dioxide molecule is bound to a ligand[11c,16b,17-18] in a metal complex. The former seldom leads to reversible absorption, whereas the latter almost invariably gives products that easily release the sulfur dioxide; presumably because the ligand-SO_2 interaction is generally weak.

1.2.1 Sulfur dioxide metal bonding and detection.

Sulfur dioxide coordinates to metals in various ways. Five different SO_2 coordination geometries have been established by X-ray crystallography (Chart I), namely: pyramidal M-SO_2[17a,19-20] [where M = a metal or a main group atom], (ii) coplanar M-SO_2[21], (iii) bridging M-SO_2-M[22], (iv) S, O-bonded[23] and lastly (v) O-bonded[24]. According to Kubas *et al.*[25] one of the simplest SO_2 coordination geometry characterisation methods is by infrared spectroscopy, since two strong bands due to SO stretching modes are normally present in the spectra of all SO_2 metal complexes. Table 1 shows the correlation between ν(SO) stretching frequencies and metal-SO_2 geometry.

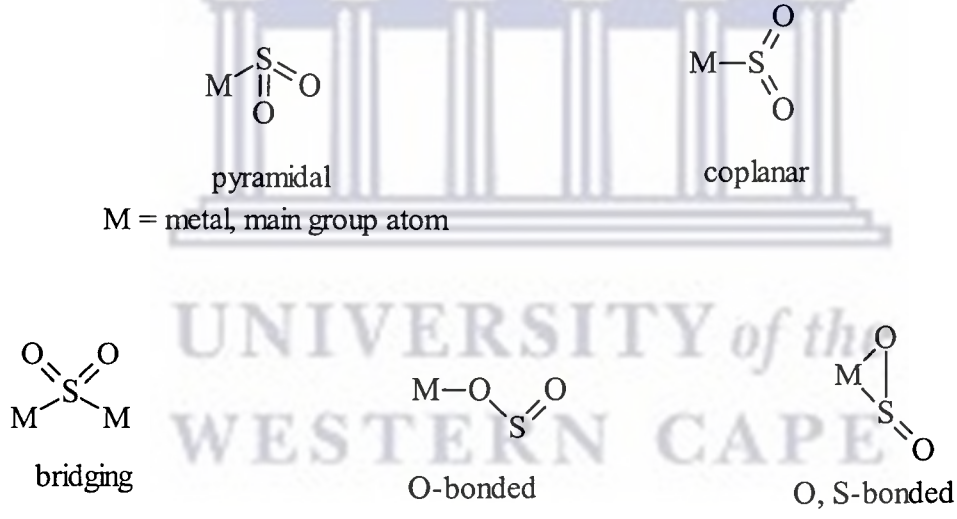

Chart I: Coordination geometries of metal-sulfur dioxide complexes.

The ranges for pyramidal M-SO_2 and bridging M-SO_2-M are nearly identical. This is not very surprising since in both instances the SO_2 is S bound and the interaction with the metal(s) results in similar M-S-O angles. Therefore differentiation between the pyramidal and bridging geometries is not usually possible on the basis of infrared evidence alone.

Table 1: Correlation of SO_2 coordination geometry and infrared stretching frequencies.

Coordination geometry	Observed ranges for ν(SO) (cm^{-1})
M-SO_2 pyramidal	1237-1150, 1065-990
M-SO_2 coplanar	1303-1250, 1130-1087
M-SO_2-M bridging	1237-1137, 1064-978
M-SO_2 S, O-bonded	1157-1107, 948-873
M-SO_2 O-bonded	1317-1210, 1135-1051

On a 1:1 basis, general correlation of geometry with SO infrared stretching frequency, reversibility of SO_2 binding, and tendency of a complex to undergo the sulfato reaction can be made, though exceptions do exist. However certain combinations of properties have been found to be diagnostic of specific geometries.[26]

1.2.2 Metal-bound SO_2 complexes.

Transition metals generally react with SO_2 by binding to the metal centre. An example can be found in recent studies by Darkwa[27] in which SO_2 reacts with Ni(dppe)(SC_6H_3RS-*o*) (R = H, Me) complexes by binding on the nickel centre. However some metal thiolato complexes containing phosphine ligands can react with sulfur dioxide via the loss of the phosphine ligand (PPh_3) from the complexes. This has been observed in the complexes $RuCp(PPh_3)_2SR$[16a] (Cp = η^5-C_5H_5; R = 4-C_6H_4Me, 1-C_3H_7, $CHMe_2$) which are activated respect to loss of PPh_3 (eq. 2) easily forming $RuCp(PPh_3)(CO)(SR)$, or in the absence of

additional ligands, trimers[28] of the type $[RuCpSR]_3$. The presence of strong π-accepting SO_2 ligand[20] stabilises the complexes $RuCp(PPh_3)(SO_2)SR$ with respect to ligand loss.

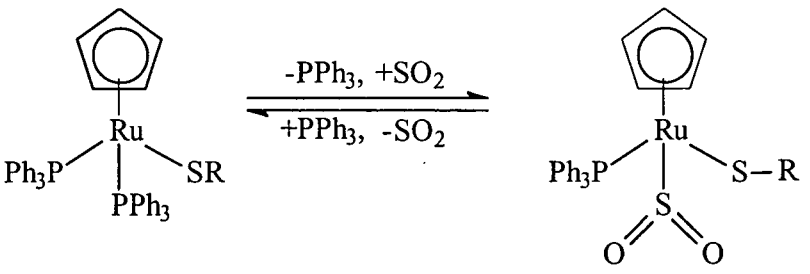

(2)

(R = 4-C_6H_4Me; 1-C_3H_7; $CHMe_2$)

From extended Huckel calculations[20a] it is established that d^8 and d^{10} transition metal complexes with strong basicity and lower energy LUMO are the ones that bound SO_2 via the metal atom. Structural evidence tends to support this view, and there now exist complexes of this type, some of which exhibits pyramidal geometry ($Pt(PPh_3)_3(SO_2)$ [20a] and $Pt(SO_2)_2(PPh_3)_2$)[20d] at the sulfur atoms and some of which (Ni(dppme)(SO_2) (dppme = 1,1,1-tris((diphenylphosphino)methyl)ethane) and $Co(PPh_3)_2(NO)(SO_2)$)[21] contain coplanar M-SO_2 groups. When compared to the isoelectronic complex $Ni(PPh_3)_3(SO_2)$, which exhibits coplanar geometry at the sulfur, the complex $Pt(PPh_3)_3(SO_2)$ is pyramidal and attests to the importance of the relative basicity of Pt compared to Ni in similar environments in determining the geometry of the M-SO_2 group.[20a]

When two or more metal centres are present, SO_2 can bridge a metal-metal bond or form a bridge between metal centres that are not supported by a metal-metal bond. Sulfur dioxide may bridge metal atoms through both sulfur and oxygen as in $[Mo(PPh_3)(CO)_2(py)(\mu\text{-}SO_2)]_2$[31a] (py = pyridine) in which the sulfur dioxide binds to two metal centres. A few heterometallic SO_2 containing clusters are known, such as the late

transition metal clusters $[Os_3Pt(\mu\text{-}H)_2(\mu\text{-}SO_2)(CO)_{10}(PCy_3)]$[31b] and $[Pt_3Au_3Cl(SO_2)_2(PCy_3)_3(P\{p\text{-}C_6H_4F\}_3)]$[31c]. Some alkyl sulfito ($M\text{-}SO_2R$) complexes are known for nickel[32a], palladium[32b], and platinum[32c] formed by the insertion of SO_2 into metal-alkyl bonds. Sulfur dioxide can also insert into a metal hydride bond, followed by an oxygen transfer process to form the $M\text{-}SO_3H$.[32d]

Another sulfur dioxide binding mode is "side-on bonding" or η^2 bonding, in which the sulfur-metal and one of the oxygen-metal distances are nearly equal. This was first found in $Rh(PPh_3)_2(NO)(\eta^2\text{-}SO_2)$[23b] and has subsequently been shown to exist in other complexes such as $Ru(PPh_3)_2Cl(NO)(\eta^2\text{-}SO_2)$[23c], $Mo(\eta^2\text{-}SO_2)(CO)_3(phen)$[11a] (phen = 1,10-phenanthroline) and $Mo(\eta^2\text{-}SO_2)_2(CO)_2(bpy)$[11a]. The complex $Rh(PPh_3)_2(NO)(\eta^2\text{-}SO_2)$ exhibits a bent metal-nitrosyl ligand binding in addition to the $\eta^2\text{-}SO_2$ and, if one considers the SO_2 to effectively occupy one coordination site, this represents an example of a four-coordinate (d^{10}) tetrahedral coordination complex. The isoelectronic complex $Co(PPh_3)(NO)(\eta^2\text{-}SO_2)$[33] on the other hand exhibits a linear metal-nitrosyl binding and a η^1-planar $Co\text{-}SO_2$ moiety, attesting to the role of the metal centre basicity plays as a contributing factor in the geometry of these SO_2 complexes. The Ru complex represents an example of a (d^8) trigonal-bipyramidal complex with the $S\text{-}O_M$ bond (O_M = metal-bound oxygen) in the equatorial plane. Two of features these two complexes have in common are (1) the presence of a fairly basic metal centre and (2) as far as the SO_2 is concerned, the close proximity of an ancillary ligand with good π-backbonding capability. As to the latter point, the relative orientation of the nitrosyl and SO_2 ligands in the two complexes shows a striking similarity in that the $S\text{-}O_M$ bond is orientated so as to

point the sulfur atom toward the nitrosyl ligand. This behaviour might be indicative of a ligand-ligand interaction and may suggest that the presence of a good π-accepting ancillary ligand contribute to the stability of the η^2-SO_2 coordination. The tendency toward the η^2 geometry would also be favoured by increased metal basicity, or in general, any perturbation which increases the energy of the potentially σ-accepting orbital or enhances the π-basicity of the metal as exemplified by $Mo(CO)_2(bpy)(SO_2)_2$[34] (bpy = 2,2'-bipyridine). Moody and Ryan[23a] have also shown by X-ray crystallography that the complex $Ru(PPh_3)_2(CO)_2(\eta^2\text{-}SO_2.SO_2)$ not only possesses the η^2-SO_2 coordination to the ruthenium, but also a second molecule of SO_2 coordinated to the terminal oxygen of the η^2-SO_2. Their study formed a foundation for the electrophilic attack on a η^2-SO_2 by the second SO_2 molecule and the importance of metal basicity for metal-SO_2 binding.

Earlier studies have also shown that η^2-SO_2 ligand in $[Fe(L)_2(\eta^2\text{-}SO_2)]$ (L = triarylphosphite, $(ArO)_3P$) can be obtained similar to the readily available $[Fe(L)_2(\eta^2\text{-}CS_2)]$ complexes[35]. It is well known that the phosphorus(III) ligand L in $[Fe(L)_2(CO)_2(\eta^2\text{-}CS_2)]$ complexes are labile, especially when they are bulky.[35] Therefore it seems reasonable to suggest that the replacement of CS_2 by SO_2 proceeds by a ligand L dissociation pathway, perhaps to give $[Fe(L)(CO)_2(CS_2)]$ with the subsequent formation of $[Fe(L)(CO)_2(CS_2)(SO_2)]$ and the displacement of CS_2 from it by free L. An alternate reaction pathway is associative with the formation of $[Fe(L)_2(CO)_2(CS_2)(SO_2)]$ having either $Fe\rightarrow SO_2$ or $FeCS_2\rightarrow SO_2$ bonding.[29] Its feasibility is a consequence of the Lewis acidity of SO_2 and hence suggest that ligand bound SO_2 complexes are possible.

1.2.3 Ligand bound SO_2 complexes.

Reactions of metal complexes in which the sulfur dioxide binds to the ligand have been studied extensively. Most of these complexes show reversible absorption of SO_2 because of the weakness of the ligand-SO_2 bond. Furthermore most of these ligand-bound SO_2 adducts are thiolato complexes,[17-18] with the sulfur of the thiolato ligand behaving as a Lewis base though this behaviour is not restricted to sulfur containing ligands. One of the earliest known ligand bound SO_2 complexes is $Pt(PPh_3)_2(CH_3)I.SO_2$[36] where the SO_2 is bound to the iodo ligand. Another complex in which SO_2 is bound to the iodo ligand is $[Cu(PPh_2Me)_2I]_2SO_2$, which contains weak I-SO_2 interactions (I-S = 3.41 Å)[17a]. Kubas *et al.*[17a] have determined the crystal structure of $Cu(PPh_2Me)_3(SPh)(SO_2)$ that confirms that the SO_2 molecule binds as a Lewis acid to the mercaptide sulfur, which in turn is coordinated to copper. The S-S distance of 2.53 Å is relatively long, and consistent with the observed lability found in these complexes. A bis thiolato adduct of a Pt(II), $Pt(PPh_3)_2(SPh)_2(SO_2)$[17a] also has the SO_2 bound to the sulfur atom.

The ability of metal thiolates to resist sulfur poisoning is one of the prerequisites for a potential catalyst for the conversion of SO_2 to harmless products. Since nickel is well known to activate thiolates towards nucleophilic behaviour[17c] as well as to promote oxygenation activity,[37a] the role of nickel as a catalyst facilitates the conversion of the nickel-thiolate-bound sulfur dioxide adduct to the corresponding sulfate compound. This is clearly discernable from the studies carried out by Darensbourg and co-workers[18a], who found that the four coordinate Ni(bme-daco) (bme-daco = N,N'-bis(mercaptoethyl)-1,5-diazacyclooctane) complex has nucleophillic thiolato sulfur sites that bind sulfur dioxide.

Further reaction of the resulting complex with SO_2 or O_2 attacks the bound SO_2 to form sulfate analogues and thus represent how metal thiolates could be used to solve SO_2 pollution problems. Recently Darkwa and co-workers[18c] have found that the nickel complexes $NiCp(PR_3)(SC_6H_4Cl)$ (Cp = η^5-C_5H_5; R = Ph_3, Bu_3, $(OPh)_3$, $(OEt)_3$ $(OMe)_3$) react with SO_2 by binding to the thiolato sulfur site. Kubas *et al.*[37b] have also demonstrated that the activation of the S=O bonds in SO_2 by transition metal complexes facilitates the cleavage of SO_2 in $(\eta^5\text{-}C_5Me_5)_2Mo_2(\mu\text{-}S_2)(\mu\text{-}SO_2)_2$ to form S_8 and a thiosulfate complex, $(\eta^5\text{-}C_5Me_5)_2Mo_2(\mu\text{-}S_2)(\mu\text{-}S)(\mu\text{-}SSO_3)$, (as shown in Scheme 1) which catalyses the homogenous hydrogenation of SO_2.

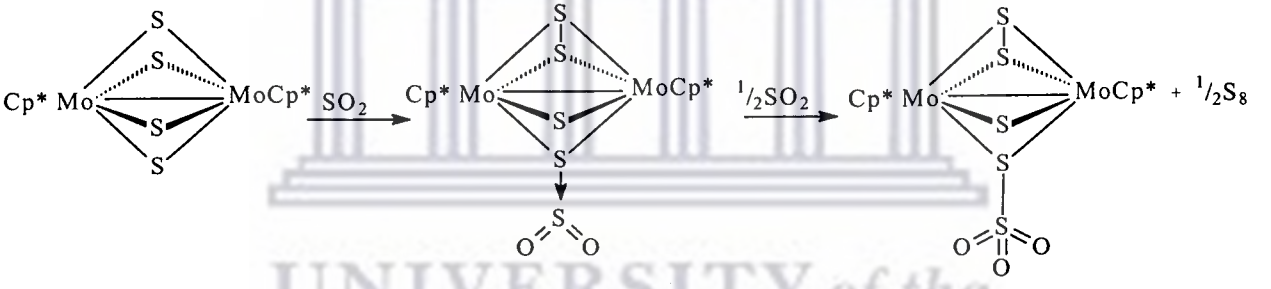

Scheme 1: Cleavage of SO_2 in $[(\eta^5\text{-}C_5Me_5)_2Mo_2(\mu\text{-}S_2)(\mu\text{-}S)_2(\mu\text{-}SSO_2)]$ to form S_8.

Catalytic conversion of SO_2 to exclusively S_8 and H_2O is also achievable using $(\eta^5\text{-}C_5H_5)_2Mo_2S_4$[17b] as a sulfur resistant catalyst and hydrogen as a reductant. The product of this reaction possesses an SO_3 unit rather than an SO_2 bound to the sulfide. The SO_3 fragment is formed by an oxygen atom transfer process, and as established by ^{18}O labeling, the source of the oxygen is the SO_2. It is conceivable that other types of reactions of SO_2, with or without metal complexes present, occur via a disproportionation

route as exemplified by the reaction of FeS with SO_2 in aqueous media to produce thiosulfate ion and Fe^{2+}.[38] The other complex in which the SO_2 binds to the bridging sulfur atom is $Cr_2(\eta^5\text{-}C_5Me_5)_2(\mu\text{-}S)_3(\mu\text{-}SSO_2)$[37c] similar to the one shown in Scheme 1.

The SO_2 disproportionation appears to be entirely a Lewis acid-base process, with the metal serving only as electron ballast. Following the report by Thon *et al.*,[38] Kubas and Ryan[11a] used Cp_2MH_2 (M = Mo, W) to reduce the air pollutant, SO_2, to innocuous products like $Cp_2M(S_2O_3)$. Research into this field of reducing SO_2 has since reached maturity and Shaver[16] has also reported a related oxygen atom disproportionation process for thiosulfinato to thiosulfonato conversion as shown in eq. 3.

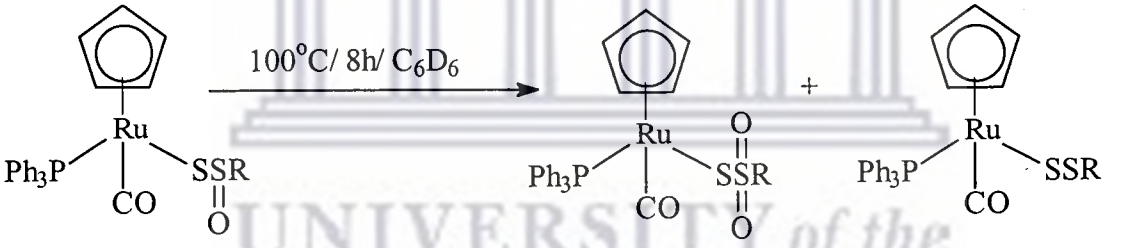

(R = 4-C_6H_4Me)

Shaver has also shown that the complexes $RuCp(PPh_3)_2SR$ (R = 4-C_6H_4Me, 1-C_3H_7, $CHMe_2$) react with SO_2 *via* the thiolato sulfur atom. Excess sulfur dioxide reacts with the resulting compound by displacing triphenylphosphine from the metal thereby forming $RuCp(PPh_3)(SO_2)(S(SO_2)R)$. This shows that SO_2 can bind to either the metal or the ligand or both in these complexes.[16] Moody *et al.*[39] have shown crystallographically that the complex $Ru(PPh_3)_2(CO)_2(\eta^2\text{-}SO_2)$ reacts with excess SO_2 in the absence of oxygen to form $Ru(PPh_3)_2(CO)_2(\eta^2\text{-}SO_2.SO_2)$. These are rare examples in which two SO_2 molecules

interact in a complex. Sulfur dioxide can also bind to two sulfur atoms of a dithiolato ligand as in the complex $[Au(SC_6H_3MeS\text{-}o)_2][n\text{-}Bu_4N]$ reported by Sadler and co-workers[18b].

It is clear from the discussion above that metal thiolato and dithiolato complexes are potential SO_2 sensors, a property that this project sorts to extend to diphosphino palladium and platinum dithiolato complexes.

1.3 Biologically active metal thiolato and metal phosphino complexes.

Some metal thiolates and metal phosphine complexes have been found to play significant roles in biological systems and as potential drugs for various ailments. Current medicinal interest in metal phosphine complexes ranges from the clinical use of the triethyl gold(I) complex, auranofin, as an antiarthritic agent, through the investigation of positively charged phosphino technetium complexes as heart-imaging agents, to the anticancer activity of certain phosphine complexes of gold(I).[40] Although auranofin is cytotoxic to tumor cells in culture, it is active only against one type of tumor. Bridged bis(phosphino) complexes such as $Au_2(dppe)Cl_2$ exhibit a wider spectrum of activity but are readily converted into four-coordinate tetrahedral gold(I) complexes by thiols in blood plasma.[41] It has been suggested that the phosphines themselves are the cytotoxic agents and that the metal ion/phosphine complex serves to protect the reagent during delivery to the appropriate target.[42] For complexes with chelating ligands, such as tetrahedral $[Au(dppe)_2]^+$, chelate ring opening is expected to be a critical step in the mode of antitumor action.[42b] The mechanism of action appears to differ from that of cisplatin (*cis*-

[$Pt(NH_3)_2Cl_2$]). The latter cross-links intrastrand guanine bases to DNA, whereas the tetrahedral gold(I) dppe complex cross-links proteins to DNA.[43] The complex [$Au(dppe)_2$]Cl does not lose activity against a subline of P388 leukemia, which is resistant to cisplatin, and moreover, [$Au(dppe)_2$]Cl and cisplatin can be administered concurrently at their respective maximum-tolerated doses to tumor-bearing mice with no lethality. The combination is more effective against moderately advanced P388 leukemia than cisplatin alone and the results indicate that the mechanism or site of action of the bis(phosphine) complex is different from that of cisplatin.[42b] Another phosphine complex that has some antitumor activity is $Au_4(dppep)Cl_4$[44] (dppep = tris(2-(diphenylphosphino)ethyl)-phosphine). Balch[45] has shown that two and four coordinate gold(I) complexes of dppep can be used as antitumor agents. Some gold(I) thiolates such as "Myocrisin" (thiomalate) and "solganol" (thioglucose) have been used as antiarthritic drugs in clinics.[46a] This prompted Sadler and coworkers[46b] to study the chemistry of gold(III) complexes of toluene-3,4-dithiol, but they showed no anticancer activity. The toluene-3,4-dithiol ligand can accommodate the square planar geometry demanded by Au(III) forming five membered-chelate rings. Other examples reported to have antiarthritic activity include dithiocarbamato and ethylene dithiolato complexes of Au(III).[47]

The discovery that diphosphine complexes of Cu(I), Ag(I) and Au(I) exhibit anticancer activity against several types of tumours,[46a] prompted investigations into the potential anticancer activity of similar complexes of Ni(II), Pd(II) and Pt(II). It has been reported that [$Pt(dppe)Cl_2$][44] (dppe = $Ph_2PCH_2CH_2PPh_2$) is inactive, because the Pt-P bonds are

too inert and the toxic diphosphine ligand is not released at the target site. Nickel(II) complexes are usually more labile than those of Pd(II) and Pt(II), but [Ni(dppe)Cl_2] is inactive probably because it is too labile and reacts rapidly with cell culture media to form the oxidised diphosphine dioxide.[48] Sadler *et al.*[49] have investigated complexes of Ni(II), Pd(II) and Pt(II) with diphosphine and phosphinoarsines and thiolate ligands and found the nickel(II) complexes to have an increased stability in comparison to chloro complexes, and that the high *trans* influence of sulfur labilises the diphosphine in the complexes of Pd(II) and Pt(II). In aqueous media the solubility of complexes containing these hydrophobic bis(diphenylphosphino)- and diphenylarsinodiphenylphosphinoethane ligands increases on coordination of the thiolate. This is important for biological testing carried out in aqueous media and greatly influences the partition of the complexes. In general the introduction of dithiolates increases the solubility but decreased the cytotoxicity of the series of complexes [M(L-L)($S(CHCO_2H)_2S$-*o*)] (M = Ni, Pd, Pt; L-L = dppe, dadpe (dadpe = 1-diphenylarsino-2-diphenylphosphinoethane); $S(CHCO_2H)_2S$ = dimercarptosuccinic acid).[49] The Pt(II) analogous of these complexes are more cytotoxic than the palladium(II) counterparts.[49]

Since thiosalicylic acid (*o*-sulfanylbenzoic acid) is able to coordinate to metal centres either through its thiolate or carboxylate groups, or both, it gives rise to a range of complexes with monodentate, bidentate chelating or bridging thiosalicylate ligands.[50] Recently, Henderson *et al.*[50c] have made use of the varied binding modes of thiosalicylic acid to synthesise the methoxy-functionalised organogold(III) thiosalicylate complex which showes marked antitumor and antimicrobial activity. The analogous

$Pt(PPh_3)(py)(SC_6H_4CO_2\text{-}o)$, $Pt(PPh_3)_2(SC_6H_4CO_2\text{-}o)$ and $Pd(PPh_3)_2(SC_6H_4CO_2\text{-}o)$ are known to have moderate antitumor activity but are less effective than gold(III) thiosalicylate complexes.[51] Therefore the potential of phosphino metal thiolates as anticancer agents makes the synthesis of such complexes important.

1.4 Cyclooligomerisation of acetylenes.

A number of transition metal complexes have been found to homogeneously catalyse the cyclisation of acetylenes. In particular, palladium(II) complexes have been extensively investigated by Maitlis *et al.*[52], who found them to be efficient catalysts for the cyclotrimerisation of acetylenes to benzenoid derivatives. Much of the transition-metal catalysed oligomerisation of acetylenes has centred on the group 10 metals, with the cheaper nickel[53] playing quite a prominent role in these studies. Acetylenes can be converted to cyclooctatetraene when heated at 60-70°C in the presence of a Ni catalyst as shown in eq. 4.

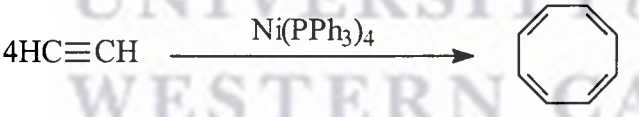

(4)

When a nickel catalyst with tertiary phosphine ligands is used under similar conditions, the acetylene is cyclotrimerised to benzene as shown in eq. 5.

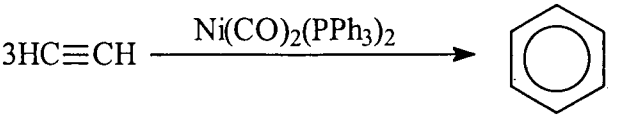

(5)

The reaction proceeds by initial coordination of one acetylene to give a mono acetylene complex, coordination of the second acetylene to form a bis-acetylene complex, and

rearrangement of this intermediate to a metallacyclopentadiene complex. Coordination of a third molecule of acetylene and its insertion into the metallacycle, followed by reductive elimination leads to the formation of a cyclotrimer. These sequence of reactions is the mechanistic pathway for the cyclotrimerisation of acetylenes. Acetylenes can also insert into a Pd-Cl bond and further insertions of the acetylene into the resulting Pd-C bond followed by cyclisation forms cyclobutadiene and benzene derivatives[54] as shown in Scheme 2.

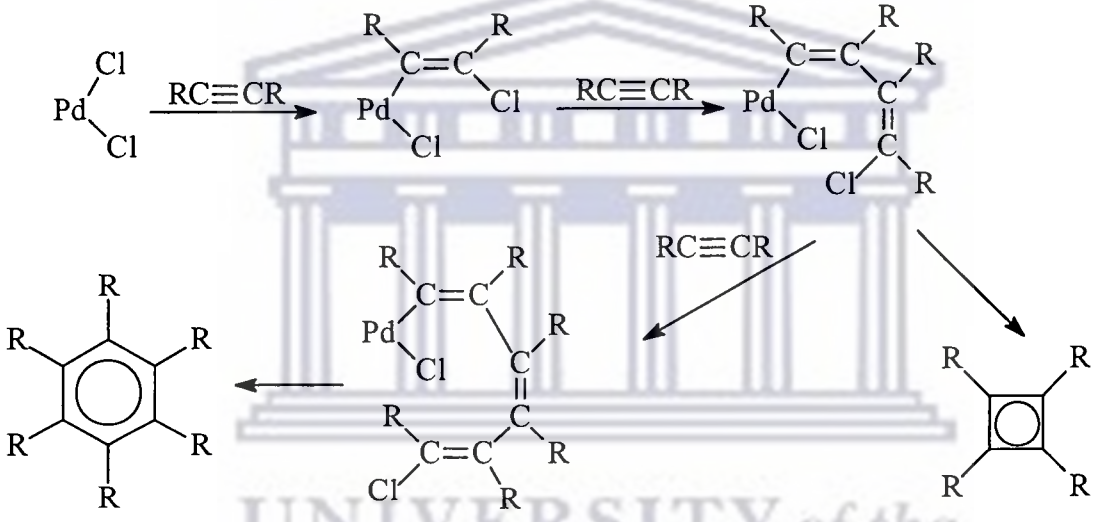

Scheme 2. Cyclooligomerisation of acetylenes *via* insertion into Pd-Cl bond.

Recently, Bennet and Wenger[54] have utilised bis(phosphino)nickel(0) complexes to catalytically cyclise a number of alkynes in solution, demonstrating the importance of phosphines in such reactions. In most cases, the main products isolated were aromatic compounds formed by cyclotrimerisation of the acetylene as a result of acetylene insertion into the Ni-benzene bonds and subsequent reductive elimination. Formation of aromatic cyclotrimer is generally favoured with more electrophilic acetylenes.

Nickel salts are well known to cyclotrimerise and cyclotetramerise acetylenes, producing benzene and cyclooctatetraene. Late-transition-metal catalysts are particularly attractive, as they tend to exhibit greater functional group tolerance than the more electron-deficient early transition metal catalysts. Two oxidation states are predominant in the use of nickel as a catalyst for acetylene cyclisation: these are nickel(II) and nickel(0). Early literature reports considered nickel(II) complexes as the active catalysts in the formation of cyclooctatetraenes[55] whereas nickel(0) complexes trimerise acetylenes to benzenoid derivatives. In general, studies involving nickel(0) are more abundant than those of nickel(II) mainly because the former readily dissolve in organic solvents whilst nickel(II) salts, that are normally used, are insoluble in such solvents. With the aid of phosphine ancillary ligands, the solubility of nickel(II) complexes in organic solvents could be achieved. Such compounds are known to trimerise[56] acetylenes. With dithiolato as coligands, phosphinonickel complexes can behave as nucleophilic agents towards acetylenes. Adduct formation, through the attachment of dienes to sulfur atoms of bis(1,2-ethylenedithiolato)nickel[57] are known and recent studies by Darkwa[27] have shown the potential ability of Ni(dppe) organochalcogenide complexes in the cyclotrimerisation of DMAD.

Further evidence of the involvement of sulfur in acetylene metal thiolate interactions is provided by the reaction of DMAD with Ni(triphos)(η^2-S_2CS) (triphos = 1,1,1-tris(diphenylphosphinomethyl)ethane) to form a five membered metallo heterocyclic

adduct, in which a dimerised DMAD moiety is attached to the carbon and sulfur of the η^2-S_2CS ligand.[58]

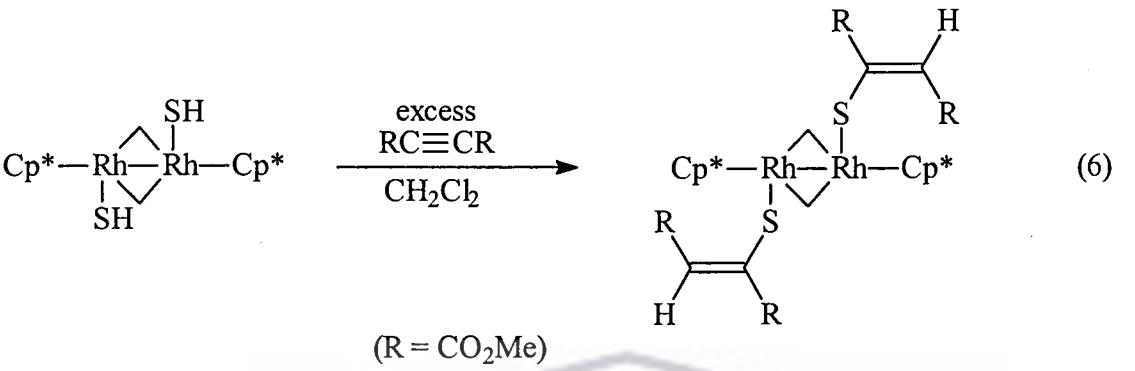

(6)

Recent work on the reaction of *trans*-$[(RhCp^*)_2(\mu\text{-}CH_2)_2(SH)_2]$ with DMAD to form *trans*-$[(RhCp^*)_2(\mu\text{-}CH_2)_2(SCR{=}CHR)_2]$ ($Cp^* = \eta^5\text{-}C_5Me_5$, $R = CO_2Me$)[59] (eq. 6) suggests that the cyclisation of acetylenes by nickel dithiolato complexes[27] could involve an initial acetylene-thiolato ligand interaction. Some of the reactions in this project were designed to provide evidence for this suggestion.

1.5. Objectives of the study.

The preceding introduction shows that work in our research group has involved, in recent years, the synthesis and reactions of Ni(dppe) thiolato complexes with sulfur dioxide and DMAD. The aim of the present study was to extend the Ni(dppe) thiolato complexes by changing both the phosphine and the metal to prepare ferrocene enchored bis(diphenylphosphino)palladium(II) and platinum(II) aryldichalcogenide complexes. The phosphine was varied from diphenylphosphino to diisopropylphosphino to improve the solubility of the complexes in the common solvents that would be used.

The second aim of the study was to investigate the stability of the complexes by varying the ionisation sources in mass spectrometry. This technique helped in identifying molecular weights of compounds, thus providing further support for the proposed structures. These structures were confirmed by single crystal X-ray crystallography. The electrochemical behaviour of the complexes was also investigated.

The third aim was to investigate the reactions of the palladium thiolates with acetylenes towards cyclooligomerisation products. One unresolved issue from the reactions of sulfur dioxide with Ni(dppe) thiolato complexes is firm evidence about the binding site of the sulfur dioxide. One aim of the present study was to change both the phosphine and metal to prepare palladium and platinum thiolato complexes that could form stable sulfur dioxide adducts.

The extent to which the above aims were realised is reported in the rest of this thesis. It would also show how successful most of the attempts to prepare various compounds were and how extensively these compounds have been characterised.

CHAPTER 2

EXPERIMENTAL

2.1 Materials and instrumentation.

All solvents were of analytical grade and were used without further purification, however they were degassed prior to use. Dichloromethane, which was used for cyclic voltammetry, was refluxed over P_2O_5 twice for 24 h, distilled under nitrogen and stored over molecular sieves. All reagents were of analytical grade and used as received. N,N,N',N'-tetramethylethylenediamine (TMEDA) and 1,2-benzenedithiol were purchased from Fluka. Palladium chloride was supplied by Next Chimica, South Africa. Chlorodiphenylphosphine, chlorodiisopropylphosphine, thiophenol, triethylamine, thiosalicylic acid, 2-mercaptophenol, 3,6-dichloro-1,2-benzenedithiol and *n*-butyllithium were purchased from Aldrich. Saarchem, South Africa supplied selenium and tellurium, while Riedel-de Haen supplied 3,4-toluenedithiol. The starting materials ferrocene[60], 1,1'-bis(diphenylphosphino)ferrocene[61] (dppf), 1,1'-bis(diisopropylphosphino)ferrocene[61] (dippf), $Pd(dppf)Cl_2$[62], $Pd(dippf)Cl_2$[63], $Pt(cod)Cl_2$[64] and $Pt(dppf)Cl_2$[65] were prepared according to the literature procedures. All the reactions were performed under an atmosphere of nitrogen using standard inert atmosphere techniques but the air-stable products were worked-up in air.

^1H and ^{31}P NMR spectra were recorded on a Varian Gemini-2000 NMR spectrometer at 200 MHz and 80.96 MHz respectively and referenced to residual $CDCl_3$ for ^1H (δ 7.26) and externally with PPh_3 for ^{31}P (δ -5.00). IR spectra were recorded on a Perkin-Elmer paragon 1000 PC FTIR spectrometer using nujol mulls. UV-vis spectra were run on a

GBC UV-vis 920 spectrophotometer. Mass spectra were recorded on a JEOL JMS-HX EBE spectrometer in the Electron Impact (EI) and Fast Atom Bombardment (FAB) modes by Dr. E.Y. Osei-Twum at the King Fahd University of Petroleum and Minerals in Saudi Arabia. Elemental analyses were performed in-house on a CARLO ERBA NA 1500 Analyzer while cyclic voltammetric data were recorded on a BAS C50W electrochemical analyzer. Dr. J. Bacsa of the University of Cape Town, South Africa, determined X-ray structures of Pd(dppf)(SC_6H_4S-*o*) and Pd(dippf)(SC_6H_3MeS-*o*) and Dr. I.A. Guzei of Iowa State University of Science and Technology, U. S. A. determined the remaining X-ray structures.

2.2 Reactions of $Pd(dppf)Cl_2$ with aryldichalcogenide reagents.

2.2.1 Reaction of $Pd(dppf)Cl_2$ with 1,2-benzenedithiol: formation of $Pd(dppf)(SC_6H_4S$-o$).1/2CH_2Cl_2$ (1a).

A mixture of $Pd(dppf)Cl_2$ (0.30 g, 0.41 mmol) and 1,2-benzenedithiol (0.058 g, 0.41 mmol) was evacuated for 15 minutes and flushed with nitrogen for a further 15 minutes in a Schlenk tube. Degassed dichloromethane (50 ml) was added, followed by triethylamine (Et_3N) (1 ml). The reddish brown solution of $Pd(dppf)Cl_2$ turned dark red on addition of Et_3N and was stirred at room temperature for 22 h, after which the mixture was filtered and the product precipitated by adding hexane. The precipitate was isolated by filtration, and washed with copious amount of water until the washings gave a negative test for chloride ions. The solid was re-dissolved in CH_2Cl_2 and dried over anhydrous $MgSO_4$. The removal of the solvent in vacuo gave analytically pure yellowish orange product. Yield = 0.24 g, 67%. Anal. calc. for $C_{40}H_{32}P_2S_2FePd.1/2CH_2Cl_2$: C,

57.67; H, 3.94%. Found C, 57.65; H, 3.59%. ^{1}H NMR ($CDCl_3$): δ 7.81 (m, 8H, PC_6H_5), 7.40 (m, 12H, PC_6H_5), 7.10 (dd, $^3J_{HH}$ = 8.00 Hz, $^3J_{HH}$ = 2.00 Hz, 2H, SC_6H_4S), 6.72 (dd, $^3J_{HH}$ = 5.90 Hz, $^3J_{HH}$ = 3.30 Hz, 2H, SC_6H_4S), 4.38 (t, $^3J_{HH}$ = 2.00 Hz, 4H, PC_5H_4), 4.20 (t, $^3J_{HH}$ = 1.90 Hz, 4H, PC_5H_4). $^{31}P\{^1H\}$ NMR: δ 25.08 (s). MS (FAB): 799 (M^+, 18); 659 (M^+-SC_6H_4S, 25). MS (EI): 659 (M^+-SC_6H_4S, 42). IR (nujol, cm^{-1}): 1712 w, 1548 m, 1459 w, 1379 s, 1283 w, 1165 w, 1094 m, 1026 w, 812 m, 736 s, 698 s, 631 m, 543 s.

Complexes **1b-1f** were prepared and worked-up in a similar manner as described for the reaction of Pd(dppf)Cl_2 with 1,2-benzenedithiol above.

2.2.2 Reaction of Pd(dppf)Cl_2 and 3,4-toluenedithiol: formation of Pd(dppf)(SC_6H_3MeS-o).CH_2Cl_2 (1b). The product was isolated as a reddish brown solid. Yield = 0.24 g, 71%. Anal. calc. for $C_{41}H_{34}P_2S_2FePd.CH_2Cl_2$: C, 56.05; H, 4.03%. Found: C, 55.49; H, 3.66%. ^{1}H NMR ($CDCl_3$): δ 7.80 (m, 8H, PC_6H_5), 7.52 (m, 12H, PC_6H_5), 6.98 (d, $^3J_{HH}$ = 8.00 Hz, 1H, SC_6H_3MeS), 6.92 (s, 1H, SC_6H_3MeS), 6.76 (dd, $^3J_{HH}$ = 8.00 Hz, $^3J_{HH}$ = 1.20 Hz, 1H, $SC_6H_3CH_3S$), 4.37 (m, 4H, PC_5H_4), 4.19 (m, 4H, PC_5H_4), 2.13 (s, 3H, SC_6H_3MeS). $^{31}P\{^1H\}$ NMR: δ 24.97 (s). MS (FAB): 813 (M^+, 20); 659 (M^+-SC_6H_3MeS, 11). MS (EI): 154 (SC_6H_3MeS, 100). IR (nujol, cm^{-1}): 1464 w, 1434 m, 1371 m, 1308 m, 1257 s, 1173 w, 1089 s, 1035 w, 997 m, 820 s, 732 s, 677 s, 635 s, 547 s, 484 s, 463 s, 433 s.

2.2.3 Reaction of Pd(dppf)Cl_2 with 3,6-dichloro-1,2-benzenedithiol: formation of Pd(dppf)($SC_6H_2Cl_2$S-o) (1c). The product was isolated as a yellowish orange solid. Yield

= 0.21 g, 59%. Anal. calc. for $C_{40}H_{30}P_2S_2Cl_2FePd$: C, 55.22; H, 3.48%. Found: C, 55.43; H, 3.34%. ^1H NMR ($CDCl_3$): δ 7.79 (m, 8H, PC_6H_5), 7.40 (m, 12H, PC_6H_5), 6.82 (s, 2H, $SC_6H_2Cl_2S$), 4.41 (t, $^3J_{HH}$ = 1.60 Hz, 4H, PC_5H_4), 4.23 (d, $^3J_{HH}$ = 1.60 Hz, 4H, PC_5H_4). $^{31}P\{^1H\}$ NMR: δ 25.48 (s). MS (FAB): 869 (M^+, 37); 659 (M^+-$SC_6H_2Cl_2S$, 41). MS (EI): 208 ($SC_6H_2Cl_2S$, 60). IR (nujol, cm^{-1}): 1707 w, 1464 m, 1375 s, 1304 w, 1270 w, 1157 m, 820 m, 749 m, 694 s, 639 m, 538 s, 459 s.

2.2.4 Reaction of Pd(dppf)Cl₂ with 2-mercaptophenol: formation of Pd(dppf)(OC₆H₄S-o) (1d). The product was isolated as an orange solid. Yield = 0.22 g, 69%. Anal. Calc. for $C_{40}H_{32}OP_2SFePd$: C, 61.20; H, 4.12%. Found: C, 60.66; H, 3.75 %. ^1H NMR ($CDCl_3$): δ 8.00 (m, 4H, PC_6H_5), 7.69 (m, 4H, PC_6H_5), 7.41(m, 6H, PC_6H_5), 7.31(m, 6H, PC_6H_5), 7.02 (d, $^3J_{HH}$ = 7.60 Hz, 1H, OC_6H_4S), 6.70 (t, $^3J_{HH}$ = 7.50 Hz, 1H, OC_6H_4S), 6.40 (t, $^3J_{HH}$ = 6.80 Hz, 1H, OC_6H_5), 6.25 (d, $^3J_{HH}$ = 8.20 Hz, 1H, OC_6H_4S), 4.71 (q, $^3J_{HH}$ = 3.80 Hz, $^3J_{HH}$ = 2.00 Hz, 2H, PC_5H_4), 4.50 (s, 2H, PC_5H_4), 4.28 (s, 2H, PC_5H_4), 3.77 (q, $^3J_{HH}$ = 3.80 Hz, $^3J_{HH}$ = 1.80 Hz, 2H, PC_5H_4). $^{31}P\{^1H\}$ NMR: δ 39.53 (d, $^2J_{PP}$ = 27.45 Hz, 1P, P *trans* S), 21.98 (d, $^2J_{PP}$ = 27.45 Hz, 1P, P *trans* O). MS (FAB): 783 (M^+, 15); 659 (M^+-OC_6H_4S, 14). MS (EI): 124 (OC_6H_4S, 84). IR (nujol, cm^{-1}): 1464 w, 1379 m, 1274 s, 1164 m, 1094 w, 1022 w, 736 s, 719 s, 690 m, 547 s, 480 s.

2.2.5 Reaction of Pd(dppf)Cl₂ with thiosalicylic acid: formation of Pd(dppf)(SC₆H₄CO₂-o).1/2CH₂Cl₂ (1e). The product was isolated as an orange solid. Yield = 0.20 g, 60%. Anal. calc. for $C_{41}H_{32}O_2P_2SFePd.^1/_2CH_2Cl_2$: C, 58.27; H, 3.89%. Found: C, 58.05; H, 3.78%. ^1H NMR ($CDCl_3$): δ 7.82 (m, 10H, PC_6H_5), 7.44 (m, 10H, PC_6H_5), 7.00 (m, 4H,

$SC_6H_4CO_2$), 4.63 (q, $^3J_{HH}$ = 3.7 Hz, 2H, PC_5H_4), 4.48 (s, 2H, PC_5H_4), 4.31 (s, 2H, PC_5H_4), 3.84 (q, $^3J_{HH}$ = 3.7 Hz, 2H, PC_5H_4). $^{31}P\{^1H\}$ NMR: δ 37.88 (d, $^2J_{PP}$ = 29.35 Hz, 1P, P *trans* S), 22.67 (d, $^2J_{PP}$ = 29.35 Hz, 1P, P *trans* O). MS (FAB): 812 (M^+, 35); 659 (M^+-$SC_6H_4CO_2$, 59). MS (EI): 152 ($SC_6H_4CO_2$, 43). IR (nujol, cm^{-1}): 1716 w, 1590 w, 1464 w, 1384 m, 1350 w, 1169 m, 1098 m, 1035 m, 854 w, 744 s, 690 s, 635 m, 547 s, 467 s.

2.2.6 Reaction of Pd(dppf)Cl₂ with 2-mercaptonicotinic acid: formation of Pd(dppf)(SC₅H₃NCO₂-o) (1f). The product was isolated as a yellow solid. Yield = 0.18 g, 53%. Anal. Calc. for $C_{40}H_{31}NO_2P_2SFePd$: C, 59.02; H, 3.85; N, 1.72%. Found: C, 59.26; H, 3.64; N, 1.68%. ^1H NMR ($CDCl_3$): δ 8.25 (m, 2H, $SC_5H_3NCO_2$), 8.04 (m, 4H, PC_6H_5), 7.69 (m, 6H, PC_6H_5), 7.51 (m, 6H, PC_6H_5), 7.31 (m, 4H, PC_6H_5), 6.89 (m, 1H, $SC_5H_3NCO_2$), 4.49 (q, $^3J_{HH}$ = 1.80 Hz, 2H, PC_5H_4), 4.56 (s, 2H, PC_5H_4), 4.28 (s, 2H, PC_5H_4), 3.64 (q, $^3J_{HH}$ = 2.00 Hz, 2H, PC_5H_4). $^{31}P\{^1H\}$ NMR: δ 39.53 (d, $^2J_{PP}$ = 29.55 Hz, 1P, P *trans* S), 21.94 (d, $^2J_{PP}$ = 29.55 Hz, 1P, P *trans* O). MS (FAB): 813 (M^+, 74); 659 (M^+-$SC_6H_3NCO_2$, 33). MS (EI): 154 ($SC_6H_3NCO_2$, 25). IR (nujol, cm^{-1}): 3441 w, 1607 w, 1468 w, 1375 w, 1304 m, 1169 m, 1094 s, 997 s, 850 w, 749 s, 673 s, 679 m, 555 s, 484 s.

2.2.7 Attempted synthesis of Pd(dppf)(SC₆H₄Te-o): formation of Pd(dppf)(SC₆H₅)₂ (1g). A Schlenk tube was fitted with a pressure equalising dropping funnel and flushed with a stream of nitrogen. A nitrogen saturated hexane (20 ml) was added to the tube, followed by *n*-butyllithium (1.6 M, 1.40 ml, 2 mmol) and then N,N,N',N'-tetramethylethylene-

diamine (TMEDA) (0.40 ml, 2 mmol). The Schlenk tube was placed in ice bath (0 °C) and a nitrogen saturated solution of thiophenol (0.11 ml, 1.00 mmol) in hexane (20 ml) was added dropwise. After the addition was complete, the reaction mixture was stirred at 0 °C for an hour and gradually allowed to warm up to room temperature, and stirred for a further 24 h. This was followed by the addition of tellurium (0.08 g, 1.00 mmol) and stirred for 5 h. A degassed solution of $Pd(dppf)Cl_2$ (0.60 g, 1.00 mmol) in dichloromethane (40 ml) was added dropwise and stirred for 8 h at room temperature. The mixture was filtered and addition of hexane to the resultant solution gave a reddish brown solid, which was recrystallised from CH_2Cl_2/hexane to give analytically pure **1g**. The product was isolated as a brick red solid. Yield = 1.29 g, 74%. Anal. calc. for $C_{46}H_{38}P_2S_2FePd$: C, 62.85; H, 4.36%. Found C, 62.23; H, 4.26%. ^1H NMR ($CDCl_3$): δ 7.75 (m, 8H, PC_6H_5), 7.36 (m, 12H, PC_6H_5), 7.17 (m, 4H, SC_6H_5), 6.77 (m, 6H, SC_6H_5), 4.30 (d, $^3J_{HH}$ = 1.80 Hz, 4H, PC_5H_4), 4.12 (d, $^3J_{HH}$ = 1.80 Hz, 4H, PC_5H_4). $^{31}P\{^1H\}$ NMR: δ 22.82 (s). MS (FAB): 878 (M^+, 8); 769 (M^+-SC_6H_5, 85). MS (EI): 554 (M^+-$2SC_6H_5$-Pd, 35). IR (nujol, cm^{-1}): 3386 w, 1657 w, 1573 s, 1379 s, 1304 w, 1279 w, 1199 w, 1169 m, 1089 s, 1014 m, 997 w, 829 m, 774 s, 690 s, 547 m, 631 w.

2.3 Reactions of $Pd(dippf)Cl_2$ with aryldichalcogenide reagents.

2.3.1 Reaction of $Pd(dippf)Cl_2$ with 1,2-benzenedithiol: formation of $Pd(dippf)(SC_6H_4S$-o) (2a).

A mixture of $Pd(dippf)Cl_2$ (0.50 g, 0.839 mmol) and 1,2-benzenedithiol (0.119 g, 0.839 mmol) in a Schlenk tube was evacuated for 10 minutes and flushed with nitrogen for a further 10 minutes in a Schlenk tube. Degassed dichloromethane (50 ml) and Et_3N (1 ml)

were added sequentially and the solution was stirred at room temperature for 3 h and filtered. The filtrate was concentrated to about 20 ml and addition of 10 ml hexane precipitated the by-product, Et_3NHCl which was filtered. Addition of excess hexane to the filtrate gave the crude product, which was recrystallised from CH_2Cl_2/hexane to give dark orange **2a**. Yield = 0.29 g, 52%. Anal. calc. for $C_{28}H_{40}P_2S_2FePd$: C, 50.57; H, 6.06%. Found C, 51.11; H, 6.01%. ^1H NMR ($CDCl_3$): δ 7.40 (dd, $^3J_{HH}$ = 4.85 Hz, $^3J_{HH}$ = 3.10 Hz, 2H, SC_6H_4S), 6.88 (dd, $^3J_{HH}$ = 5.90 Hz, $^3J_{HH}$ = 3.20 Hz 2H, SC_6H_4S), 4.48 (m, 8H, PC_5H_4), 2.64 (m, 4H, $PCH(CH_3)_2$), 1.48 (m, 12H $PCH(CH_3)_2$), 1.19 (m, 12H, $PCH(CH_3)_2$). $^{31}P\{^1H\}$ NMR: δ 47.19 (s). MS (FAB): 664 (M^+, 15); 524 (M^+-SC_6H_4S, 8). MS (EI): 524 (M^+-SC_6H_4S, 40). IR (nujol, cm^{-1}): 1556 m, 1014 m, 1287 m, 1245 m, 1199 m, 1165 s, 1102 s, 1080 w, 1030 s, 934 w, 887 w, 829 m, 736 s, 656 w, 627 s, 538 m.

Complexes **2b-2f** were prepared and worked-up in a similar manner as described for the reaction of $Pd(dppf)Cl_2$ with 1,2-benzenedithiol above.

2.3.2 Reaction of Pd(dippf)Cl₂ with 3,4-toluenedithiol: formation of Pd(dippf)(SC₆H₃MeS-o).CH₂Cl₂ (2b). The product was isolated as an orange solid. Yield = 0.32 g, 56%. Anal. calc. for $C_{29}H_{42}P_2S_2FePd.CH_2Cl_2$: C, 47.17; H, 5.81%. Found C, 46.75; H, 5.77%. ^1H NMR ($CDCl_3$): δ 7.28 (d, $^3J_{HH}$ = 7.00 Hz, 1H, SC_6H_3MeS), 7.22 (s, 1H, SC_6H_3MeS), 6.70 (dd, $^3J_{HH}$ = 8.00 Hz, $^3J_{HH}$ = 1.40 Hz, 1H, SC_6H_3MeS), 4.49 (s, 4H, PC_5H_4), 4.46 (s, 4H, PC_5H_4), 2.64 (m, 4H, $PCH(CH_3)_2$), 2.24 (s, 3H, SC_6H_3MeS), 1.47 (m, 12H, $PCH(CH_3)_2$), 1.18 (m, 12H, $PCH(CH_3)_2$). $^{31}P\{^1H\}$ NMR: δ 42.15 (d, $^2J_{PP}$ = 18.30 Hz, 1P); 41.87 (d, $^2J_{PP}$ = 18.30 Hz, 1P). MS (FAB): 680 (M^+, 100); 524 (M^+-

SC_6H_3MeS, 16). MS (EI): 680 (M^+, 84); 524 (M^+-SC_6H_3MeS, 56). IR (nujol, cm^{-1}): 1383 w, 1285 w, 1262 w, 1245 w, 1195 w, 1159 m, 1116 m, 1066 w, 1035 w, 970 w, 930 w, 879 m, 865 m, 850 m, 813 s, 793 s, 731 s, 700 m, 653 s, 626 s, 540 s.

2.3.3 Reaction of $Pd(dippf)Cl_2$ with 3,6-dichloro-1,2-benzenedithiol: formation of $Pd(dippf)(SC_6H_2Cl_2S\text{-}o)$ (2c). The product was obtained as a yellow solid. Yield = 0.33 g, 55%. Anal. calc. for $C_{28}H_{38}Cl_2P_2S_2FePd$: C, 45.86; H, 5.22%. Found C, 46.04; H, 5.38%. ^1H NMR ($CDCl_3$): δ 6.97 (s, 2H, $SC_6H_2Cl_2S$), 4.51 (s, 4H, PC_5H_4), 4.49 (d, $^3J_{HH}$ = 3.20 Hz, 4H, PC_5H_4), 2.68 (m, 4H, $PCH(CH_3)_2$), 1.49 (m, 12H, $PCH(CH_3)_2$), 1.20 (m, 12H, $PCH(CH_3)_2$). $^{31}P\{^1H\}$ NMR: δ 41.92 (s). MS (FAB): 734 (M^+, 46); 524 (M^+-$SC_6H_2Cl_2S$, 19). MS (EI): 734 (M^+, 72); 524 (M^+-$SC_6H_2Cl_2S$, 56). IR (nujol, cm^{-1}): 1527 w, 1379 w, 1342 w, 1274 m, 1194 w, 1169 s, 1068 s, 1035 s, 963 w, 892 w, 816 m, 774 m, 728 m, 652 m, 623 s, 597 m.

2.3.4 Reaction of $Pd(dippf)Cl_2$ with 2-mercaptophenol: formation of $Pd(dippf)(OC_6H_4S\text{-}o).1/2CH_2Cl_2$ (2d). The product was isolated as a shiny dark brown solid. Yield = 0.38 g, 70%. Anal. calc. for $C_{28}H_{40}OP_2SFePd.1/2CH_2Cl_2$: C, 49.51; H, 5.98%. Found C, 49.25; H, 6.21%. ^1H NMR ($CDCl_3$): δ 7.35 (d, $^3J_{HH}$ = 8.4 Hz, 1H, OC_6H_4S), 7.01 (d, $^3J_{HH}$ = 7.6 Hz, 1H, OC_6H_4S), 6.82 (t, $^3J_{HH}$ = 8.20 Hz, 1H, OC_6H_4S), 6.54 (t, $^3J_{HH}$ = 8.20 Hz, 1H, OC_6H_4), 4.54 (s, 4H, PC_5H_4), 4.46 (s, 4H, PC_5H_4), 2.36 (m, 4H, $PCH(CH_3)_2$), 1.42 (m, 12H, $PCH(CH_3)_2$), 1.20 (m, 12H, $PCH(CH_3)_2$). $^{31}P\{^1H\}$ NMR: δ 55.18 (d, $^2J_{PP}$ = 12.14 Hz, 1P, P *trans* S); 48.28 (d, $^2J_{PP}$ = 12.14 Hz, 1P, P *trans* O). MS (FAB): 648 (M^+, 28); 524 (M^+-OC_6H_4S, 8). MS (EI): 648 (M^+, 35); 604 (M^+-^{i}Pr, 9). IR

(nujol, cm^{-1}): 2621 w, 1581 w, 1548 w, 1379 s, 1274 s, 1169 s, 1119 w, 1030 s, 934 w, 883 m, 850 m, 803 m, 732 s, 698 s, 652 m, 628 m, 602 m.

2.3.5 Reaction of $Pd(dippf)Cl_2$ with thiosalicylic acid: formation of $Pd(dippf)(SC_6H_4CO_2\text{-}o)$ (2e).

The product was isolated as brown oil and kept for one week at -15 °C to precipitate. Yield = 0.57 g, 45%. Anal. calc for $C_{29}H_{40}O_2P_2SFePd$: C, 51.46; H, 5.96%. Found C, 51.02; H, 6.94%. ^1H NMR ($CDCl_3$): δ 7.42 (m, 2H, $SC_6H_4CO_2$), 7.01 (m, 2H, $SC_6H_4CO_2$), 4.50 (m, 8H, C_5H_4), 2.80 (m, 4H, $PCH(CH_3)_2$), 1.49 (m, 12H, $PCH(CH_3)_2$), 1.20 (m, 12H, $PCH(CH_3)_2$). $^{31}P\{^1H\}$ NMR: δ 59.16 (d, $^2J_{PP}$ = 11.17 Hz, 1P, P *trans* S); 51.63 (d, $^2J_{PP}$ = 11.17 Hz, 1P, P *trans* O). MS (FAB): 677 (M^+, 66); 524 (M^+-$SC_6H_4CO_2$, 76). MS (EI): 677 (M^+, 54); 635 (M^+-^{i}Pr, 9). IR (nujol, cm^{-1}): 2730 w, 2593 w, 2347 w, 1678 m, 1581 m, 1464 s, 1379 s, 1300 w, 1236 w, 1165 m, 1030 s, 934 w, 879 w, 837 w, 791 w, 740 w, 719 s, 652 m, 623 m.

2.3.6 Reaction of $Pd(dippf)Cl_2$ with 2-mercaptonicotinic acid: formation of $Pd(dippf)(SC_5H_3NCO_2\text{-}o).1/2CH_2Cl_2$ (2f). The product was isolated as a yellowish orange solid. Yield = 0.45 g, 45%. Anal. calc. for $C_{28}H_{39}NO_2P_2SFePd.^1/_2CH_2Cl_2$: C, 49.19; H, 6.00; N, 1.94%. Found C, 48.81; H, 6.30; N, 2.11%. ^1H NMR ($CDCl_3$): δ 8.35 (m, 2H, $SC_5H_3NCO_2$), 7.01 (dd, $^3J_{HH}$ = 4.90 Hz, $^3J_{HH}$ = 1.80 Hz, 1H, $SC_5H_3NCO_2$), 4.53 (m, 8H, C_5H_4), 2.83 (m, 4H, $PCH(CH_3)_2$), 1.51 (m, 12H, $PCH(CH_3)_2$), 1.23 (m, 12H, $PCH(CH_3)_2$). $^{31}P\{^1H\}$ NMR: δ 59.66 (d, $^2J_{PP}$ = 12.71 Hz, 1P, P *trans* S); 52.34 (d, $^2J_{PP}$ = 12.71 Hz, 1P, P *trans* O). MS (FAB): 678 (M^+, 29); 524 (M^+-$SC_6H_3NCO_2$, 12). MS (EI):

635 (M^+-^{i}Pr, 8). IR (nujol, cm^{-1}): 1720 w, 1602 w, 1560 m, 1459 m, 1375 s, 1249 m, 1165 m, 1077 w, 1043 s, 934 w, 883 m, 770 s, 719 s, 656 m, 606 s.

2.3.7 Attempted synthesis of Pd(dippf)(SC_6H_4Te-o): formation of Pd(dippf)(SC_6H_5-o)$_2$ .CH_2Cl_2 (2g).

The procedure followed in the preparation of **2g** is the same as described in section **2.2.7** but using Pd(dippf)Cl_2 in place of Pd(dppf)Cl_2. The product was isolated as a brick red solid. Yield = 0.62 g, 68%. Anal. calc. for $C_{34}H_{46}P_2S_2FePd.CH_2Cl_2$: C, 50.77; H, 5.84%. Found C, 50.60; H, 5.94%. ^{1}H NMR ($CDCl_3$): δ 7.30 (m, 4H, SC_6H_5), 6.92 (m, 6H, SC_6H_5), 4.47 (s, 8H, PC_5H_4), 3.02 (sept, 4H, $PCH(CH_3)_2$), 1.50 (q, $^3J_{HH}$ = 16.40 Hz, $^3J_{HH}$ = 7.40 Hz, 12H, $PCH(CH_3)_2$), 1.19 (q, $^3J_{HH}$ = 14.00 Hz, $^3J_{HH}$ = 7.00 Hz, 12H, $PCH(CH_3)_2$). $^{31}P\{^1H\}$ NMR: 47.63 (s). MS (FAB): 743 (M^+, 7), 634 (M^+-SC_6H_5, 80). MS (EI): 635 (M^+- SC_6H_5, 100). IR (nujol, cm^{-1}): 3386 w, 1657 w, 1573 s, 1379 s, 1304 w, 1279 w, 1199 w, 1169 m, 1089 s, 1014 m, 997 w, 829 m, 744 s, 690 s, 547 m, 631 w.

2.4. Reactions of Pt(dppf)Cl_2 with aryldichalcogenide reagents.

2.4.1 Reaction of Pt(dppf)Cl_2 with 1,2-benzenedithiol: formation of Pt(dppf)(SC_6H_4S-o).CH_2Cl_2 (3a). A mixture of Pt(dppf)Cl_2 (0.40 g, 0.49 mmol) and 1,2-benzenedithiol (0.069 g, 0.49 mmol) in a Schlenk tube was evacuated for 10 minutes and flushed with nitrogen for a further 10 minutes in a Schlenk tube. Degassed dichloromethane (50 ml) and Et_3N (1 ml) were added sequentially and the solution was stirred at room temperature for 3 h and filtered. The filtrate was concentrated to about 20 ml and addition of 10 ml hexane precipitated the by-product, Et_3NHCl which was filtered. Addition of excess

hexane to the filtrate gave the crude product, which was recrystallised from CH_2Cl_2/hexane. The product was obtained as a yellowish solid. Yield = 0.32 g, 73%. Anal. calc. for $C_{40}H_{32}P_2S_2FePt.CH_2Cl_2$: C, 50.52; H, 3.52%. Found C, 50.11; H, 3.02%. ^1H NMR ($CDCl_3$): δ 7.81 (m, 8H, PC_6H_5), 7.41 (m, 12H, PC_6H_5), 7.27 (m, 2H, SC_6H_4S), 6.68 (m, 2H, SC_6H_4S), 4.36 (s, 4H, PC_5H_4), 4.23 (d, $^3J_{HH}$ = 1.8 Hz, 4H, PC_5H_4). $^{31}P\{^1H\}$ NMR: δ 22.82 (s, 2P, J_{Pt-P} = 1471.85 Hz). MS (FAB): 889 (M^+, 85); 812 (M^+-Ph, 10). MS (EI): 889 (M^+, 100), 781 (M^+-SC_6H_5, 9). IR (nujol, cm^{-1}): 1556 m, 1410 m, 1287 m, 1199 m, 1165 s, 1102 s, 1080 w, 1030 s, 934 w, 887 w, 829 m, 736 s, 656 w, 627 s, 538 m.

Complexes **3b-3f** were prepared and worked-up in a similar manner as described for the reaction of $Pd(dppf)Cl_2$ with 1,2-benzenedithiol above.

2.4.2 Reaction of $Pt(dppf)Cl_2$ with 4-methyl-1,2-benzenedithiol: formation of $Pt(dppf)(SC_6H_3MeS\text{-}o)1/2CH_2Cl_2$ (3b). The product was isolated as a yellow solid. Yield = 0.40 g, 54%. Anal. calc. for $C_{41}H_{34}P_2S_2FePt.1/2CH_2Cl_2$: C, 52.68; H, 3.73%. Found C, 52.76; H, 3.85%. ^1H NMR ($CDCl_3$): δ 7.81 (m, 8H, PC_6H_5), 7.39 (m, 12H, PC_6H_5), 7.14 (d, $^3J_{HH}$ = 7.60 Hz, 1H, SC_6H_3MeS), 7.08 (s, 1H, SC_6H_3MeS), 6.50 (dd, $^3J_{HH}$ = 7.60 Hz, $^3J_{HH}$ = 1.30 Hz, 1H, SC_6H_3MeS), 4.35 (s, 4H, PC_5H_4), 4.22 (s, 4H, PC_5H_4), 2.15 (s, 3H, SC_6H_3MeS). $^{31}P\{^1H\}$ NMR: δ 22.83 (s, 2P, J_{Pt-P} = 1470.80 Hz). MS (FAB): 904 (M^+, 96); 826 (M^+-Ph, 4). MS (EI): 904 (M^+, 100); 782 (M^+-SC_6H_4Me, 4). IR (nujol, cm^{-1}): 1463 m, 1387 s, 1308 w, 1295 w, 1264 m, 1171 m, 1096 s, 1034 m, 1003 w, 821 m, 724 s, 698 s, 636 m, 561 s.

2.4.3 Reaction of $Pt(dppf)Cl_2$ with 3,6-dichloro-1,2-benzenedithiol: formation of $Pt(dppf)(SC_6H_2Cl_2S\text{-}o)$ (3c). The product was isolated as a greenish yellow solid. Yield = 0.26 g, 55%. Anal. calc. for $C_{40}H_{30}Cl_2P_2S_2FePt$: C, 50.12; H, 3.15%. Found C, 50.41; H, 3.42%. ^1H NMR ($CDCl_3$): δ 7.80 (m, 8H, PC_6H_5), 7.39 (m, 12H, PC_6H_5), 6.80 (s, 2H, $SC_6H_2Cl_2S$), 4.38 (s, 4H, PC_5H_4), 4.25 (s, 4H, PC_5H_4). $^{31}P\{^1H\}$ NMR: δ 22.52 (s, 2P, $J_{Pt\text{-}P}$ = 1466.43 Hz). MS (FAB): 958 (M^+, 100); 749 (M^+-$SC_6H_2Cl_2S$, 12). MS (EI): 958 (M^+, 100), 922 (M^+-Cl, 5). IR (nujol, cm^{-1}): 1526 w, 1471 m, 1379 m, 1334 m, 1272 s, 1171 m, 1096 s, 1069 s, 1029 m, 1007 m, 830 s, 751 m, 711 s, 636 s, 561 s.

2.4.4 Reaction of $Pt(dppf)Cl_2$ with 2-mercaptophenol: formation of $Pt(dppf)(OC_6H_4S\text{-}o).1/2CH_2Cl_2$ (3d). The product was isolated as a yellow solid. Yield = 0.24 g, 56%. Anal. calc. for $C_{40}H_{32}OP_2SFePt.1/2CH_2Cl_2$: C, 53.10; H, 3.63%. Found C, 53.51; H, 3.77%. ^1H NMR ($CDCl_3$): δ 7.94 (m, 4H, PC_6H_5), 7.71 (m, 4H, PC_6H_5), 7.34 (m, 12H, PC_6H_5), 7.11 (d, $^3J_{HH}$ = 8.40 Hz, 1H, OC_6H_4S), 6.62 (t, $^3J_{HH}$ = 7.80 Hz, 1H, OC_6H_4S), 6.40 (t, $^3J_{HH}$ = 7.80 Hz, 1H, OC_6H_4S), 6.31 (d, $^3J_{HH}$ = 8.40 Hz, 1H, OC_6H_4S), 4.62 (q, $^3J_{HH}$ = 1.80 Hz, $^3J_{HH}$ = 3.80 Hz, 2H, PC_5H_4), 4.45 (s, 2H, PC_5H_4), 4.28 (s, 2H, PC_5H_4), 3.91 (q, $^3J_{HH}$ = 1.80 Hz, $^3J_{HH}$ = 3.80 Hz, 2H, PC_5H_4). $^{31}P\{^1H\}$ NMR: δ 26.40 (d, $^2J_{PP}$ = 21.98 Hz, $J_{Pt\text{-}P}$ = 1518.40 Hz, 1P, P *trans* S); 13.05 (d, $^2J_{PP}$ = 21.98 Hz, $J_{Pt\text{-}P}$ = 1749.54 Hz, 1P, P *trans* O). MS (FAB): 873 (M^+, 40), 765 (M^+-SC_6H_4, 3). MS (EI): 873 (M^+, 100), 745 (M^+-SC_6H_4O, 4). IR (nujol, cm^{-1}): 1560 m, 1272 m, 1237 m, 1184 s, 1096 s, 1025 m, 998 w, 848 m, 746 s, 693 s, 640 s, 567 s.

2.4.5 Reaction of $Pt(dppf)Cl_2$ with thiosalicylic acid: formation of $Pt(dppf)(SC_6H_4CO_2$-o) (3e). The product was isolated as a yellow solid. Yield = 0.26 g, 59%. Anal. calc. for $C_{41}H_{32}O_2P_2SFePt$: C, 54.62; H, 3.58%. Found C, 55.22; H, 3.81%. ^1H NMR ($CDCl_3$): δ 7.82 (m, 8H, PC_6H_5), 7.40 (m, 12H, PC_6H_5), 7.09 (m, 2H, $SC_6H_4CO_2$), 6.98 (m, 2H, $SC_6H_4CO_2$), 4.58 (q, $^3J_{HH}$ = 3.80 Hz, 2H, PC_5H_4), 4.45 (s, 2H, PC_5H_4), 4.30 (s, 2H, PC_5H_4), 3.90 (q, $^3J_{HH}$ = 3.80 Hz, 2H, PC_5H_4). $^{31}P\{^1H\}$ NMR: δ 26.87 (d, $^2J_{PP}$ = 22.59 Hz, J_{Pt-P} = 1472.26 Hz, 1P, P *trans* S); 14.27 (d, $^2J_{PP}$ = 22.59 Hz, J_{Pt-P} = 1981.90 Hz, 1P, P *trans* O). MS (FAB): 902 (M^+, 45); 749 (M^+-$SC_6H_4CO_2$, 25). MS (EI): 858 (M^+-CO_2, 100). IR (nujol, cm^{-1}): 1617 m, 1595 w, 1330 w, 1175 m, 1131 m, 1100 s, 1034 m, 1007 m, 830 w, 746 s, 698 s, 636 m, 561 s.

2.4.6 Reaction of $Pt(dppf)Cl_2$ with 2-mercaptonicotinic acid: formation of $Pt(dppf)(SC_6H_3NCO_2$-o) (3f). The product was isolated as a yellow solid. Yield = 0.25 g, 57%. Anal. calc. for $C_{40}H_{31}NO_2P_2SFePt$: C, 53.23; H, 3.46; N, 1.55%. Found C, 52.90; H, 3.24; N, 1.50%. ^1H NMR ($CDCl_3$): δ 8.27 (m, 1H, $SC_6H_4NCO_2$), 7.91 (m, 4H, PC_6H_5), 7.53 (m, 16H, PC_6H_5), 6.90 (m, 1H, $SC_6H_3NCO_2$), 6.37 (m, 1H, $SC_6H_4NCO_2$), 4.82 (m, 2H, PC_5H_4), 4.59 (s, 2H, PC_5H_4), 4.29 (s, 2H, PC_5H_4), 3.70 (m, 2H, PC_5H_4). $^{31}P\{^1H\}$ NMR: δ 25.81 (d, $^2J_{PP}$ = 23.84 Hz, J_{Pt-P} = 1472.26 Hz, 1P, P *trans* S); 14.97 (d, $^2J_{PP}$ = 23.84 Hz, J_{Pt-P} = 1973.80 Hz, 1P, P *trans* O). MS (FAB): 902 (M^+, 65); 858 (M^+-CO_2, 8). MS (EI): 858 (M^+-CO_2, 84). IR (nujol, cm^{-1}): 1626 w, 1578 w, 1330 w, 1171 m, 1153 s, 1091 m, 1025 s, 994 m, 861 m, 830 s, 746 s, 689 s, 640 s, 561 s.

2.4.7 Attempted synthesis of Pt(dppf)(SC_6H_4Te-o): formation of Pt(dppf)(SC_6H_5-o)$_2$.CH_2Cl_2 (3g).

The procedure followed in the preparation of **3g** is the same as described in section **2.2.7** but using Pt(dppf)Cl_2 in place of Pd(dppf)Cl_2. The product was isolated as a yellow solid. Yield = 0.35 g, 73%. Anal. calc. for $C_{46}H_{38}P_2S_2FePt.CH_2Cl_2$: C, 53.62; H, 3.83 %. Found C, 53.76; H, 4.23 %. ^{1}H NMR ($CDCl_3$): δ 7.78 (m, 8H, PC_6H_5), 7.32 (m, 12H, PC_6H_5), 7.17 (m, 4H, SC_6H_5), 6.78 (m, 6H, SC_6H_5), 4.29 (s, 4H, PC_5H_4), 4.13 (d, 4H, $^3J_{HH}$ = 1.80 Hz). $^{31}P\{^1H\}$ NMR: δ 24.54 (s, 2P, J_{Pt-P} = 1463 Hz). MS (FAB): 968 (M^+, 5), 859 (M^+-SC_6H_5, 80). MS (EI): 860 (M^+-C_6H_5, 18). IR (Nujol, cm^{-1}): 3386 w, 1657 w, 1573 s, 1379 s, 1304 w, 1279 w, 1199 w, 1169 m, 1089 s, 1014 m, 997 w, 829 m, 744 s, 690 s, 631 w, 547 m.

2.5 X-ray crystal structure determination of Pd(dppf)(SC_6H_4S-*o*) (1a), Pd(dippf)(SC_6H_4S-*o*) (2a), Pd(dippf)(SC_6H_3MeS-*o*) (2b), Pd(dippf)(SC_6H_5)$_2$ (2g), Pt(dppf)(SC_6H_4S-*o*) (3a) and Pt(dppf)(SC_6H_4O-*o*) (3d).

A representative crystallographic experiment is that of Pt(dppf)(SC_6H_4S-*o*) (**1a**) described as follows:

Data collection.

A red crystal with approximate dimensions 0.2 × 0.2 × 0.2 mm^3 was selected under oil under ambient conditions and attached to the tip of a glass a capillary. The crystal was mounted in a stream of cold nitrogen at 173(2) K and centered in the X-ray beam by using a video camera. The crystal evaluation and data collection were performed on a Bruker CCD-1000 diffractometers with Mo-K_α (λ = 0.71073 Å) radiation and the

diffractometer to crystal distance of 5.08 cm. The initial cell constants were obtained from three series of ω scans at different starting angles. Each series consisted of 20 frames collected at intervals of 0.3 ° in a 6 ° range about ω with the exposure time of 10 seconds per frame. A total of 77 reflections was obtained. The reflections were successfully indexed by an automated indexing routine built in the SMART program. The final cell constants were calculated from a set of 6412 strong reflections from the actual data collection. The data were collected by using the hemisphere data collection routine. The reciprocal space was surveyed to the extent of a full sphere to a resolution of 0.80 Å. A total of 51364 data were harvested by collecting three sets of frames with 0.4 ° scans in ω with an exposure time of 10 seconds per frame. These highly redundant datasets were corrected for Lorentz and polarisation effects. The absorption correction was based on fitting a function to the empirical transmission surface as sampled by multiple equivalent measurements.[66]

Structure solution and refinement.

The systematic absences in the diffraction data were uniquely consistent for the space group *Pbcm* and $Pca2_1$ but only the latter, non-centrosymmetric space group $Pca2_1$ yielded chemical reasonable and computationally stable results of refinement.[67] A successful solution by the direct methods provided most non-hydrogen atoms from the *E*-map. The remaining non-hydrogen atoms were located in an alternating series of least squares cycles and difference Fourier maps.[68] All non-hydrogen atoms were refined with anisotropic displacement coefficients. All hydrogen atoms were included in the structure factor calculation at idealised positions and were allowed to ride on the neighbouring

atoms with relative isotropic displacement coefficients. There are two symmetry independent molecules of the complex present in the asymmetric unit. These molecules are related by a non-crystallographic inversion centre. There are also two molecules of solvate dichloromethane present in the asymmetric unit. The crystal specimen proved to be a merohedral twin with an 85:15 twin component contribution. The final least squares refinement of 884 parameters against 15952 data resulted in residuals R (based on F^2 for I $\geq 2\sigma$) and wR (based on F^2 for all data) of 0.0220 and 0.0424 respectively. The final difference Fourier map was featureless. The ORTEP diagrams were drawn with 30% probability ellipsoids. A summary of data collection and structure refinement is given in Table 9.

2.6 Electrochemical experiments.

Cyclic voltammetry measurements of the complexes were performed on a BAS C50W electrochemical analyzer using a three-electrode system. The three electrodes used were a platinum disc as a working electrode, a platinum wire as an auxiliary electrode and a silver/silver chloride reference electrode. All experiments were carried out at room temperature under a dry nitrogen atmosphere on sample concentrations of 10^{-3} M, with 0.15 M tetrabutylammonium-tetrafluoroborate, [n-Bu_4N][BF_4], as a supporting electrolyte (0.15 M) at a scan rate of 100 $mV.s^{-1}$. Potentials were referenced to an internal ferrocene/ferrocenium couple added at the end of each experiment and quoted versus the saturated calomel electrode (SCE).[69] Results of the electrochemistry experiments are reported in Table 15.

2.7 Reactions of M(dppf) (M = Pd, Pt) and Pd(dippf) aryldichalcogenide complexes with dimethylacetylene dicarboxylate (DMAD).

In a typical reaction, excess DMAD (0.5 ml, 4.07 mmol) and Pd(dppf)(SC_6H_4S-*o*) (0.065 g, 0.081 mmol) in CH_2Cl_2/toluene (1:1) (60 ml) was refluxed for 48 h. The light-yellow solution changed to dark orange after 48 h. It was concentrated to about 2 ml and chromatographed on silica gel. The eluent was a 1:4 mixture of CH_2Cl_2/Ether. The eluate was evaporated to dryness to give a white solid, which was recrystallised from CH_2Cl_2/hexane to yield hexamethylbenzene hexacarboxylate (HMBC), $C_6(CO_2Me)_6$. The HMBC obtained was characterised by ^1H NMR, $^{13}C\{^1H\}$ NMR, GC-mass spectrometry and by elemental analysis. Yield = 1.24 g, 28%. Anal. calc. for $C_{18}H_{18}O_{12}$: C, 50.71; H, 4.26%. Found C, 50.55; H, 4.23%. ^1H NMR ($CDCl_3$): δ 3.88 (s, 18 H). $^{13}C\{^1H\}$ NMR ($CDCl_3$): δ 165.12 (s), 133.89 (s), 53.48 (s). MS (EI): m/z 426 (M^+, 14), 395 (M^+-OMe, 100).

The reactions of **1b, 1d, 2a-b** and **2d** with DMAD were performed in a similar manner as described above. However when these complexes were used the major product isolated was a four-membered cyclised product, tetramethylcyclobut-1,3-dienetetracarboxylate (TMCTC). The TMCTC obtained was characterised by ^1H NMR, $^{13}C\{^1H\}$ NMR, GC-mass spectrometry and by elemental analysis. Anal. Calc. for $C_{12}H_{12}O_8$: C, 50.71; H, 4.26%. Found C, 50.23; H, 4.71%. ^1H NMR ($CDCl_3$): δ 3.87 (s, 12H). $^{13}C\{^1H\}$: δ 165.12 (s), 133.84 (s), 53.25 (s). MS (EI): 285 (M^+, 4), 225 (M^+-CO_2Me, 78).

CHAPTER 3

SYNTHESIS

3.1 Synthesis and spectroscopic characterisation of complexes.

The starting materials, $M(dppf)Cl_2$ (M = Pd, Pt) and $Pd(dippf)Cl_2$ were treated with equimolar amounts of the aryldichalcogen reagents, 1,2-benzenedithiol (1,2-$(HS)C_6H_4(SH)$ **(a)**), 3,4-toluenedithiol ($(HS)C_6H_3Me(SH)$) **(b)**, 3,6-dichloro-1,2-benzenedithiol ($(HS)C_6H_2Cl_2(SH)$) **(c)**, 2-mercaptophenol ($(HS)C_6H_4(OH)$) **(d)**, thiosalicylic acid ($(HS)C_6H_4(CO_2H)$) **(e)** and thionicotinic acid ($(HS)C_5H_3N(CO_2H)$) **(f)** in either CH_2Cl_2 or toluene in the presence of the organic base triethylamine (Et_3N) to afford the complexes of the type shown in Scheme 3. The $Pd(dippf)Cl_2$ and $Pt(dppf)Cl_2$ reactions were performed in a similar manner as in Scheme 3. Toluene was used as a solvent in most of the reactions because the by-product, Et_3NHCl, is not soluble in toluene and if the product is soluble in toluene, the by-product could be filtered off fairly easily. However in instances where the products were insoluble in toluene, CH_2Cl_2 was used and the by-product was extracted with water.

The reactions were found to take place only after the addition of the base as evidenced by the colour changes that occurred immediately after the addition of the base. The role of the base in these reactions was to deprotonate the acidic protons of aryldichalcogen compounds and to remove the halogen from the metal halide, thereby forming the amine salt $Et_3NH^+Cl^-$ as the by-product. The metal products had two characteristic colours in solution and in the solid state. The palladium complexes were generally orange while the platinum ones were yellow. They were isolated in moderate to high yields, ranging from

52-79%. All the products were solids and soluble in CH_2Cl_2 but insoluble in hexane, except Pd(dippf)($SC_6H_4CO_2$-*o*) (**2e**) which was isolated as a dark orange thick oil but soluble in CH_2Cl_2. To solidify **2e**, this oil was dissolved in CH_2Cl_2 and the solution layered with hexane and kept as –15°C for several days after which it solidified. It is interesting to note that most of the complexes isolated crystallised with one or half a molecule of CH_2Cl_2. This was clearly discernible from the ^1H NMR spectra as a distinct peak at 5.29 ppm. In some cases the solid state X-ray structures showed either $CHCl_3$ or CH_2Cl_2 inclusion molecules, these being the solvents in which the crystals were grown.

All the complexes were fully characterised by IR and NMR spectroscopy, mass spectrometry and by elemental analysis. Further characterisation of **1a**, **2a**, **2b**, **2h**, **3a** and **3d** by single crystal X-ray diffraction studies confirmed the structures deduced from the spectroscopic data. These detailed characterisations are described in the subsequent sections of this thesis.

3.2 Characterisation of homoleptic dithiolato metal complexes.

3.2.1 Infrared spectral data of homoleptic dithiolato metal complexes.

The main region of interest in IR spectroscopy for analytical purposes is from 400-4000 cm^{-1}. This region may be divided into two sections, namely the "main" region (1000-4000 cm^{-1}) and the "finger-print" region (400-1000 cm^{-1}). Assignment of specific functional groups is usually made from the main region of the IR spectrum. In this project the absorption in the main region was very weak and some of the peaks could not be

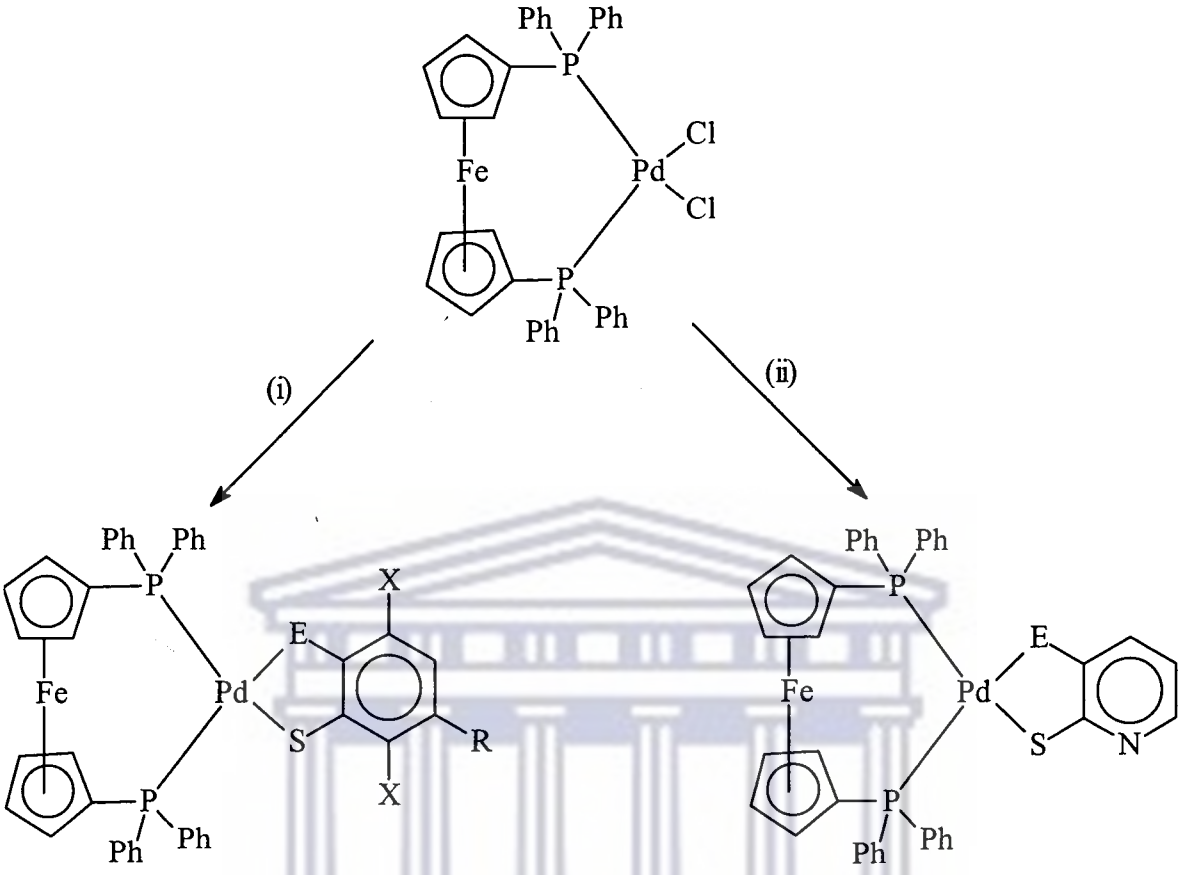

Compound	R	X	E
1a	H	H	S
1b	Me	H	S
1c	H	Cl	S
1d	H	H	O
1e	H	H	CO_2
1f	H	H	CO_2

Legend: (i) Et_3N, 1,2-$(HS)C_6H_3R(EH)$, (E = S, R = H, Me; R = H, E = O, CO_2), Et_3N, 1,2-$(HS)C_6H_2Cl_2(SH)$; (ii) Et_3N, 1,2-$(HS)C_5NH_3(CO_2H)$.

Scheme 3. General synthetic scheme illustrated with Pd(dppf) complexes.

observed due to overlap with nujol peaks, hence assignment of functional groups were made using the fingerprint region. However, the presence of these functional groups was confirmed from other analytical techniques such as ^{1}H NMR.

Most of the IR spectra of the complexes were similar and typified by **1b** whose spectrum is shown in Fig. 1. Tables 2a and 2b summarise the IR data for selected functional groups of homoleptic complexes of Pd(dppf), Pd(dippf) and Pt(dppf) complexes. The diphenylphosphino and the dithiolato ligands had peaks between 425 and 477 cm^{-1} as a group of four to five peaks and also between 484 and 694 cm^{-1} assignable to C_6H_5 and C_6H_4 respectively. These peaks were generally very strong relative to the other peaks. They were also observed in M(dppf)Cl_2 (M = Pd, Pt) and Pd(dippf)Cl_2 which were used as starting materials but were stronger in the metal halides starting materials relative to the phenyl peaks in the thiolato complexes. In **1b** phenyl peaks were observed at 425, 463, 484, 513, 543, 635, and 694 cm^{-1}. Phenyl peaks are observed at 490, 514, 536, and 695 cm^{-1} in NiCp(PPh_3)X[18c] (where Cp = η^5-C_5H_5 and X = Br, Cl) and also at 430, 485, 520, 660, 690 and 700 cm^{-1} in Ni(dppe)(SC_6H_3MeS-*o*), Ni(dppe)(SC_6H_4S-*o*) and [Ni(dppe)Cl]$_2$(μ-SC_6H_4S-*m*).[18d] In studies carried out by Nakamoto[70] phenylphosphine peaks were observed at 616 and 709 cm^{-1}. By comparing IR peak value found in new complexes with those in the literature, the peaks between 425 and 477 cm^{-1} could be assigned to the thiolatophenyl peaks while the peaks between 484 and 686 cm^{-1} are assigned to the phenylphosphine peaks in these new complexes.

The characteristic peaks for the pentahapto cyclopentadienyl rings are generally found between 720 and 950 cm^{-1}. Parr *et al.*[71] observed cyclopentadienyl peaks at 835 cm^{-1}. In **1b** the cyclopentadienyl peaks appeared at 751 and 890 cm^{-1}. Based on the IR data, it was evident that the three main functional groups namely: the diphenylphosphino, the aryldichalcogenide and the cyclopentadienyl ring are all present in the complexes. However, the IR results did not show any significant changes brought about by the substituents on the aryl ring of the thiolato ligands as Tables 2a and 2b show.

Table 2a. Infrared spectral data for selected functional groups of Pd(dppf) and Pt(dppf) homoleptic dithiolato complexes.

Complex	Aryldithiolato ligands (cm^{-1})	Phenylphosphine ligands (cm^{-1})	η^5-C_5H_4P (cm^{-1})
1a	429, 471	484, 517, 543, 639, 686	740, 761, 816
1b	425, 463	484, 513, 543, 635, 695	751, 800, 816
1c	425, 463	488, 513, 543, 635, 690	728, 799, 820
1g	432, 477	487, 547, 615, 679, 694	736, 750, 824
3a	428, 466	484, 513, 545, 641, 698	731, 758, 830
3b	428, 465	484, 512, 556, 640, 698	732, 755, 832
3c	426, 463	484, 510, 547, 645, 689	742, 790, 845
3g	435, 468	486, 506, 547, 631, 690	744, 752, 829

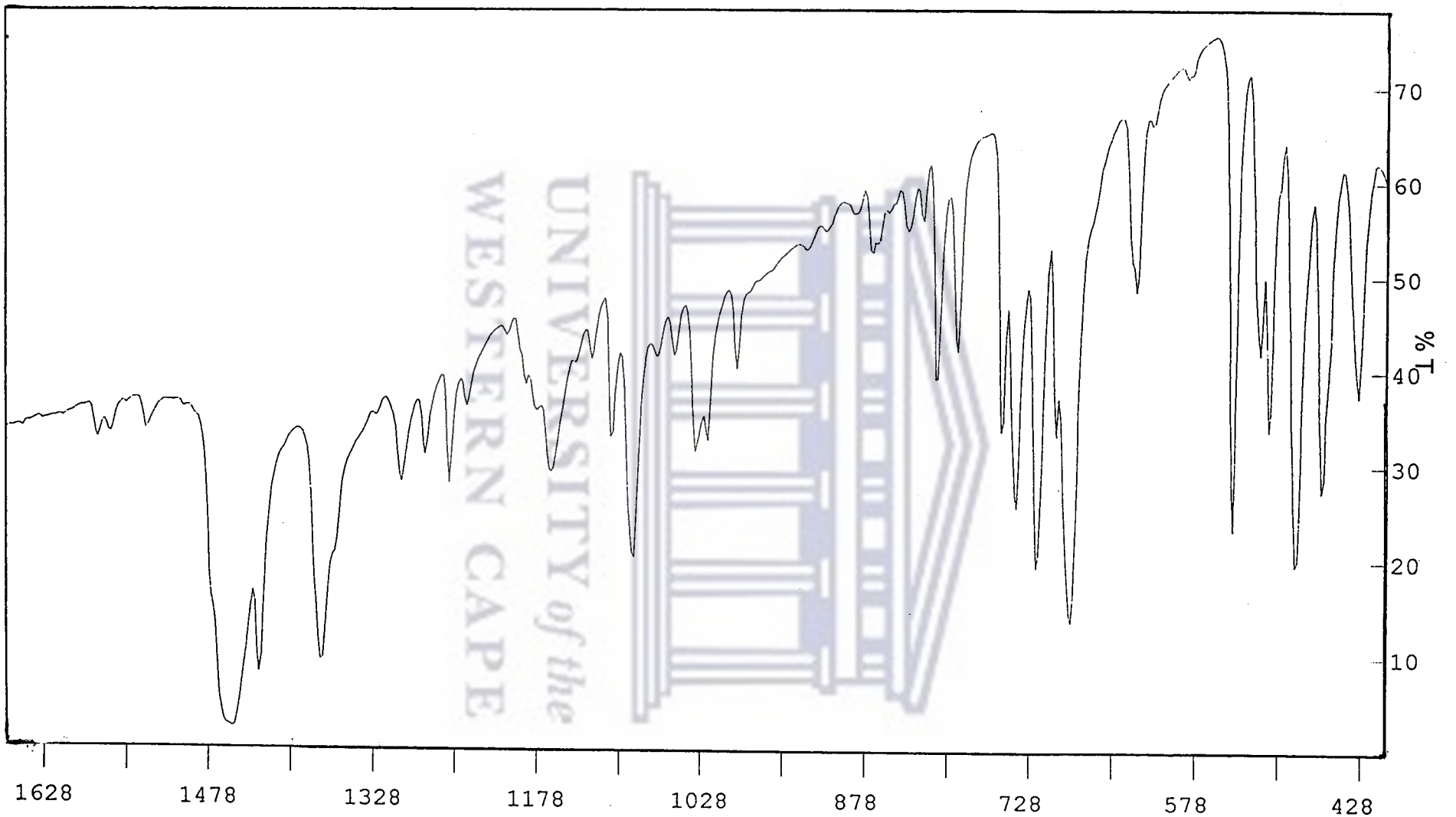

Fig. 1. Infrared spectrum of **1b** as nujol mulls.

Table 2b. Infrared spectral data for selected functional groups of Pd(dippf) homoleptic dithiolato complexes.

Complex	Aryldithiolato ligands (cm^{-1})	η^5-C_5H_4P (cm^{-1})
2a	626, 638	736, 799, 820
2b	627, 648	732, 795, 838
2c	627, 652	728, 778, 838
2g	630, 650	720, 740, 842

3.2.2 ^{1}H NMR spectral data of homoleptic dithiolato metal complexes.

Further characterisation of the complexes by ^{1}H NMR spectroscopy showed that the spectra of complexes **1a-1c**, **2a-2c**, and **3a-3c** were generally similar irrespective of the metal centre or the phosphine, although there were some shifts of peaks. A representative spectrum of these complexes is that of compound **2a** with its dppf analogue (**1a**) as an insert (Fig. 2) to show the effect of the phosphine on the chemical shifts of the aryl and cyclopentadienyl protons. Table 3 is a summary of the ^{1}H NMR data of the homoleptic dithiolato metal complexes.

The homoleptic complexes displayed two sets of multiplets in the region 7.87-7.71 ppm and 7.49-7.26 ppm. This is the region where phenyl protons are generally found. The two sets of peaks were in a ratio of 2:3 respectively. Pilato and co-workers[72] reported similar phenyl proton peaks to be in the regions 7.83-7.76 and 7.47-7.42 ppm; 7.83-7.77 and 7.50-7.44 ppm; and 7.86-7.76 and 7.54-7.49 ppm for phenyl protons of the complexes

Pd(dppe){S_2C_2(2-quinoxaline)(H)}, Pt(dppe){S_2C_2(2-quinoxaline)(H)}, and Pd(dppe){S_2C_2(2-pyridine)(H)} (dppe = 1,2-bis(diphenylphosphino)ethane) respectively, all of which were in the ratio 2:3 respectively. Hayashi *et al.*[73] reported the x-ray structure of Pd(dppf)Cl_2 and the ^{1}H NMR spectrum of this complex to have two sets of multiplets in the region 8.00-7.68 ppm and 7.50-7.25 ppm. These peaks were also attributed to the phenyl protons. Even when the metallocene is changed from ferrocene to ruthenocene analogues as in Pt(dppr)Cl_2 and Pd(dppr)Cl_2[74] (dppr = 1,1'-bis(diphenylphosphino)ruthenocene), the multiplets were observed in the regions 7.91-7.34 ppm and 7.88-7.33 ppm respectively. In a different study by Brown and Guiry the complex, Pd(dppr)Cl_2, had phenyl peaks in the regions 8.05-7.70 ppm and 7.60-7.30 ppm.[75] It could thus be inferred that the two sets of peaks in the regions 7.87-7.71 ppm and 7.49-7.26 ppm for **1a-1c** and **3a-3c** are due to the phenyl protons of the dppf ligand, with the protons *ortho* to the phosphorus atom lying downfield due to the deshielding effect of the phosphorus atom nearby. These multiplets (7.87-7.71 ppm) integrate for eight protons, which is in agreement with the eight protons *ortho* to the phosphorus atom. In **1a** the phenylphosphino proton peaks appeared around 7.80-7.40 ppm. The set of peaks between 7.49-7.26 ppm, which integrate for 12 protons could then be assigned to the *meta* and *para* protons of the phenyl rings attached to the phosphorus in the phosphine ligands.

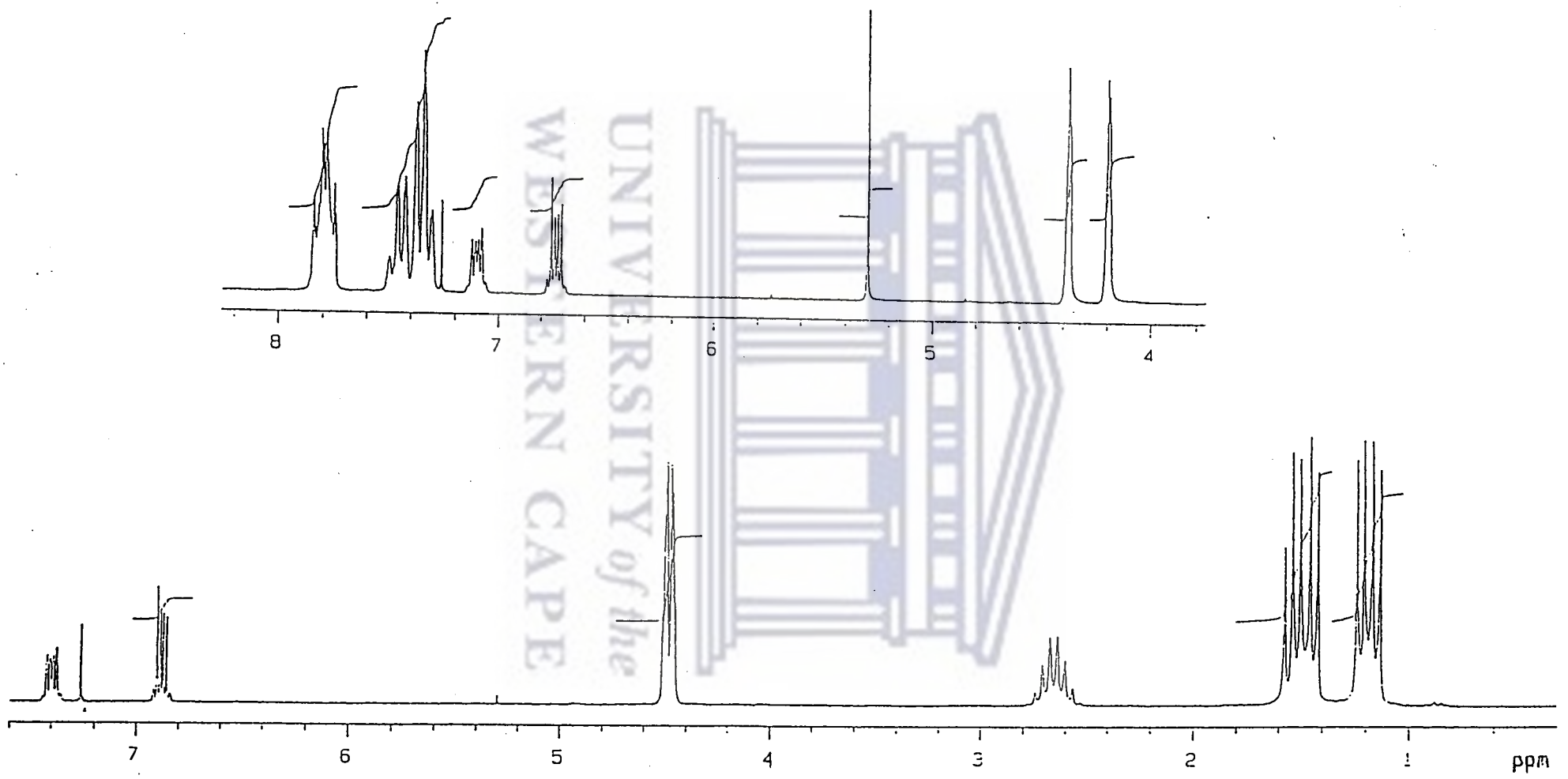

Fig. 2. ^{1}H NMR spectrum of **2a** and **1a** (insert).

Table 3. ^1H NMR spectral data of Pd(dppf), Pd(dippf) and Pt(dppf) dithiolato complexes.

Complex	η^5-C_5H_4P (ppm)		Diphenylphosphine ligand (ppm)		Diisopropylphosphine ligand (ppm)		Aryldithiolato ligand (ppm)		
1a	4.38	4.20	7.81	7.40	-	-	7.10	6.72	-
2a	4.48	4.45	-	-	1.48	1.19	7.40	6.88	-
3a	4.36	4.23	7.81	7.41	-	-	7.27	6.68	-
1b	4.37	4.19	7.80	7.52	-	-	6.98	6.76	6.92
2b	4.49	4.46	-	-	1.47	1.18	7.28	6.70	7.22
3b	4.35	4.22	7.81	7.39	-	-	7.14	6.50	7.08
1c	4.41	4.23	7.79	7.40	-	-	-	6.82	-
2c	4.51	4.49	-	-	1.49	1.20	-	6.97	-
3c	4.38	4.25	7.80	7.39	-	-	-	6.80	-

The substituted cyclopentadienyl ring for the free dppf ligand and in the complexes had two sets of peaks, with the free dppf ones better separated. Compound **1a** exhibited two triplets at 4.38 and 4.20 ppm. Similar peaks have been observed in the ^{1}H NMR spectrum of Pd(dppf)Cl_2 that was prepared for these reactions. Hayashi *et al.*[76] also detected peaks around 4.18 and 4.36 ppm for Pd(dppf)Cl_2 and assigned them to the cyclopentadienyl protons. In two different studies, the cyclopentadienyl peaks were found at 4.53 and 4.81 ppm by Hor[74] and at 4.40 and 4.19 ppm by Brown[75] for the same complex, Pd(dppr)Cl_2. The difference in these peak values for the same compound can be attributed to the different solvents in which they were run. Since in 1,1'-diphenylferrocene the cyclopentadienyl protons were detected at 4.45 and 4.19 ppm[77], the peaks at 4.38 (triplet) and 4.20 ppm for **1a** are without doubt due to the cyclopentadienyl protons of the ferrocenyl moiety with the protons *ortho* to the phosphorus lying downfield (4.38 ppm) and the protons at the *meta* position lying at 4.20 ppm. The triplet arises from the coupling of phosphorus with the nearest protons because the phosphorus has a spin of $^1/_2$. The triplet was not always easy to resolve due to small magnetic field used.

In addition to the phenyl peaks associated with the dppf ligand, there were other phenyl peaks found in the ^{1}H NMR spectra of the dppf complexes. These peaks are associated with the thiolato ligands. The peaks were easily discernible when the phosphine was dippf and hence easier to assign. Fig. 2 illustrates this. Two sets of multiplets were observed at 7.10 and 6.72 ppm in the ^{1}H NMR spectrum of **1a** for SC_6H_4S-*o*. Similar peaks were observed in the ^{1}H NMR spectrum of **2a** at 7.40 and 6.88 ppm and in **3a** at 7.27 and 6.68 ppm. The downfield multiplet at 7.10 ppm in **1a** is due to the aryl protons

ortho to the two sulfur atoms while the one upfield at 6.72 ppm is due to the two protons *meta* to the sulfur atoms. If these two sets of protons at 3,6 and 4,5 positions of the aryl ring were both chemically and magnetically equivalent, they should give rise to two doublets due to the coupling of these protons with each other. From the spectrum it is apparent that the peaks are multiplets primarily due to the fact that the protons at 3 and 6 positions of the aryl ring are not magnetically equivalent although they lie in the same chemical environment. As a result of this H_A and $H_{A'}$ can couple. Similarly H_B and $H_{B'}$ can couple as shown in Scheme 4. This results in an AA'BB' spin system and represent an example of a four-spin system. Generally the spectra of four-spin systems consisting of two pairs of chemically equivalent nuclei are relatively easy to recognise. They are symmetrical with respect to the centre of the spectrum, but in order to differentiate this from other spin-patterns one needs to use a combination of frequency (ν) and coupling constants (J).

The other spin system in which symmetry is found is AA'XX'. Spectra of AA'BB' and AA'XX' spin systems are always found when a molecule contains two pairs of protons such that the protons within each pair can be imagined to exchange positions by rotation about a plane of symmetry.[78] The most important examples are disubstituted benzene derivatives with two different substituents *para* to each other or with two identical substituents *ortho* to each other, as in the 1,2-benzenedithiolate ligand shown in Scheme 4. As a result of the symmetry $\nu_A = \nu_{A'}$; $\nu_B = \nu_{B'}$ (where ν = frequency) and also $J_{AB} = J_{A'B'}$; $J_{AB'} = J_{A'B}$ (where J = coupling constant). The spectrum also depends on the chemical shift difference $\Delta\nu = \nu_A - \nu_B$ and the coupling constants $J_{AA'}$ and $J_{BB'}$ as observed

in the ^{1}H NMR spectrum of $C_6H_4Cl_2$.[78] The only distinction between AA'BB' and AA'XX' spectra is from the number of lines that each spectrum has. Each half of the AA'BB' spectrum can have up to 12 lines and of the AA'XX' spectrum up to 10 lines. It is possible to analyse spectra of this type manually, but a more convincing analysis is usually performed by simulation.[78] The spectra of complexes reported here were assigned manually, using the above described criteria.

From the expansion of the aryldithiolato regions in the ^{1}H NMR spectra of the complexes, it can be inferred that complexes **1a**, **2a** and **3a** have AA'BB' spin system. This conclusion is based on the 12 lines observed in each half of the ^{1}H NMR spectrum of the 1,2-benzenedithiolate ligand.

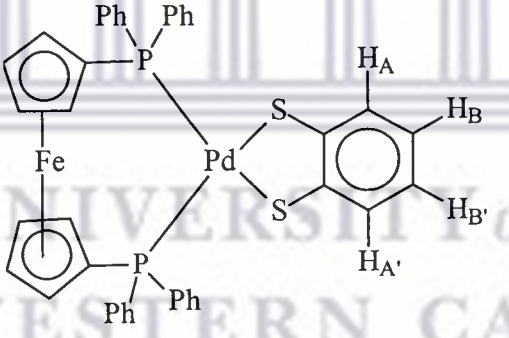

Scheme 4. Diagram to illustrate coupling of the aryldithiolato protons in **1a** for the AA'BB' spin system.

The effect of the phosphine ligand on the ^{1}H NMR spectrum can be deduced by comparing the spectrum of **1a**, in which the phosphine is diphenylphosphine, with that of **2a** which has isopropyl groups attached to the phosphorus. A closer look at the ^{1}H NMR spectral data (Table 3) reveals that the cyclopentadienyl ligand protons are deshielded in

2a relative to **1a** (Fig. 2). This is primarily due to the isopropylphosphine being a better Lewis base than the phenylphosphine, and consequently donates more electron density to the metal atom.

In the ^{1}H NMR spectra of **1c**, **2c** and **3c** the aryldithiolato ligand protons *ortho* to the chlorine atom appears at 6.82, 6.97 and 6.80 ppm respectively and all of them are singlets integrating for two protons. The ^{1}H NMR spectra of **1b**, **2b** and **3b** had singlets at 2.13, 2.24 and 2.15 ppm respectively integrating for three protons. These signals were assigned to the methyl group of the toluene ligand, while the broad singlets at 6.92, 7.22 and 7.08 ppm for **1b**, **2b** and **3b** respectively were due to the proton between the sulfur and the methyl group (i.e. at position 2 of the toluene-based ligand). There were doublets at 6.98 ($^{3}J_{HH}$ = 8.00 Hz), 7.28 ($^{3}J_{HH}$ = 7.00 Hz) and 7.14 ppm ($^{3}J_{HH}$ = 7.60 Hz) and a doublet of a doublet at 6.76, 6.70 and 6.50 ppm for **1b**, **2b** and **3b** respectively. These could be assigned to the protons at positions 5 and 6 respectively of the toluene dithiolato ligand. The signal downfield is a doublet due to coupling with the proton at position 6 while the latter one couples with the proton in position 5 and is further split by the proton in position 2 of the dithiolato ligand into a doublet of a doublet. The smaller coupling constants of the doublets show the long range coupling of these protons with the proton at the second position of the ligand.

In complexes where the phosphine was diisopropylphosphine, the alkyl protons were observed upfield. This freed the phenyl region leaving only the aryldithiolato peaks, where in dppf complexes aryl peaks overlapped with the phenyl peaks for the Pd(dppf)

and Pt(dppf) series. The presence of the hydrogen in position 2 of the isopropyl group makes the two methyl groups inequivalent. Thus the peaks for these methyl groups appear at 1.48 and 1.19 ppm for **2a**, 1.47 and 1.18 ppm for **2b**, and at 1.49 and 1.20 ppm for **2c**. The C-H protons appear as septuplet a bit downfield at 2.64, 2.64 and 2.68 ppm for **2a**, **2b** and **2c** respectively. The septuplet arises from the interaction of the C-H proton of the isopropyl group with the two CH_3 protons. This is rationalised from the multiplicity equation, $M = 2nI + 1$ (where $I = 1/2$ for proton nuclei and n being the number of equivalent neighbour nuclei). The equation then reduces to $M = n + 1$ and for the two CH_3 groups in the neighbourhood, we expect the C-H proton peak to be a septuplet.

From the above ^{1}H NMR assignments and the accompanying discussion, it is clear that the Pd and Pt complexes isolated contain the dppf or dippf ligands and the three aryldithiolato ligands SC_6H_4S-*o*, SC_6H_3Me-*o* and $SC_6H_2Cl_2S$-*o* bonded as bidentate ligands.

3.2.3 $^{31}P\{^1H\}$ NMR spectral data for the homoleptic dithiolato metal complexes.

The $^{31}P\{^1H\}$ NMR spectra of all the Pd(dppf) and Pd(dippf) homoleptic aryldithiolato complexes displayed spectra consisting of only singlet peaks.[18d,79] This shows that the two phosphorus atoms are equivalent. The effect of the aryl substituents on the chemical shifts of the phosphorus atoms can be observed from the $^{31}P\{^1H\}$ NMR spectra of the Pd(dppf) complexes (Table 4). In particular, **1b** lies upfield (24.97 ppm) with respect to **1a** (25.08 ppm) and **1c** (25.48 ppm). The methyl group donates more electron density via

the aryl ring to the phosphorus atom, which shields that particular phosphorus atom. The chlorine atoms in **1c** withdraw electron density and consequently, the phosphorus atom shows a downfield peak compared to **1a** and **1b**. In all these complexes, the effect is a long range one as observed by the slight differences in chemical shifts.

As the phosphine was varied from diphenylphosphine to diisopropylphosphine, the chemical shifts of the phosphorus atoms also changed. This is not surprising as each of the phosphine is expected to have different electronic and steric effects. In order to compare the effect of the phosphines on the $^{31}P\{^{1}H\}$ NMR chemical shifts, the dithiolato ligand was kept as SC_6H_4S-*o*, while the phosphine was varied from diphenylphosphine to diisopropylphosphine as in complexes **1a** and **2a** respectively. For **2a**, the phosphorus peak was found to lie at 47.19 ppm and that of **1a** at 25.08 ppm. This observation could be explained by the σ-donor ability of the phosphines. Alkylphosphines are better σ-donors than arylphosphines, and as a result of that we expect diisopropylphosphines to donate more electron density into the metal centre. A more significant contribution, however, is the ability of the metal to backdonate electron density to the phosphorus. The elements in period 3, such as Si, P, and S have empty d-orbitals in their valence shells. These d-orbitals are of low energy to allow them to overlap with the d-orbitals of the metal atoms, thus giving rise to d_π-d_π backbonding, similar to d_π-p_π backbonding found in CO metal complexes.

If for a series of PR_3 ligands the σ-donation to a metal atom is poor, then the d-orbitals on the phosphorus atom become lower in energy and d_π-d_π backbonding is enhanced. Since

σ-donation to the metal is assumed to be low, then π-backbonding would remove the electron density from the metal atom. In particular, for phenylphosphines as in Pd(dppf)(SC_6H_4S-*o*) (**1a**), σ-donation to the metal will be low, thus enhancing π-backbonding. The electron density withdrawn from the metal tend to shield the phosphorus atom and it came as no surprise when the phosphorus peak lied upfield in Pd(dppf)(SC_6H_4S-*o*) relative to the one in Pd(dippf)(SC_6H_4S-*o*) (**2a**). For the complex Pd(dippf)(SC_6H_3MeS-*o*), the $^{31}P\{^1H\}$ NMR spectrum had two doublets with an AB spin pattern (Fig. 3a) at 42.15 and 41.87 ppm. This AB spin pattern is similar to the one observed for the mixed aryldichalcogenide complex, Ni(dppe)(SC_6H_4Se-*o*).[27] However when the phosphine was dppf, the $^{31}P\{^1H\}$ NMR spectra of Pd(dppf)(SC_6H_3MeS-*o*) and Pt(dppf)(SC_6H_3MeS-*o*) had only singlet peaks. The reason for this AB spin pattern observed for Pd(dippf)(SC_6H_3MeS-*o*) could not be established. A summary of the $^{31}P\{^1H\}$ NMR chemical shifts of the Pd(II) aryldichalcogenide complexes is shown in Table 4.

Table 4. The $^{31}P\{^1H\}$ NMR spectral data of the homoleptic dithiolato Pd(II) complexes.

Pd(dppf)		Pd(dippf)	
Complex	Chemical shift (ppm)	Complex	Chemical shift (ppm)
1a	25.08 (s)	**2a**	41.19 (s)
1b	24.97 (s)	**2b**	42.15 (d, $^2J_{PP}$ = 18.30 Hz); 41.87 (d, $^2J_{PP}$ = 18.30 Hz)
1c	25.48 (s)	**2c**	41.92 (s)

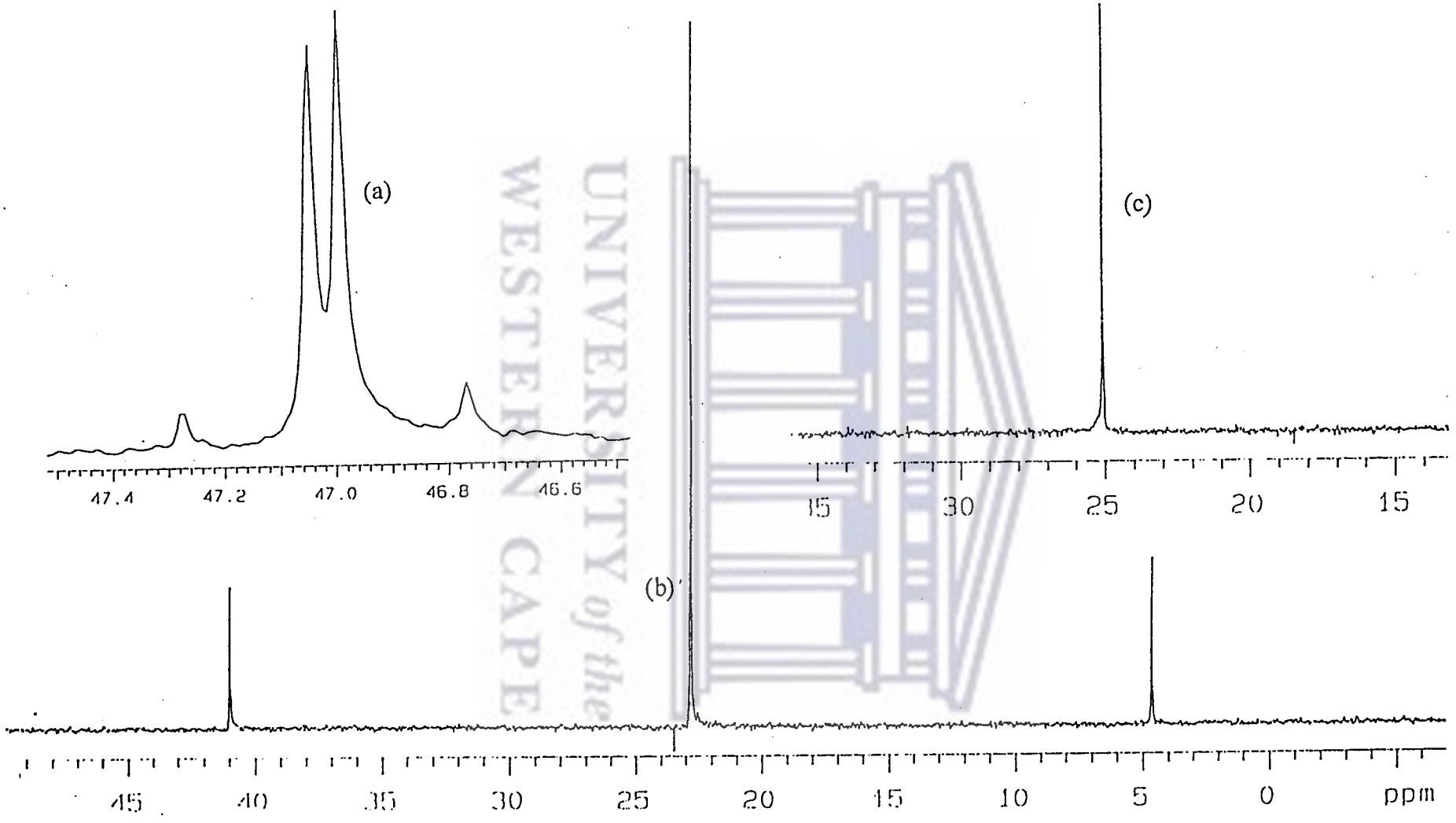

Fig. 3. $^{31}P\{^{1}H\}$ NMR spectrum of **2b** (a), **3b** (b) and **1a** (c)

The $^{31}P\{^{1}H\}$ NMR spectra of the dithiolato platinum complexes were different from their palladium analogues. This is mainly due to the NMR active ^{195}Pt nucleus. The natural abundance of ^{195}Pt is 33.7 % and has a spin of ½. In general, all the $^{31}P\{^{1}H\}$ NMR spectra of the homoleptic aryldithiolato complexes of Pt(II) consisted of a singlet peak flanked by a pair of ^{195}Pt satellites. Typical spectrum would consist of three peaks with an intensity ratio of 1:4:1. In **3b** the singlet appeared at 22.83 ppm with the two satellites at 4.66 and 40.99 ppm. This splitting pattern was also observed in **3a** and **3c** and the coupling constants in each case were of the same magnitude and are summarised in Table 5. Similar spectra have been reported by Ghilardi *et al.* for the complex $Pt(C_2H_4)(PPh_3)_2$.[80] Also in a different study by Grim and co-workers[81], the complex $Pt(C_2H_5(C_6H_5)P)_2Cl_2$ exhibited *cis* and *trans* isomers and both isomers could be detected in the $^{31}P\{^{1}H\}$ NMR spectrum which consists of two singlets and two pairs of platinum satellites for the *cis* and *trans* isomers. The platinum satellites helped to identify the two isomers. In fact examples of ^{195}Pt coupling to phosphorus abound in the literature[49,50b,80-82] and serves as a quick diagnosis to establish the identity of Pt-P bonding. This is exemplified by the work of Colacio *et al.*[82b] where the J_{Pt-P} are in the range 2428-2683 Hz for [Pt(dppm)(bpy)(μ-TT)] and [Pt(dppm)(μ-TT)$_2$] (where TT = thiotheophylline and bpy = 2,2'-bipyridine). Other examples include $Pt(PPh_3)_2(SC_2H_4S\text{-}o)$[82c] and Pt(dppe)$(S(CHCO_2H)_2S\text{-}o)$[49] which have J_{Pt-P} of 2590 and 2363 Hz respectively. The results in this project were no exception and helped to identify the Pt products in the reactions performed. The coupling constants of the phosphorus with the ^{195}Pt isotopes (J_{Pt-P}) were in the range 1466-1472 Hz (Table 5). This is found to be consistent with square planar platinum(II) geometry and are in the range for equivalent *cis* phosphine configuration.[50b,82]

Table 5. The $^{31}P\{^{1}H\}$ NMR spectral data of Pt(dppf) homoleptic dithiolato complexes.

Complex	$^{31}P\{^{1}H\}$ chemical shift (ppm)	J_{Pt-P} (Hz)
3a	22.82 (s)	1471.85
3b	22.83 (s)	1470.80
3c	22.52 (s)	1466.43

3.3 Attempted one-pot synthesis of M(dppf)(SC_6H_4E-*o*) (M = Pd, Pt; E = Se and Te).

In order to fully compare the properties of the mixed aryldichalcogenide complexes attempts were made to synthesize complexes of the general formula, M(dppf)(SC_6H_4E) (M = Pd, Pt; E = Se, Te). The synthetic procedure followed is that reported by Rauchfuss *et al.*,[82a] which involves the lithiation of thiophenol and stabilisation of the intermediate with tetramethylethylenediamine (TMEDA). The next step in the synthesis involves the reaction of the intermediate, $LiSC_6H_4Li$-*o*, with the appropriate chalcogen, followed by the *in-situ* reaction with M(dppf)Cl_2 (M = Pd, Pt) or Pd(dippf)Cl_2 as illustrated in Scheme 5.

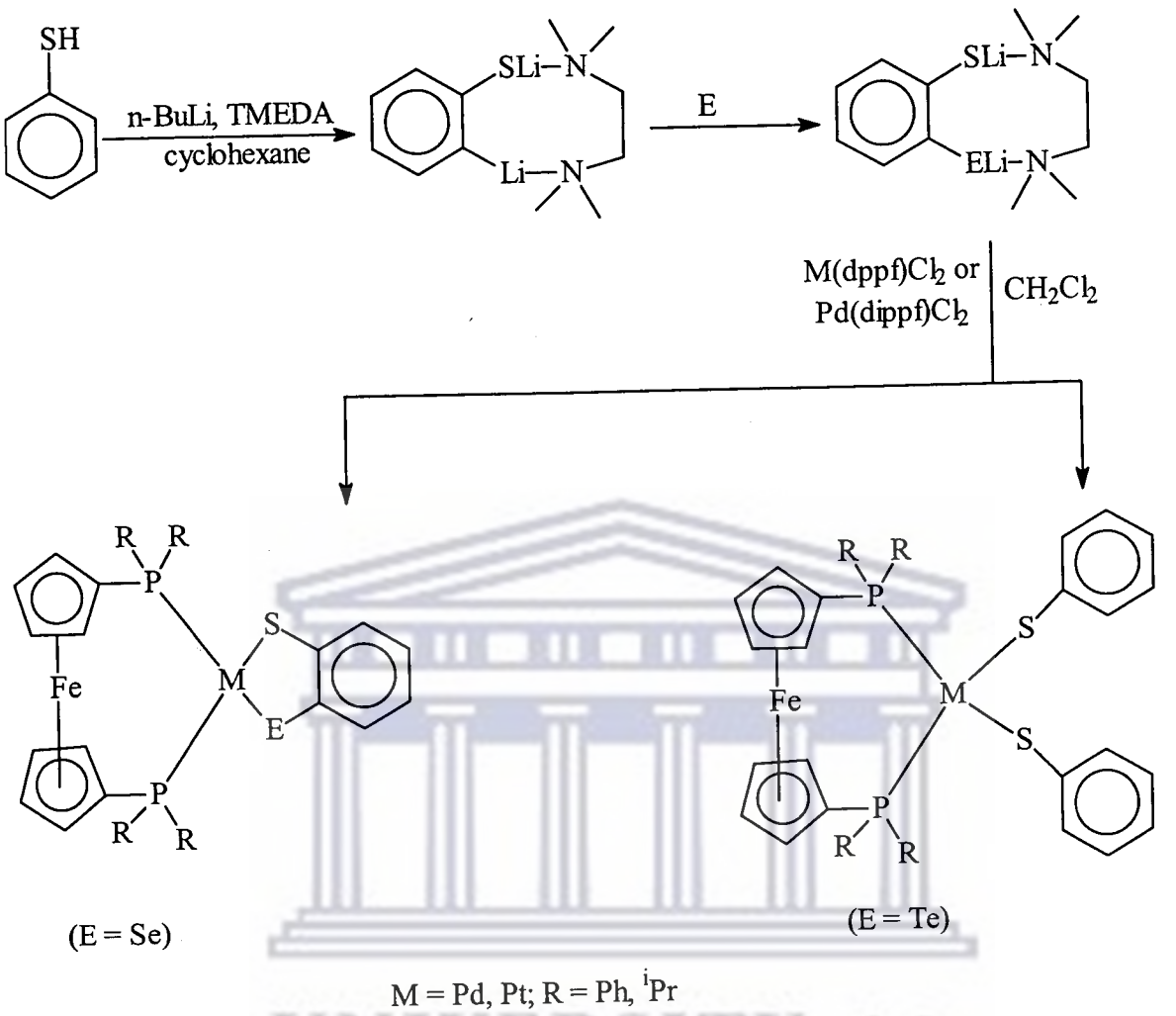

Scheme 5: *In situ* reactions of $M(dppf)Cl_2$ and $Pd(dippf)Cl_2$ with $LiSC_6H_4ELi$-*o* (M = Pd, Pt; E = Se, Te)

With E = Se, the transformation gave a mixture of products, which was difficult to separate on silica and alumina columns. Evidence for the expected product was found in the ^1H NMR chemical shifts of the cyclopentadienyl region of the dppf complexes where four peaks (two broad singlets and two quartets) were observed. The peaks are similar to those observed in the other mixed chalcogenide complexes as exemplified by the ^1H NMR spectrum of $Pd(dppf)(SC_6H_4O$-*o*) **(1d)** in Fig. 6 which is discussed latter. Also,

FAB mass spectrometry showed molecular ion peak of the selenium complexes at m/z = 769, 712 and 936 for Pd(dppf)(SC_6H_4Se-*o*) (Fig. 4), Pd(dippf)(SC_6H_4Se-*o*) and Pt(SC_6H_4Se-*o*) respectively. Some of the peaks detected in the FAB mass spectrometry are m/z of 877, 743, and 968 corresponding to Pd(dppf)($SC_6H_5)_2$, Pd(dippf)($SC_6H_5)_2$ and Pt(dppf)($SC_6H_5)_2$ respectively and indicating a mixture of products. On the contrary, when E was Te, the tellurium appeared not to have reacted to form the anticipated intermediate, $LiSC_6H_4TeLi$-*o*. As a result the *in-situ* reaction with Pd and Pt starting materials were found to contain two moles of thiophenolate ligand coordinated to the metal centre. This was detected from both the elemental analysis and NMR data of the complexes. The yields of M(dppf)($SC_6H_5)_2$ (M = Pd, Pt) and Pd(dippf)($SC_6H_5)_2$ from this source were generally moderate (68-74%). However over 80% yields were obtained when the Pd(dppf)Cl_2, Pd(dippf)Cl_2 and Pt(dppf)Cl_2 were reacted directly with thiophenol as in eq. 7.

$$M(dppf)Cl_2 + 2HSC_6H_5 \xrightarrow[-2Et_3NHCl]{2Et_3N} M(dppf)(SC_6H_5)_2 \quad (M = Pd, Pt) \qquad (7)$$

All the compounds isolated from the one pot reactions were fully characterised by IR, ^1H and $^{31}P\{^1H\}$ NMR spectroscopy and mass spectrometry. The IR spectra of complexes **1g**, **2g** and **3g** had strong peaks in the phenyl regions, in accordance with the earlier observation for the other homoleptic dithiolato complexes. The rest of the peaks followed similar assignments as summarised in Table 2. Compounds **1g**, **2g**, and **3g** had two sets of multiplets with the downfield multiplets for the aryl protons *ortho* to the sulfur atom at 7.17, 7.30 and 7.17 ppm respectively in the ^1H NMR spectra. The other multiplets

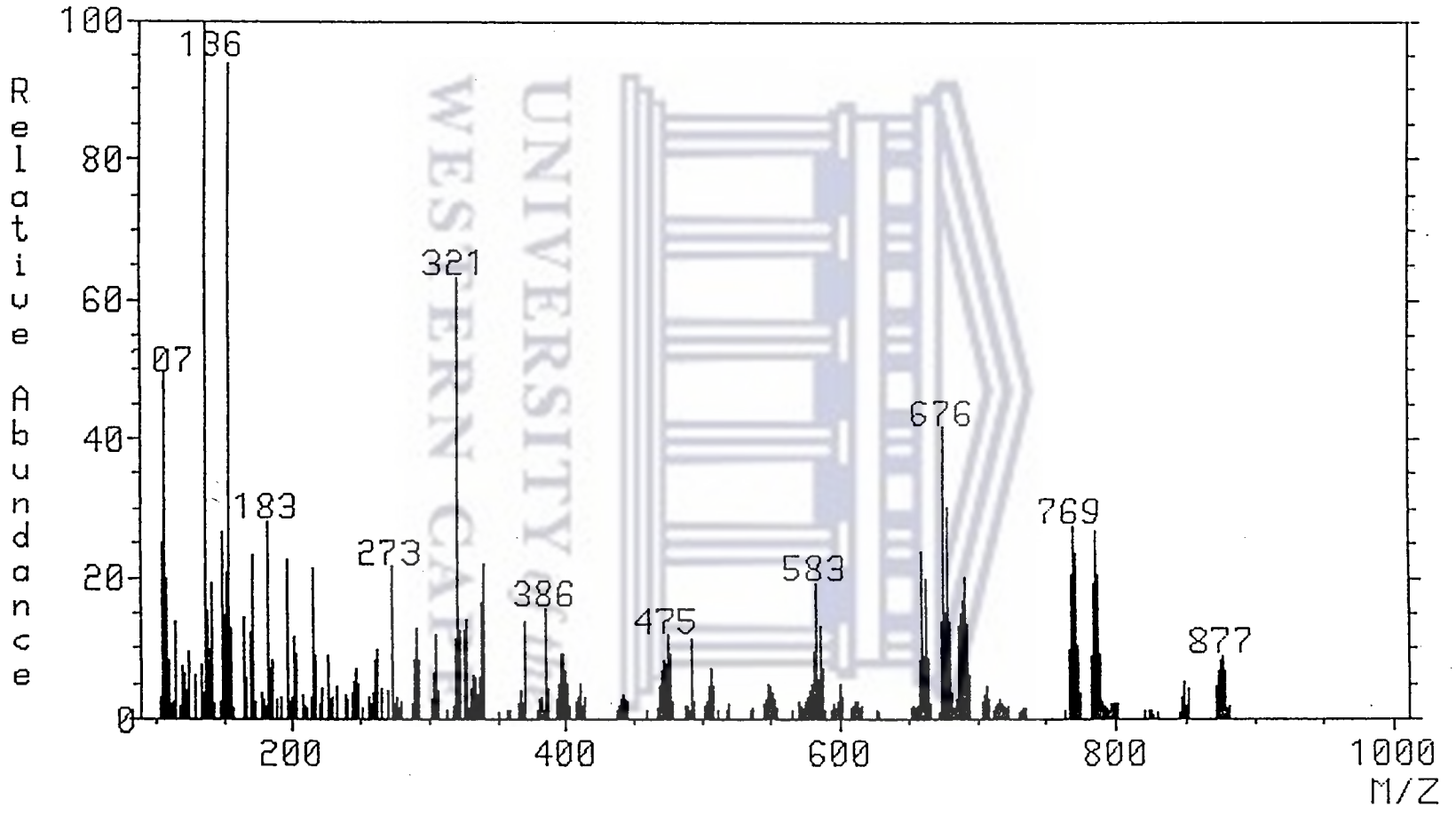

Fig. 4. FAB mass spectrum of Pd(dppf)(SC_6H_4Se-*o*).

integrated for three protons and were assigneed to the remaining aryl protons. Peak values were 6.77, 6.92 and 6.78 ppm for compounds **1g**, **2g** and **3g** respectively. The phenyl proton peaks in **1g** and **3g** were found in the regions 7.75-7.78 ppm and 7.32-7.36 ppm. The former set of peaks accounts for eight protons of the phenyl protons *ortho* to the phosphorus atoms, whilst the latter set of peaks was from the remaining phenyl protons. For **2g**, the isopropyl proton peaks were found at 1.50 and 1.19 ppm for the CH_3 while the CH peak was at 3.02 ppm. The $^{31}P\{^1H\}$ NMR spectra of **1g**, **2g** and **3g** had singlet peaks at 22.82, 47.63 and 24.54 ppm respectively, thus showing the equivalence of the two phosphorus atoms. Single crystal X-ray structure of **2g** discussed latter confirmed the proposed structures of **1g**, **2g** and **3g** obtained from the analytical data.

3.4 Characterisation of mixed aryldichalcogenide metal complexes.

3.4.1 Infrared spectral data of the mixed aryldichalcogenide metal complexes.

As shown in Scheme 3, when the thiol ligand was 2-mercaptophenol, thiosalicylic acid and 2-mercaptonicotinic acid, the products isolated had O and S atoms binding to Pd or Pt. These are referred to in this thesis as the mixed aryldichalcogenide complexes. By changing the aryldichalcogenide ligand from aryldithiolato to mixed aryldichalcogenide, the IR stretching frequencies did not shift significantly. A representative IR spectrum is that of **2e** shown in Fig. 5 and the IR data is summarised in Table 6. Here too, the phenyl peaks were generally observed between 460-560 cm^{-1} as a group of strong peaks and also in the 680-740 cm^{-1} region. For the diisopropylphosphine complexes, the 680-740 cm^{-1} region had only weak or no peaks while the 460-560 cm^{-1} region had strong peaks. This simplified the assignment of the phenylphosphine and the aryldithiolato peaks. It could be

inferred that the peaks in the 460-560 cm^{-1} region are due to the phenylphosphines. The alkyl peaks of the isopropylphosphine complexes overlapped with the nujol peaks in the IR spectrum. This made the assignment of the alkyl groups of diisopropylphosphine very difficult. The presence of these groups could be identified from the ^1H NMR spectral data discussed in section 3.2.2 of this thesis.

Table 6a. Infrared spectral data for selected functional groups of the mixed aryldichalcogenide complexes of Pd(dppf) and Pt(dppf).

Complex	SC_6H_4E-*o* (cm^{-1})	Phenylphosphine ligand (cm^{-1})	η^5-C_5H_4P (cm^{-1})
1d	426, 462	488, 513, 551, 672, 698	736, 789, 824
1e	429, 463	488, 512, 541, 631, 698	736, 801, 825
1f	429, 463	487, 501, 520, 639, 698	744, 790, 835
3d	426, 467	490, 520, 552, 636, 689	737, 780, 844
3e	425, 463	484, 508, 561, 636, 693	736, 751, 861
3f	432, 458	485, 508, 556, 596, 640	732, 751, 830

Table 6b. Infrared spectral data for selected functional groups of the mixed arydichalcogenide complexes of Pd(dippf).

Complex	SC_6H_4E-*o* (cm^{-1})	η^5-C_5H_4P (cm^{-1})
2d	627, 649	727, 736, 832
2e	623, 652	719, 740, 837
2f	631, 656	718, 766, 838

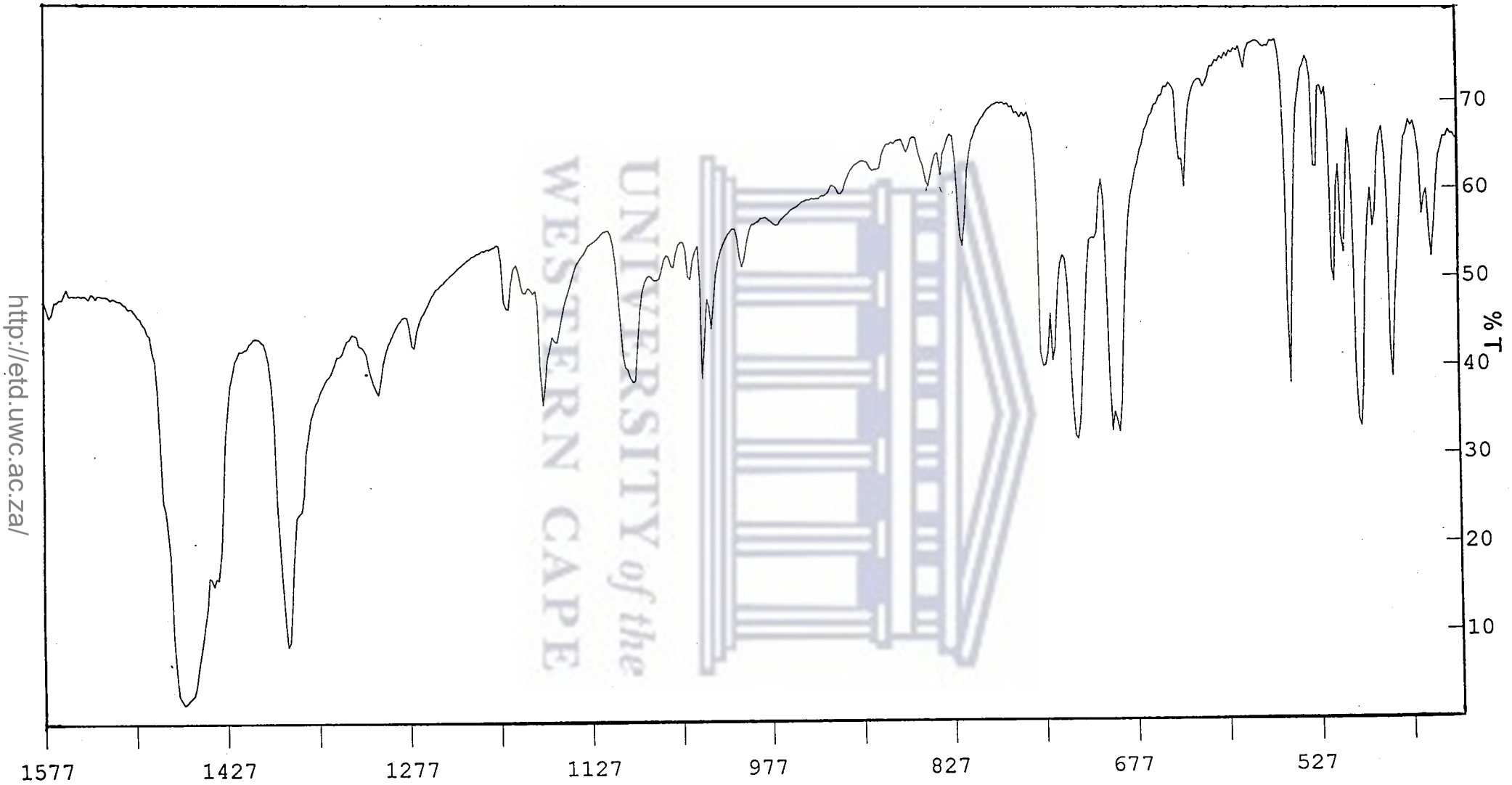

Fig. 5. Infrared spectrum of **2d** as nujol mulls.

3.4.2 ^{1}H NMR spectral data of the mixed aryldichalcogenide metal complexes.

The phenylphosphine proton peaks appeared as a set of three to four multiplet peaks, unlike in the homoleptic complexes where the phenylphosphine proton peaks appeared as a set of two multiplets. A typical spectrum is that of Pd(dppf)(SC_6H_4O-*o*) (**1d**) shown in Fig. 6 with the cyclopentadienyl region expanded as an insert. The **1d** spectrum had phenyl peaks at 8.00, 7.69 and 7.32 ppm. These peaks were assigned on the basis of the difference in the polarisability of the two chalcogen atoms with the protons *ortho* to the phosphorus atom *trans* to sulfur at 8.00 ppm and those *trans* to oxygen at 7.69 ppm. These peaks are quartets due to their coupling with the phosphorus atom and the protons at carbons 2 and 6 of the phenyl ring. The remaining phenylphosphine protons were detected as a multiplet around 7.32 ppm that is not fully resolved. However the integration of these multiplets, and two downfield sets described earlier on, show the right number of protons to confirm that there are two phenyl rings attached to each phosphorus atom in the dppf ligand as shown in Table 7.

The effect of the different chalcogen atoms can be clearly seen in the cyclopentadienyl region of the ^{1}H NMR spectrum (Fig. 6). Contrary to the two peaks observed in the dithiolato complexes, the mixed aryldichalcogenide complexes displayed spectra consisting of four sets of cyclopentadienyl peaks. These four sets of peaks consist of two quartets; one downfield and the other one upfield and two broad singlets between the quartets. For **1d** the quartets were at 4.71 and 3.77 ppm with the singlets at 4.50 and 4.28 ppm. The peaks are quartets due to coupling of protons at carbons 2 and 5 with the

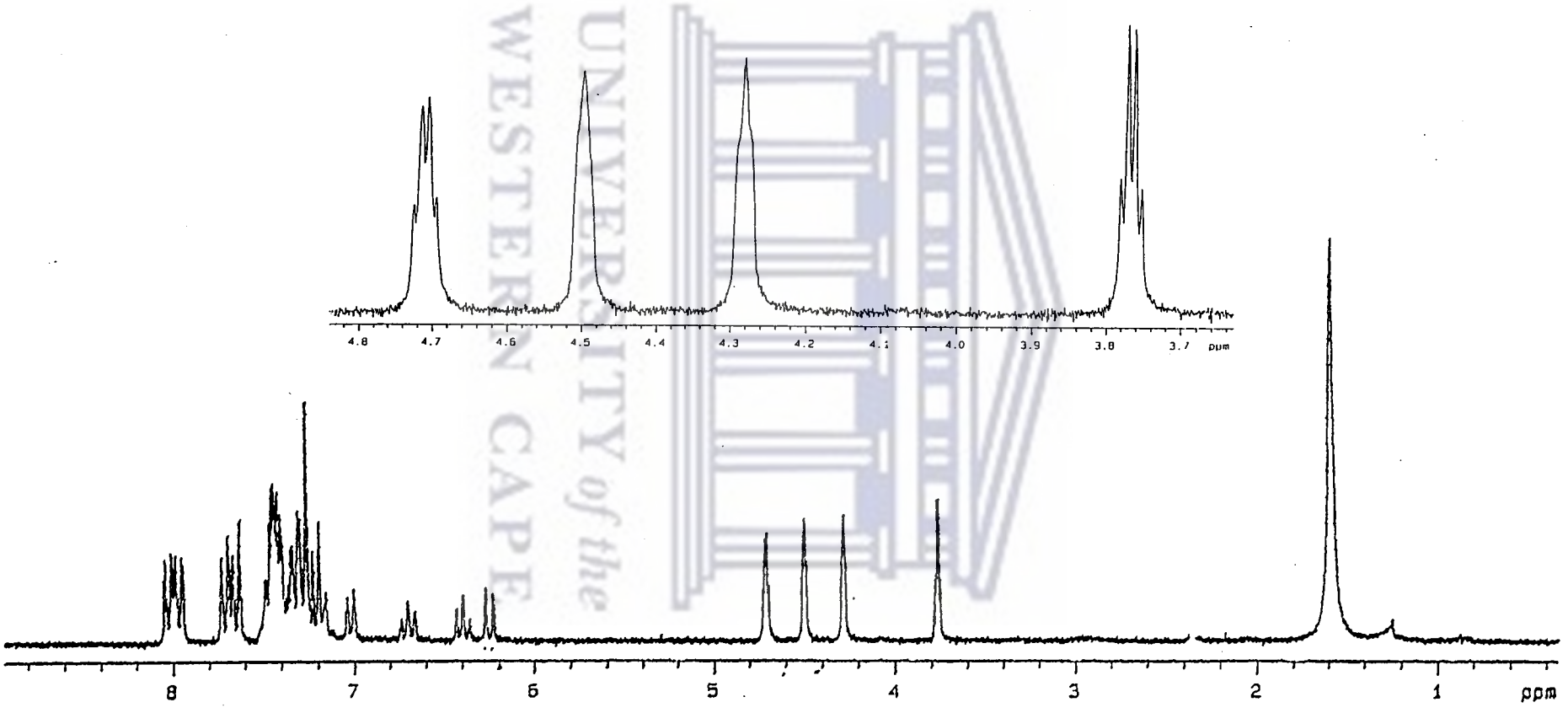

Fig. 6. The ^{1}H NMR of **1d** with its cyclopentadienyl region as an insert.

phosphorus atom and the other cyclopentadienyl protons. The quartet at 4.71 ppm is due to the protons at carbon 2 and 5 of the cyclopentadienyl ligand *trans* to the sulfur atom, while the peak at 3.77 ppm is due to the protons *trans* to the oxygen atom. The broadness of the singlets shows weak coupling of the protons at carbons 3 and 4 with protons at carbons 2 and 5. The assignments of these protons were made on the basis of the *trans*-influence which is related to the *trans* effect.

Trans-influence is a phenomenon where electronic rather than steric effects lead to stereospecific reactions and is mostly observed in square planar d^8 metal ions like Pt(II). Where the *trans* effect is observed, a ligand (strong σ base or π acid) weakens and ultimately breaks a metal-ligand bond *trans* to it. There is also a ground state influence of a *trans* ligand on a metal-ligand bond that has been extensively studied. It involves the ability of a ligand to weaken the metal-ligand bond *trans* to it without completely breaking this bond as is observed for the *trans* effect. This is referred to as the *trans* influence which is a thermodynamic effect.[83-84] Studies of *trans*-influence have been made on square planar palladium(II) and platinum(II) complexes. Of relevance to this project is the results from the $^{31}P\{^1H\}$ coupling constant data that suggest the Pt-P bond in *cis*- and *trans*-$Pt(PR_3)_2X_2$ complexes to have a greater 6s character when the two phosphorus ligands are *cis* rather than *trans* to each other.[83a] This would suggests that in the *trans* isomer the difference in X ligands results in electron density distortion on the phosphorus. If an ion is a negative high charge, it will hold its outer electrons only weakly and can easily be distorted by a positive ion, it is said to be polarisable. The

greater the polarisability of an anion, the less ionic the bond will be between it and a cation.[85]

Because of the *trans*-influence for the mixed aryldichalcogenide ligands, the more polarisable atom deshields the phosphorus atom *trans* to it. As a result of the deshielding effect, the cyclopentadienyl protons associated with the phosphorus atom *trans* to sulfur lie downfield relative to the cyclopentadienyl protons associated with the phosphorus atom *trans* to the less polarisable oxygen atom.

There is no clear trend in the ^{1}H NMR of the cyclopentadienyl protons when the metal was changed from Pd to Pt. In **1d** the singlet at 4.50 ppm was assigned to the protons at carbons 3 and 4 of the cyclopentadienyl ligand *trans* to the sulfur atom while the one at 4.28 ppm is due to similar protons *trans* to the oxygen atom. These are expected to be doublets but appeared as broad singlet peaks which suggests that the strength of the magnet of the NMR spectrometer is not strong enough to show the coupling. In **3d** the singlets appeared at 4.45 and 4.28 ppm respectively.

The arylthiolato protons for complexes containing ligands **d-f** were different from the **a-c** ligands. These were similarly assigned on the basis of the difference in polarisability of the chalcogenide atoms. For **1d** (Fig. 6) the spectrum consisted of two doublets at 7.02 and 6.25 ppm and two triplets at 6.70 and 6.40 ppm. The doublet at 7.02 ppm is due to the aryl proton *ortho* to the sulfur while the one at 6.25 ppm is due to the proton *ortho* to the oxygen atom. The triplet at 6.70 ppm is due to the proton *para* to the sulfur atom and the one at 6.40 ppm is due to the proton *meta* to the sulfur atom for **1d**. The coupling

Table 7. ^1H NMR spectral data of the mixed aryldichalcogenide metal complexes.

Complex	η^5-C_5H_4P (ppm)				Aryldithiolato protons (ppm)			
1d	4.71	4.50	4.28	3.77	7.02	6.70	6.40	6.25
2d	4.54	4.46	-	-	7.35	7.01	6.82	6.54
3d	4.62	4.45	4.28	3.91	7.11	6.62	6.40	6.31
1e	4.63	4.48	4.31	3.84	7.06	6.97	-	-
2e	5.50	4.49	-	-	7.42	7.01	-	-
3e	4.58	4.45	4.30	3.90	7.09	6.98	-	-
1f	4.84	4.56	4.28	3.64	8.25	6.89	-	-
2f	4.53	4.47	-	-	8.35	7.01	-	-
3f	4.82	4.59	4.29	3.70	8.27	6.90	6.37	-

observed for these peaks are triplets due to coupling to the two neighbouring protons of the aryl ring. Similar peak values and patterns were found for **2d** and **3d**. In **1e** the thiolato aryl protons appeared at 7.06 and 6.97 ppm as a set of two multiplets. Similar peak patterns were found in **2e** and **3e** as shown in Table 7. The protons closer to the nitrogen of the pyridine based thiolato ligand lie most downfield at 8.25, 8.35 and 8.27 for **1f**, **2f** and **3f** respectively. These protons are very close to the more electronegative nitrogen atom and as a result are deshielded. All the mixed chalcogenide complexes followed similar proton assignment as summarised in Table 7 and the experimental section of the respective complexes.

3.4.3 $^{31}P\{^{1}H\}$ NMR spectral data of the mixed aryldichalcogenide metal complexes.

3.4.3.1 $^{31}P\{^{1}H\}$ NMR spectral data of palladium complexes.

Unlike the $^{31}P\{^{1}H\}$ NMR spectra peaks observed for the homoleptic series, when the aryldichalcogenide ligand was mixed chalcogenide, the $^{31}P\{^{1}H\}$ NMR peaks were no longer singlets. The spectra of all the mixed chalcogenide complexes of Pd(dppf) and Pd(dippf) complexes displayed spectra that had two doublets consistent with two inequivalent phosphorus nuclei (Fig. 7). The spectra are similar to that reported for Ni(dppe)(SC_6H_4O-*o*) where two doublets were observed.[27] In **1e** the two doublets were found at 37.33 and 22.46 ppm while in **2e** they were found at 59.16 and 51.63 ppm.

When there are two inequivalent phosphorus nuclei as observed here, two possible spin patterns namely: AX and AB could be applicable. In an AX spin pattern, the chemical shift difference $\Delta\nu$ between the coupled nuclei is greater than the coupling constant, i.e. J

< Δν whereas for an AB spin pattern, $J > \Delta\nu$.[86] By applying these criteria, the $^{31}P\{^{1}H\}$ NMR spectra of the mixed aryldichalcogenide complexes of palladium were assigned to an AX spin pattern.

Table 8. The $^{31}P\{^{1}H\}$ NMR spectral data of the mixed aryldichalcogenide complexes of Pd(II) complexes.

Complex	Chemical shifts (ppm)	Δν (ppm)	J_{PP} (Hz)
1d	32.44 (d); 21.98 (d)	10.46	27.44
1e	37.33 (d); 22.46 (d)	14.87	28.98
1f	39.52 (d); 21.94 (d)	17.58	29.55
2d	55.18 (d); 48.28 (d)	6.90	12.14
2e	59.16 (d); 51.63 (d)	7.53	11.17
2f	59.66 (d); 52.34 (d)	7.32	12.71

All the complexes which contain oxygen and sulfur in the ligands gave an AX spectrum quite similar to those found in Ni(dppe)(SC_6H_4O-*o*)[27]. The chemical shifts of the doublets associated with each of the phosphorus atom of the dppf and dippf ligand can be linked to the *trans*-influence of the chalcogen atom *trans* to the phosphorus atom. This is based on the more polarisable chalcogen having a better *trans*-influence. For example in **1e**, the chemical shift of the phosphorus atom *trans* to the sulfur atom was found to be 39.52 ppm whilst the one *trans* to the oxygen atom was 22.46 ppm. Representative spectra of **1e**

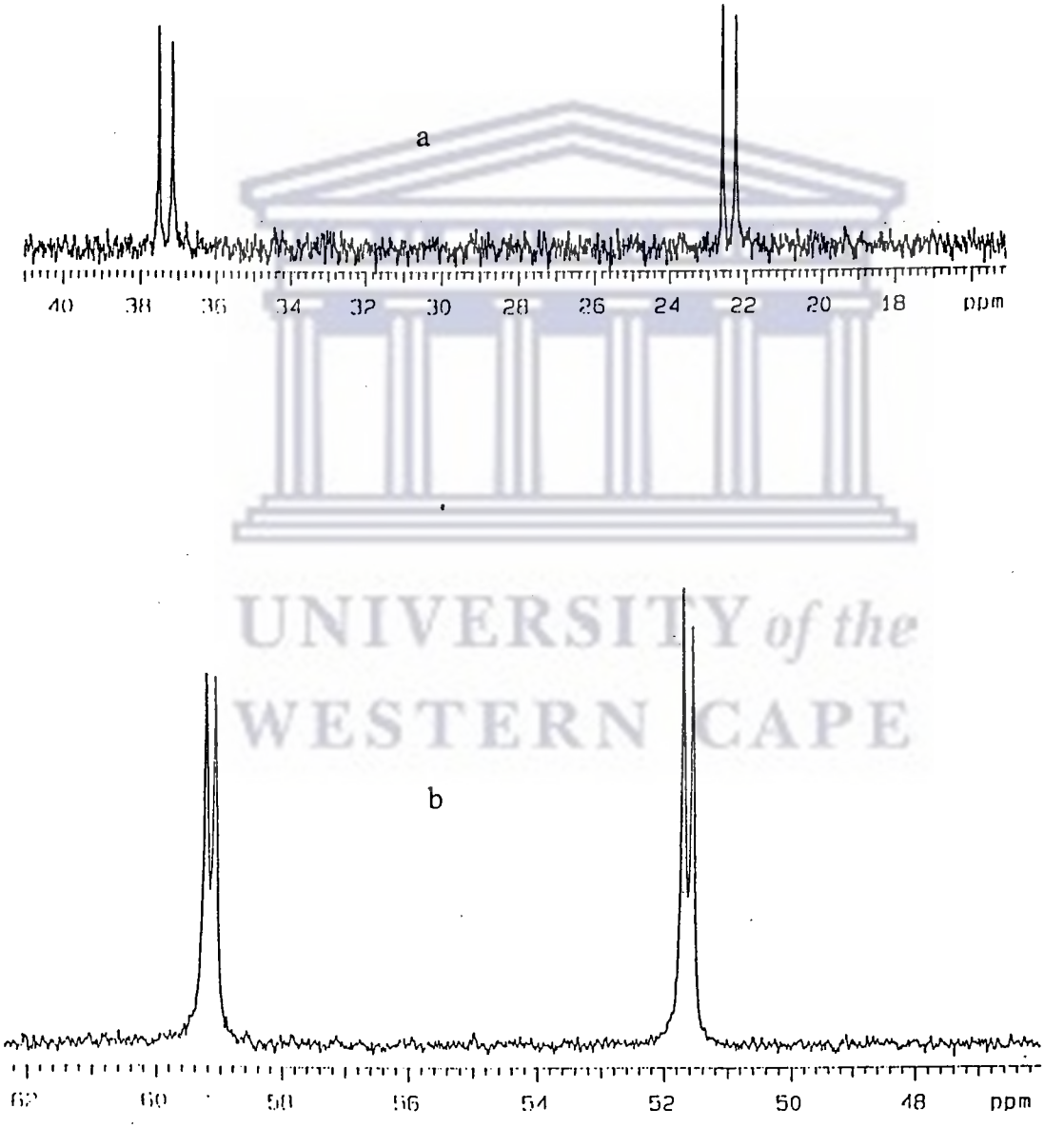

Fig. 7. The $^{31}P\{^{1}H\}$ NMR spectrum of **1e** (a) and **2e** (b)

and **2e** are shown in Fig. 7 and illustrate the dppf and dippf effects. Comparison of **2d** and **2e** shows that the presence of the more electron withdrawing carbonyl group in **2e** deshields the phosphorus relative to that in **2d**. The effect is more pronounced in **2f** because of the nitrogen group in the ring. Overall the downfield shift is **2f** > **2e** > **2d**. The same order was observed in the dppf analogues as illustrated in Table 7. The coupling constants also follow the same pattern decreasing from **2f** > **2d**. The coupling constant of **2e** seems anomalous with a value lower than that of **2d**. This cannot be readily explained. The use of $^{31}P\{^{1}H\}$ NMR spectra to identify *trans*-influence has been observed by Henderson *et al.* for Pt(dppe)($SC_6H_4CO_2$-*o*).[50b] Even for the homoleptic complex, M(dppe){S_2C_2(2-pyridine)(H)} (M = Ni, Pd, Pt)[72], the influence of the pyridine nitrogen results in different electronic environment similar to that produced by the polarisability differences described above. The result is two broad $^{31}P\{^{1}H\}$ NMR singlets (57.4 and 57.2 ppm) for the dppe phosphorus in Ni(dppe){S_2C_2(2-pyridine)(H)}[72]. It appears from these results that ^{31}P NMR spectroscopy is a viable measure of the *trans*-influence of atoms that offers a routine experimental route to detect this effect.

3.4.3.2 The $^{31}P\{^{1}H\}$ NMR data of platinum mixed aryldichalcogenide complexes.

An even more interesting coupling pattern was found when the metal was platinum. The $^{31}P\{^{1}H\}$ NMR spectra of the mixed aryldichalcogenide complexes of Pt(II) displayed a set of six doublets (Fig. 8). Two of these doublets were more intense and about five folds in intensity than that of the remaining four doublets. The two intense doublets are due to the two phosphorus nuclei of the dppf ligand with the four less intense doublets being satellites of the NMR active ^{195}Pt nucleus. These were assigned in accordance with the

analogues **3a-3c** in which it was found that the platinum satellites are always less intense than the phosphorus peaks. The peak patterns were similar to **3a - 3c** except that the two phosphorus atoms in the mixed aryldichalcogenide complexes are inequivalent. As a result of this inequivalence, each phosphorus atom is expected to give a singlet peak and two platinum satellites. However the inequivalence of these phosphorus nuclei makes them to couple thereby splitting the singlets into doublets. This applies to platinum satellites as well; resulting in a spectrum that consists of six doublets, two from the phosphorus nuclei and four from the platinum satellites. A representative spectrum is that of **3e** shown in Fig. 8. Peak assignments here, based on *trans*-influence described earlier, means the phosphorus *trans* to sulfur would lie downfield and that *trans* to oxygen would be upfield, with their associated Pt satellites. The ^{195}Pt satellite peaks associated with the phosphorus *trans* to sulfur are marked with asterisks in Fig. 8. The unmarked peaks are due to the satellites associated with the phosphorus *trans* to the oxygen atom.

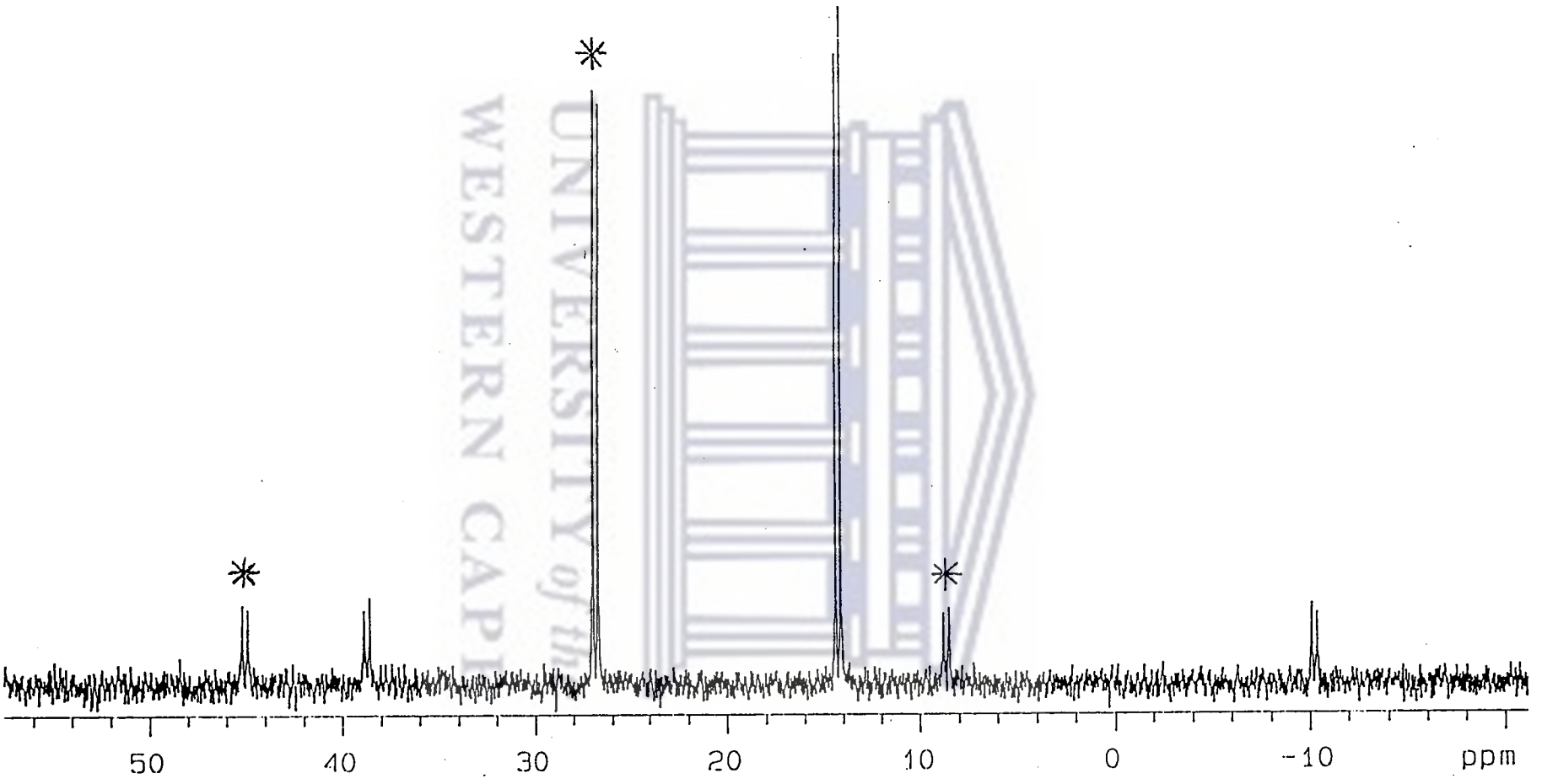

Fig. 8. $^{31}P\{^{1}H\}$ NMR spectrum of **3e**.

CHAPTER 4

MOLECULAR STRUCTURES

4.1 Mass spectrometry of homoleptic aryldithiolato and mixed aryldichalcogenide metal complexes of Pd(II) and Pt(II).

One of the characterisation tools used in this project was mass spectrometry and this chapter describes the use of mass spectrometry to determine molecular ions of products isolated. Mass spectrometry involves the vaporisation of a compound, its ionisation and the analysis of the ions produced. For unipositive ions, the molecular mass is thus determined. The ionisation generally produces excited gaseous ions that may undergo fragmentation to give a series of peaks in the mass spectrum corresponding to the ionic fragmentation products.

Mass spectrometry is a good analytical tool in synthetic chemistry that helps to identify molecular weights of compounds. By so doing, it helps in providing further support for the proposed structures of compounds as suggested by other analytical tools such as IR, NMR and elemental analysis. Since in most cases, an ion corresponding to the molecular ion is observed, molecular weight measurement is straightforward. Analysis of the pattern may show which groups are lost readily, and give some idea of the structure of the ions even when molecular ions are not detected. Analysis of the energy necessary to produce ionisation of the molecule followed by the appearance of a given fragmentation product can, under certain conditions, give useful thermodynamic data and some information on bond strengths.[83]

An attraction of mass spectrometry as an analytical tool is its high sensitivity. Generally less than a milligram of compound is necessary to give a spectrum, and used as an analytical method, very small quantities of an element may be detected. Mass spectrometry was used to further characterise compounds in this project and also as a measure of stability by varying the ionisation source. The two ionisation sources that were used are electron impact (EI) and fast atom bombardment (FAB).

None of the Pd(dppf) complexes showed the molecular ion peak in the EI mode. However, when all the complexes were subjected to FAB mass spectroscopy, they displayed their molecular ion peaks. Representative EI and FAB spectra are that of **1f** shown in Fig. 9 with its FAB fragmentation pattern in Scheme 6. This indicates that the electron impact ionisation source was too harsh for the complexes but the complexes could stand the softer FAB. The same effect was observed by Darkwa *et al.* in the study of the stability of Ni(dppe)(SC_6H_4E-*o*) (E = S, O, CO_2).[27] The complexes that contain the pyridine based ligand (**1f**, **2f** and **3f**) were found to decompose if kept for more than 24 h in solution even under an inert nitrogen atmosphere and it came as no surprise when these complexes showed no molecular ion peak in the electron impact mode. In some cases, the molecular ion peak in the EI spectrum was not the base peak but some Pd(dppf) complexes had m/z = 154 as their base peak. This m/z = 154 peak is assigned to the aryldichalcogenide ligand.

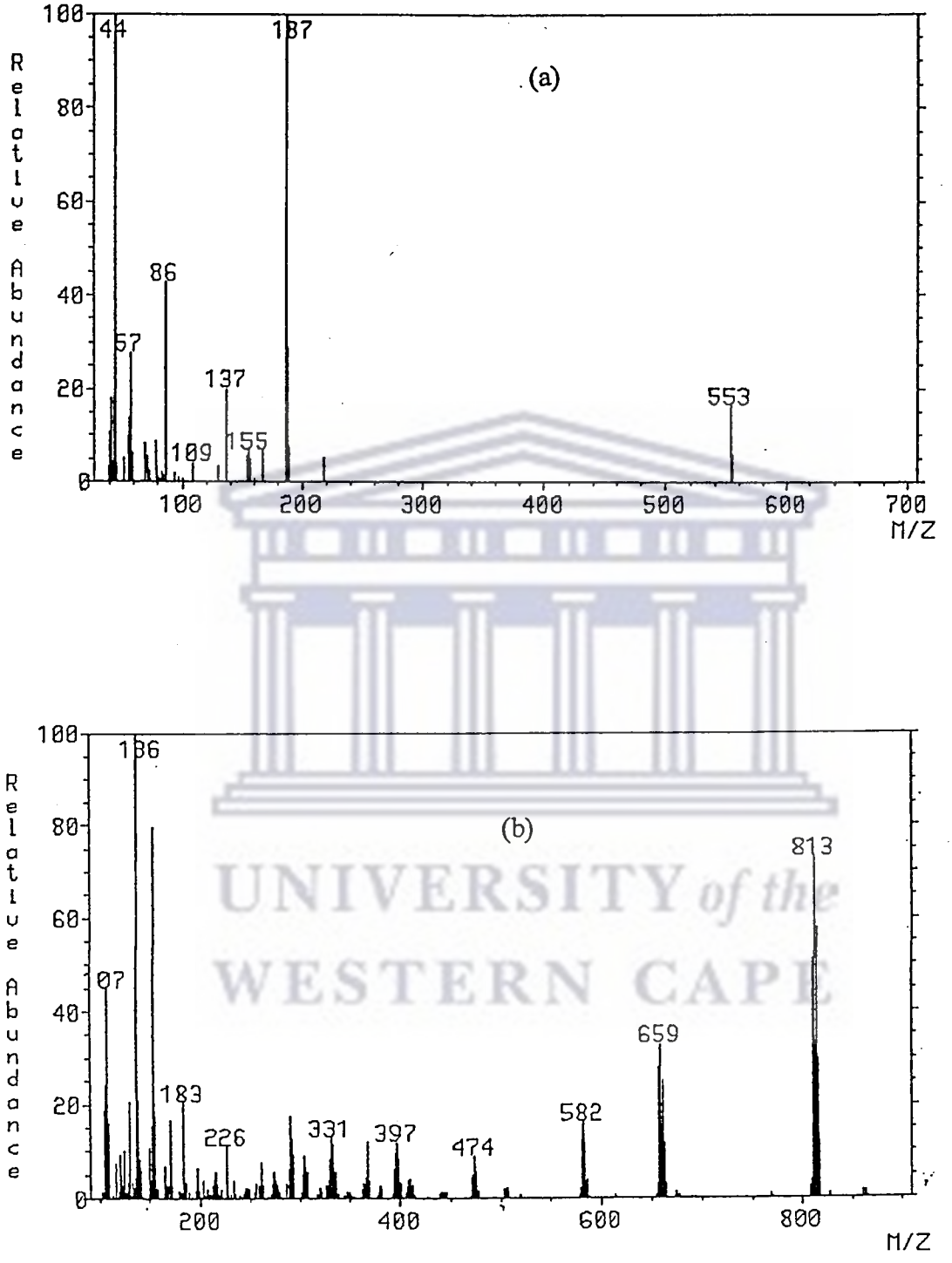

Fig. 9. EI (a) and FAB (b) mass spectra of **1f**.

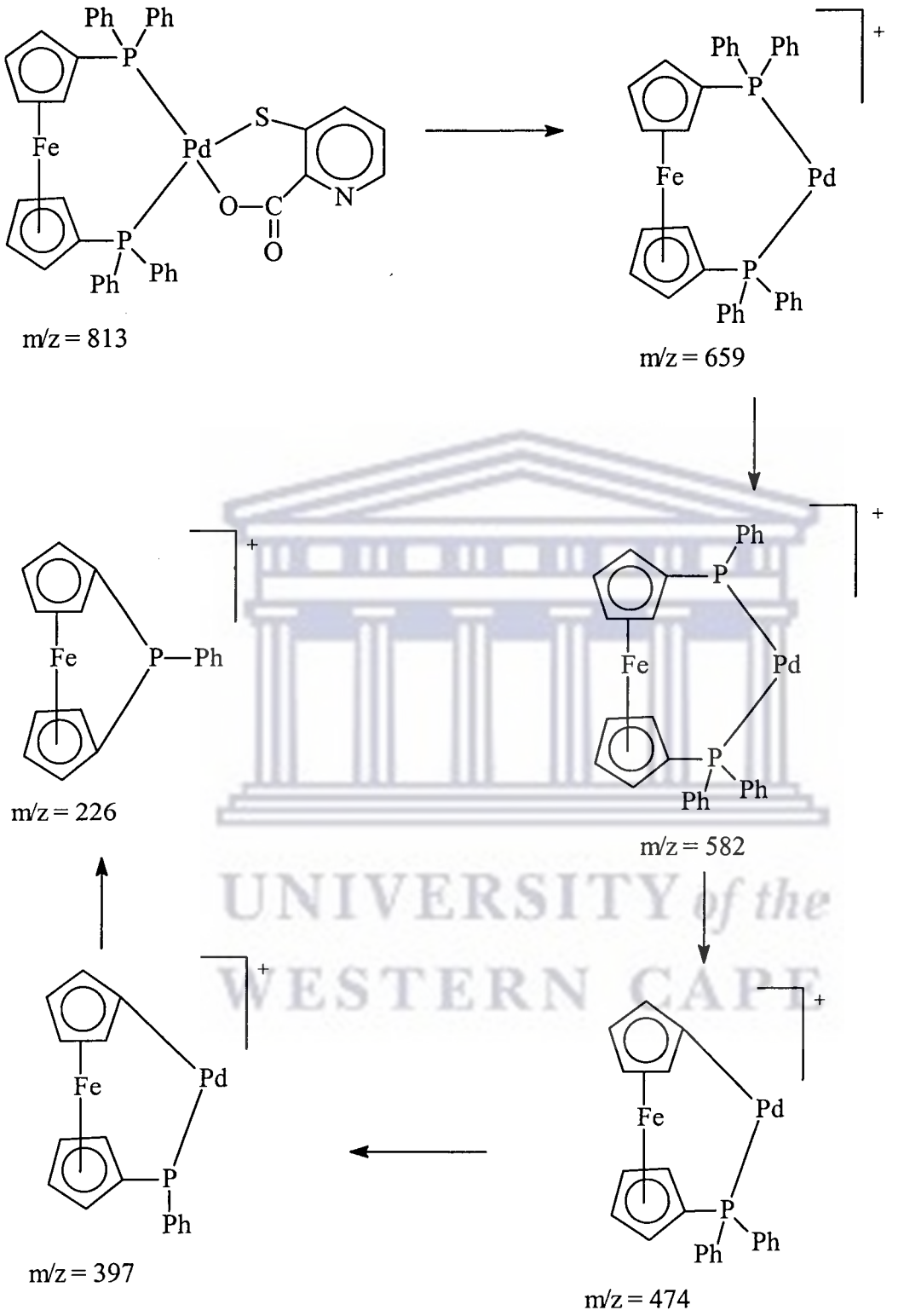

Scheme 6. FAB mass spectral fragmentation pattern of **1f**.

The fragmentation pattern (Scheme 6) shows how the complexes behave in the mass spectrometer. All the Pd(dppf) complexes lost the aryldichalcogenide ligand quite readily in the FAB mode, followed by the consecutive loss of the two phenyl groups (m/z = 77) and then the palladium metal (m/z = 106). The Pd(dippf) complexes on the other hand, lost an isopropyl group in the EI mode while the aryldichalcogenide ligand was lost first in the FAB mode.

The two Pt(II) complexes **3e** and **3f** did not show any molecular ion peak and were found to loose the CO_2 fragment in the EI mode. This was evidenced by the loss of a fragment with m/z = 44 and the remaining fragment (m/z = 858, 100%; in the case of **3e**) was found to be the base peak, suggesting that a more stable fragment is formed. The other platinum complexes (**3a-3d**) displayed molecular ion peaks in both the EI and FAB modes. These molecular ion peaks were base peaks (100% intensity) in the EI mode. All the aryldithiolato complexes of Pt(dppf), **3a**, **3b** and **3c** lost the phenyl group (m/z = 77) first in the FAB mode. Unlike the fragmentation pattern in the Pd(dppf) complexes, the Pt(dppf) complexes showed no regular fragmentation pattern. The fragmentation pathway is quite different from the one postulated for the Pd(dppf) complexes, hence a universal sequential loss of fragments could not be established for **3a-c**. It appears that there are some rearrangements that could not be accounted for in most of these complexes. Some of these peaks are at m/z = 391, 421 and 745.

Based on the EI mass spectrometry data the platinum complexes appear to be more stable than the palladium complexes although CO_2 was lost quite readily in the mixed

chalcogenide complexes. The molecular ion peaks, which were found to be the base peaks in both the EI and FAB modes, strongly suggest a better stability.

4.2 Determination of molecular structures by X-ray crystallography.

In structural elucidation, single crystal X-ray structures usually serve as a confirmation of a structure in the solid state. There are however instances where the solid state structure differs from that identified in solution. For the structures reported in this thesis, the solid state structures were the same as those proposed from solution NMR data, thus confirming the proposed structures from IR, NMR spectrometry and elemental analysis. The complexes whose structures were determined by single crystal X-ray diffraction are Pd(dppf)(SC_6H_4S-*o*) (**1a**), Pd(dippf)(SC_6H_4S-*o*) (**2a**), Pd(dippf)(SC_6H_3MeS-*o*) (**2b**), Pd(dippf)(SC_6H_5)$_2$ (**2g**), Pt(dppf)(SC_6H_4S-*o*) (**3a**) and Pt(dppf)(SC_6H_4O-*o*) (**3d**). Three of the complexes (**1a**, **2b** and **3a**) crystallised with the chlorinated solvents from which single crystals were grown. Complex **1a** was crystallised by slow evaporation of a solution that was used to run ^{1}H NMR spectrum in $CDCl_3$, thus the $CHCl_3$ molecule found in the unit cell must be the small amount of non-deuterated chloroform in the NMR solvent. The rest of the complexes were crystallised from a mixture of CH_2Cl_2/hexane (2:1) at -15°C. These solvents of crystallisation confirmed their presence in the solid as detected by ^{1}H NMR and by microanalysis. The crystallographic data of complexes **1a**, **2a**, **2b**, **3a** and **3d** is shown in Table 9.

*Table 9. Crystallographic data for complexes **1a**, **2a**, **2b**, **3a** and **3d**.*

	1a.$CHCl_3$	**2a**	**2b**.CH_2Cl_2	**3a**.CH_2Cl_2	**3d**
Formula	$C_{41}H_{33}Cl_3P_2S_2FePd$	$C_{28}H_{40}P_2S_2FePd$	$C_{30}H_{46}Cl_2P_2S_2FePd$	$C_{41}H_{34}Cl_2P_2S_2FePt$	$C_{40}H_{32}OP_2SFePt$
FW	920.33	664.91	765.88	974.58	873.60
T(K)	293(2)	173(2)	173(2)	173(2)	173(2)
Wavelength (Å)	0.71	0.71	0.71	0.71	0.71
Crystal system	Monoclinic	Orthorhombic	Monoclinic	Orthorhombic	Monoclinic
Space group	$P2_1/n$	$P2_12_12_1$	$P2_1/n$	$Pca2_1$	$P2_1/c$
a, Å	14.48(3)	11.07(7)	18.79(2)	20.20(9)	10.11(6)
b, Å	13.43(3)	14.65(9)	9.42(7)	13.29(6)	18.56(10)
c, Å	20.21(4)	18.06(11)	20.06(2)	27.27(12)	17.96(10)
α, deg	90	90	90	90	90
β, deg	104.28	90	111.73(3)	90	99.69(10)
γ, deg	90	90	90	90	90

Volume ($Å^3$), Z	3807.5(13), 4	2928.30(3), 4	3297.50(5), 4	7322.40(6), 8	3322.90(3)
Density (calc) ($Mg.m^{-3}$)	1.61	1.51	1.54	1.77	1.75
Crystal size (mm^3)	0.24x0.20x0.17	0.40x0.30x0.10	0.17x0.17x0.17	0.20x0.20x0.20	0.40x0.30x0.30
No. of reflections collected/unique	27868/8346 [R(int) = 0.0434]	34296/5988 [R(int) = 0.0321	15619/7536 [R(int) = 0.0357	49562/15952 [R(int) = 0.0286]	18588/6661 [R(int) = 0.0261]
Goodness-of-fit on F^2	1.033	1.041	1.040	1.018	1.004
Final R indices [I>2sigma (I)]	R_1 = 0.0310, wR_2 = 0.0647	R_1 = 0.0262, wR_2 = 0.0606	R_1 = 0.0365, wR_2 = 0.0792	R_1 = 0.0220, wR_2 = 0.0424	R_1 = 0.0237, wR_2 = 0.0480

4.2.1 The molecular structures of 1a, 2a and 2b.

The ORTEP diagrams of **1a**, **2a** and **2b** are shown in Figures 10, 11 and 12 with selected bond distances and bond angles in Tables 10, 11 and 12 respectively. The geometry around the Pd atom in **1a**, **2a** and **2b** is distorted square planar with two *cis* sulfur and two *cis* phosphorus atoms. The bite angles that have sulfur atoms are in the range 87.09(3)-88.34(3)° while those that have phosphorus atoms are in the range 97.24(3)-102.44(3)°. The P-Pd-P bite angle of 97.24(3)° for **1a** is larger than that found in Pd(dppe)(3-$NH_2C_6H_4$)(S-^{t}Bu) (84.89(8)°)[87]. This can be ascribed to the bulkiness of the ferrocenyl moiety, which tend to enlarge P-Pd-P bite angles. In different studies by Hayashi[73] and Dierkes *et al.*[88], large P-Pd-P bite angles were found to play a significant role in catalytic applications. The P-Pd-P bite angle in **1a** is comparable to the value of 99.07° found in Pd(dppf)Cl_2[73] but smaller than the values 102.44(3) and 101.88(3)° found in **2a** and **2b** respectively. Larger phosphorus bite angles were found in the dippf complexes and are amongst the largest found for diphosphinoferrocene complexes. Even in the complex Pd(dippf)$(SC_6H_5)_2$[89], the P-Pd-P angle of 101.09(2)° was found to be large. The bite angles are large in **2a** (102.44(3)°) and **2b** (101.88(3)°) due to the more bulky isopropyl groups. These larger bite angles in **2a** and **2b** lead to the concomitant reduction of the S-Pd-S bond angles of 87.09(3)° and 87.30(3)° respectively compared to the same angle in **1a** (88.34(3)°).

The Pd-P bond distances in **1a**, **2a** and **2b** are consistently similar, with one of the two Pd-P distances in each compound slightly longer. If one assumes that a normal Pd-P bond distance is 2.29 Å (the value obtained by averaging 2422 Pd-P bond distances reported in

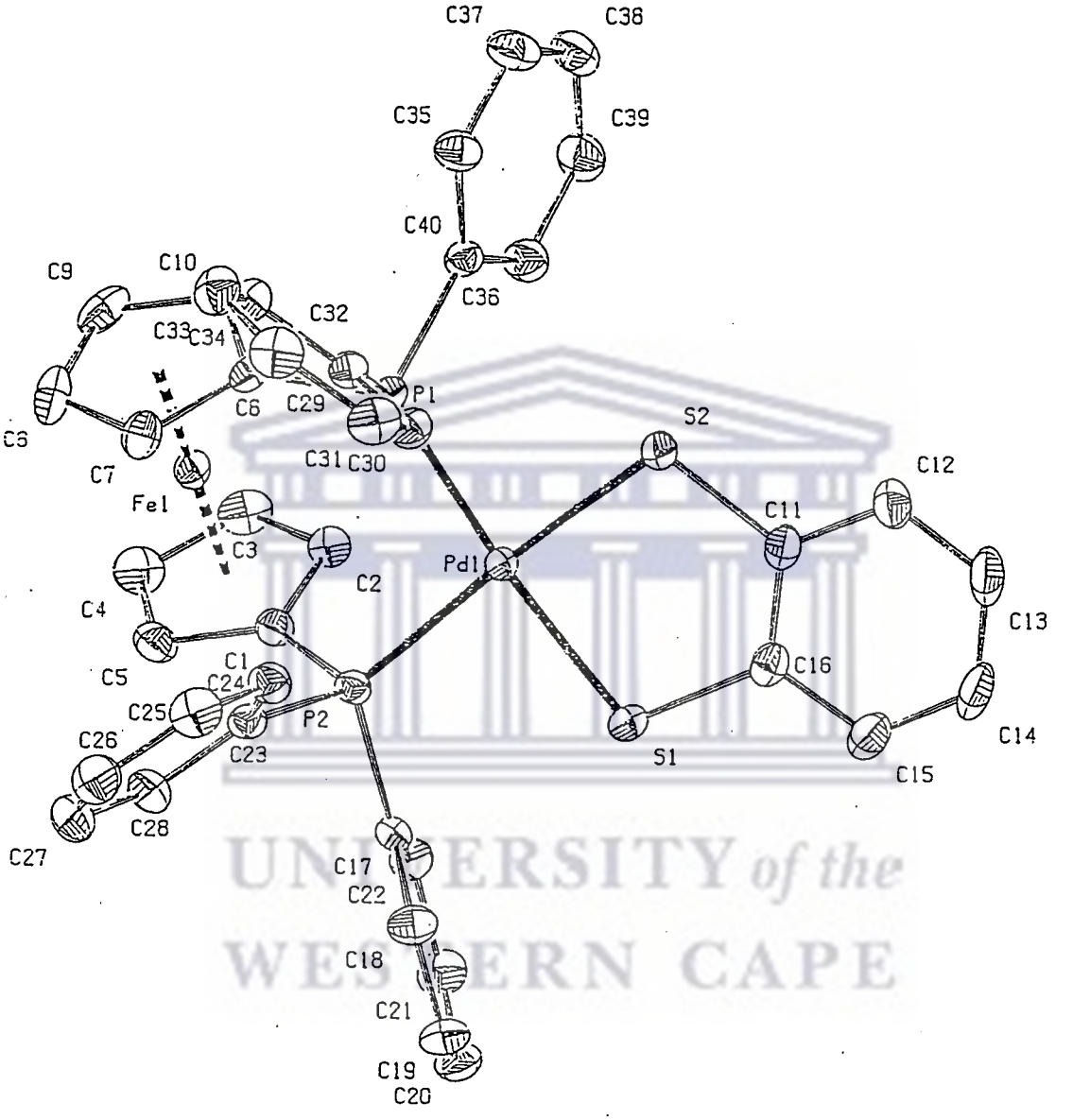

Fig. 10 The ORTEP drawing of **1a**.

Table 10: Selected bond distances and bond angles of Pd(dppf)(SC_6H_4S-o).

Bond distances (Å)			
Pd-S(1)	2.296(8)	P(2)-C(1)	1.797(2)
Pd-S(2)	2.304(8)	P(2)-C(23)	1.825(2)
Pd-P(1)	2.329(9)	P(2)-C(17)	1.827(2)
Pd-P(2)	2.312(7)	P(1)-C(6)	1.815(2)
S(1)-C(16)	1.762(3)	P(1)-C(40)	1.826(2)
S(2)-C(11)	1.757(2)	P(1)-C(29)	1.824(2)

Bond angles (°)			
S(1)-Pd-S(2)	88.34(3)	C(23)-P(2)-Pd	112.21(8)
S(1)-Pd-P(2)	88.12(3)	C(17)-P(2)-Pd	117.54(7)
S(2)-Pd-P(2)	176.45(2)	C(6)-P(1)-Pd	121.85(7)
S(1)-Pd-P(1)	174.40(2)	C(40)-P(1)-Pd	112.41(8)
S(2)-Pd-P(1)	86.31(3)	C(29)-P(1)-Pd	112.42(8)
P(2)-Pd-P(1)	97.24(3)	C(16)-S(1)-Pd	104.51(8)
C(1)-P(2)-Pd	112.85(8)	C(11)-S(2)-Pd	104.83(9)

Table 11: Selected bond distances and bond angles of Pd(dippf)(SC_6H_4S-o)

Bond distances (Å)			
Pd-S(2)	2.305(9)	P(1)-C(1)	1.802(4)
Pd-S(1)	2.309(8)	P(1)-C(11)	1.864(4)
Pd-P(2)	2.343(8)	P(1)-C(14)	1.877(4)
Pd-P(1)	2.336(10)	P(2)-C(6)	1.816(3)
S(1)-C(23)	1.742(4)	P(2)-C(17)	1.855(4)
S(2)-C(28)	1.749(4)	P(2)-C(20)	1.867(3)

Bond angles (°)			
S(2)-Pd-S(1)	87.09(3)	C(28)-S(2)-Pd	105.48(14)
S(2)-Pd-P(1)	168.80(3)	C(1)-P(1)-Pd	119.98(12)
S(1)-Pd-P(1)	86.50(4)	C(11)-P(1)-Pd	112.59(15)
S(2)-Pd-P(2)	85.14(3)	C(14)-P(1)-Pd	113.90(14)
S(1)-Pd-P(2)	168.64(3)	C(6)-P(2)-Pd	121.83(11)
P(1)-Pd-P(2)	102.44(3)	C(17)-P(2)-Pd	113.43(12)
C(23)-S(1)-Pd	105.48(13)	C(20)-P(2)-Pd	112.12(11)

the Cambridge Structural Database (CSD)),[90] then the Pd-P bond distances in **1a**, **2a** and **2b** are slightly longer than normal. In particular, the average Pd-P bond lengths of 2.320 (**1a**), 2.339 (**2a**) and 2.331 Å (**2b**) are longer than Pd-P bond lengths found in [Ru(η^5-$C_5H_4O)_2$]$PdPPh_3$ (2.295(1) Å)[91] and $Pd(dppf)Cl_2$ (2.301(5) Å)[73]. Even if one compares

the obtained Pd-P bond lengths with that reported for $Pd(dppm)Cl_2$, $Pd(dppe)Cl_2$ and $Pd(dppp)Cl_2$, the literature values[92] are still shorter than that found in **1a**, **2a** and **2b**. As was the case with Pd-P bond distances, one out of the two Pd-S bond distances in each complex is slightly longer. The average Pd-S bond distances in **1a** (2.300 Å), **2a** (2.307 Å) and **2b** (2.310 Å) are similar to typical Pd-S bond distances (2.300 Å) obtained by averaging 340 such distances extracted from the CSD.[90] The ferrocene moiety is quite typical with the rings in a staggered conformation. This is easily determined by taking selective torsion angles of two cyclopentadienyl ring atoms of one ring and the corresponding two atoms of the other cyclopentadienyl ring.

4.2.2 The molecular structures of 3a and 3d.

The molecular structures of **3a** and **3d** are shown in Figures 13 and 14 with selected bond distances and bond angles in Tables 13 and 14. The ferrocene moiety is quite typical, with the pentahapto cyclopentadienyl rings in a staggered conformation. The mercaptophenolate ligand is chelated to the Pt via the sulfur atom and oxygen atoms. The geometry about the platinum atom is a distorted square planar with two *cis* phosphorus atoms, the oxygen and sulfur atoms also in a *cis* configuration for **3d**. The ligand bite angles that have sulfur atoms are in the range 85.89(7)-88.26(4)° but both Pt complexes have *cis*-angles of 96.19(3)° for the phosphorus atoms. The P-Pt-P bite angles of 96.19(3)° is smaller than that found in $Pt(dppf)Cl_2$ (99.30°)[93] and Pt(dppf)(bph) (98.60°) (bph = biphenyl).[93] This bite angle is larger than P-Pt-P angles found for the series Pt(dppm)(7,8-bzq) (72.1°), Pt(dppe)(bzq) (84.5°) and Pt(dppp)(bzq) (91.6°) (bzq = benzoquinoline)[94]. The larger P-Pt-P bite angle can be attributed to the large size of dppf

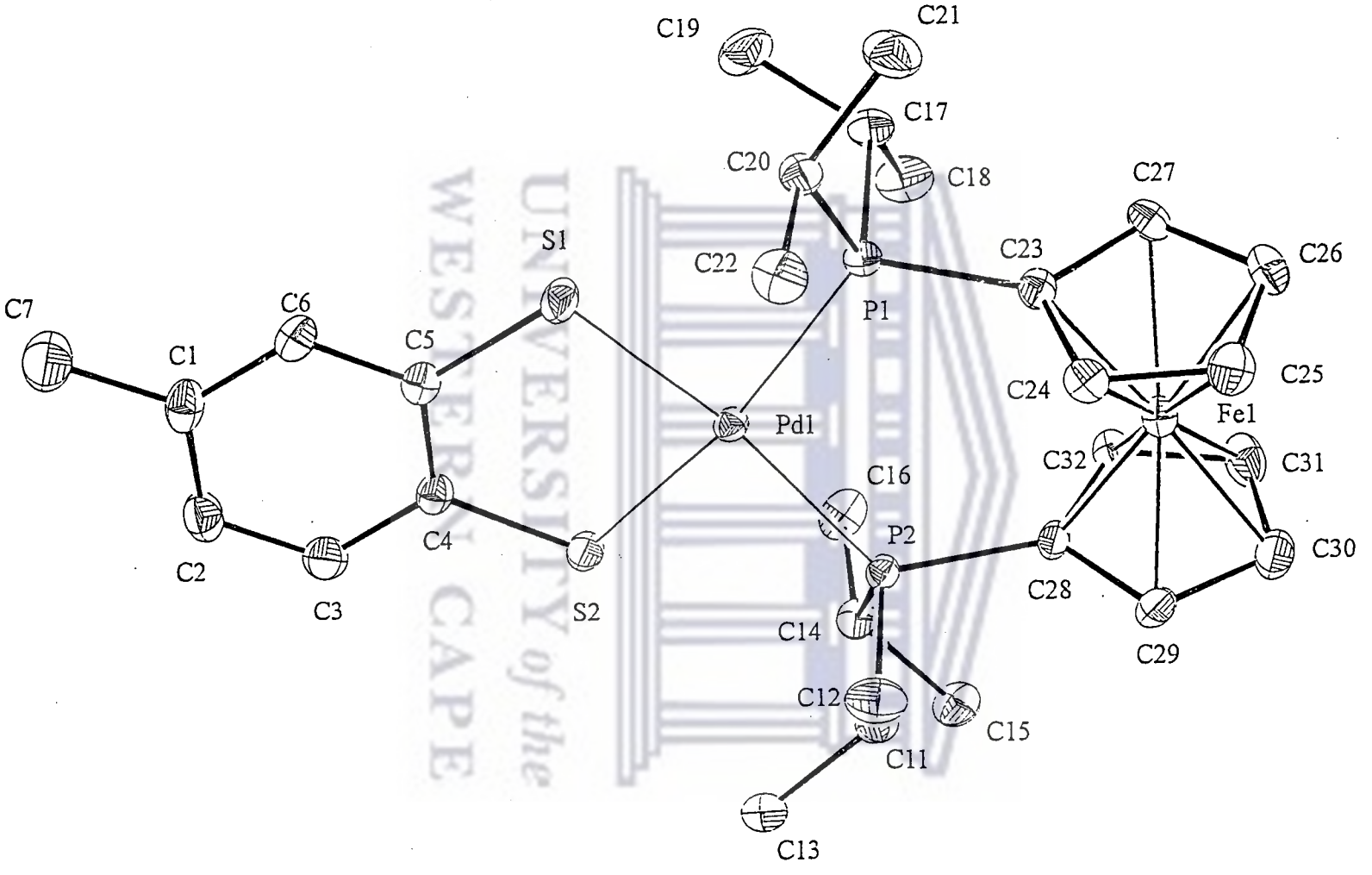

Fig. 12 The ORTEP drawing of **2b**.

Table 12: Selected bond distances and bond angles of Pd(dippf)(SC_6H_3MeS-o)

Bond distances (Å)			
Pd-S(2)	2.319(8)	P(1)-C(23)	1.824(3)
Pd-S(1)	2.301(8)	P(1)-C(17)	1.855(3)
Pd-P(2)	2.333(8)	P(1)-C(20)	1.859(3)
Pd-P(1)	2.329(8)	P(2)-C(28)	1.829(3)
S(1)-C(5)	1.752(3)	P(2)-C(11)	1.849(3)
S(2)-C(4)	1.764(3)	P(2)-C(14)	1.861(3)

Bond angles (°)			
S(1)-Pd-S(2)	87.30(3)	C(4)-S(2)-Pd	104.86(10)
S(2)-Pd-P(1)	169.41(3)	C(23)-P(1)-Pd	120.99(9)
S(1)-Pd-P(1)	84.94(3)	C(17)-P(1)-Pd	114.32(10)
S(2)-Pd-P(2)	86.67(3)	C(20)-P(1)-Pd	111.43(11)
S(1)-Pd-P(2)	170.66(3)	C(28)-P(2)-Pd	122.32(9)
P(1)-Pd-P(2)	101.88(3)	C(11)-P(2)-Pd	113.27(10)
C(5)-S(1)-Pd	106.00(10)	C(14)-P(2)-Pd	112.24(10)

ligand compared to dppm, dppe and dppp ligands. The enforced P-Pt-P angle suppresses the O-Pt-S bond angle to 85.89(7)° and tend to strain also the O-Pt-P(2) bond angle to 81.52(7)° in **3d**. In **3a** the large bite angle reduces the S-Pt-S angle to 88.26(4)°.

The Pt-P bond distances in **3a** (2.308(10) and 2.309(10) Å) are closer to the normal distance of 2.29 Å (mean value for 5404 Pt-P bond distances extracted from the CSD)[90], whilst the Pt-P bond distances in **3d** had two sets of values, both shorter than normal (2.226(8) and 2.289(9) Å). The Pt-P bond distance of the phosphorus atom *trans* to the sulfur atom in **3d** is 2.289(9) Å compared to 2.226 Å for the Pt-P bond distance of the phosphorus atom *trans* to the oxygen atom in this complex. This is the effect of the *trans*-influence of the sulfur atom on the phosphorus *trans* to it, and is similar to the trend found in $Pt(PPh_3)_2(SC_6H_4CO_2\text{-}o)$ (Pt-P *trans* to sulfur being 2.303(11) Å and Pt-P *trans* to oxygen being 2.250(11) Å).[50b]

The Pt-S bond distances in **3a** are similar to the Pd-S ones. These are however shorter than Pt-S bonds reported for $Pt(PPh_3)_2(SC_6H_4CO_2\text{-}o)$ (2.322(2) Å)[50b] and $Pt(SC_6H_4CO_2\text{-}o)(XyNC)$ (XyNC = 2,6-xylyl) (2.340(8) Å).[51] Henderson *et al.*[50b] have ascribed this to the high *trans*-influence of PPh_3 as compared to the low *trans*-influence of pyridine in $Pt(PPh_3)(py)(SC_6H_4CO_2\text{-}o)$ (Pt-S = 2.255(3) Å)[51]. The *trans*-influence of dppf could lie between that of PPh_3 and py and hence the intermediate value of Pt-S observed for **3d**.

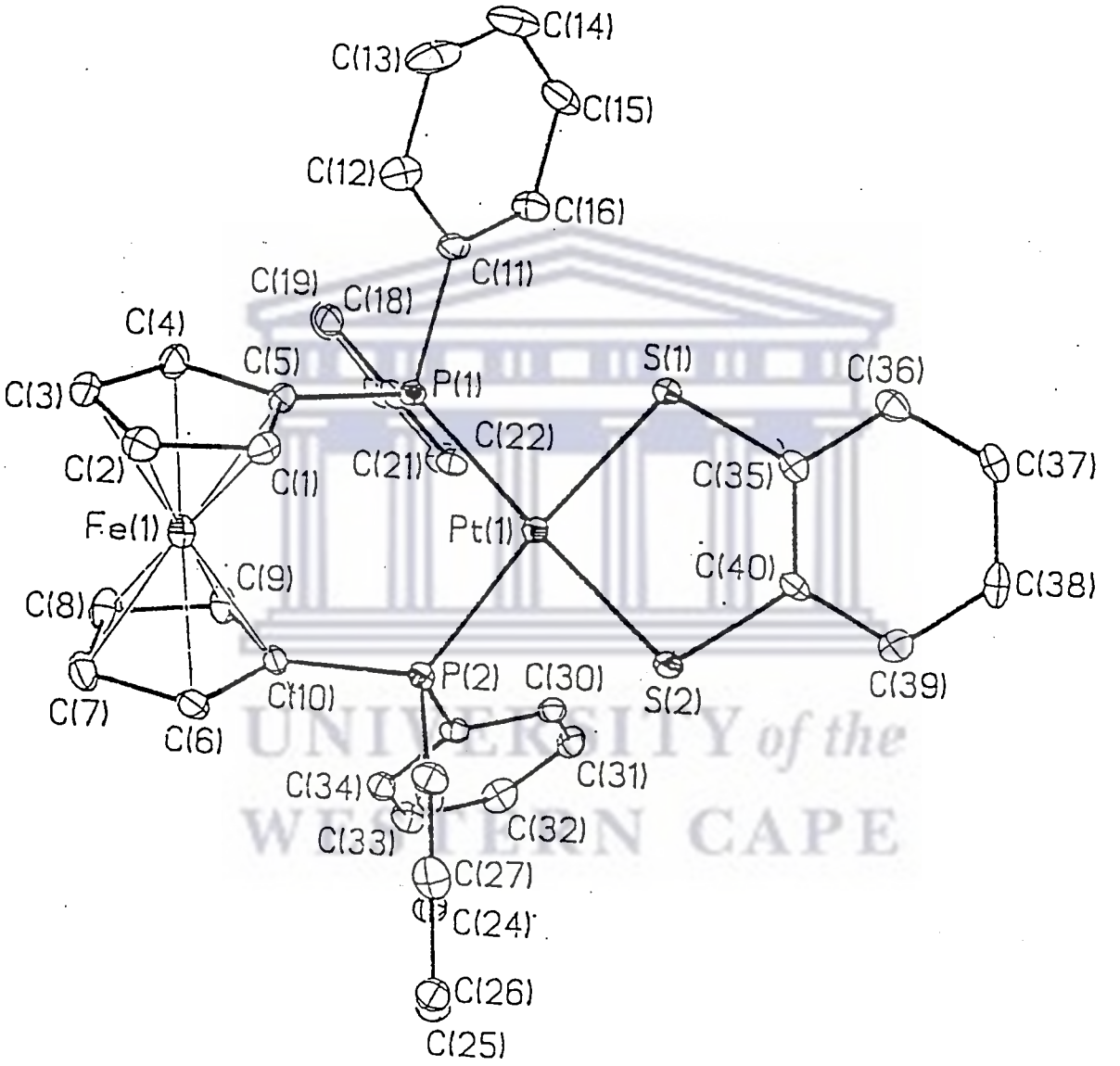

Fig. 13 The ORTEP drawing of **3a**.

Table 13: Selected bond distances and bond angles of Pt(dppf)(SC_6H_4S-o)

Bond distances (Å)			
Pt-S(2)	2.308(10)	P(1)-C(5)	1.790(4)
Pt-S(1)	2.309(10)	P(1)-C(17)	1.825(4)
Pt-P(2)	2.301(10)	P(1)-C(11)	1.833(4)
Pt-P(1)	2.288(9)	P(2)-C(10)	1.821(4)
S(1)-C(35)	1.761(4)	P(2)-C(29)	1.826(4)
S(2)-C(40)	1.765(4)	P(2)-C(23)	1.836(4)

Bond angles (°)			
S(2)-Pt-S(1)	88.26(4)	C(40)-S(2)-Pt	104.53(15)
S(2)-Pt-P(1)	177.42(4)	C(5)-P(1)-Pt	112.71(13)
S(1)-Pt-P(1)	89.17(4)	C(17)-P(1)-Pt	112.79(14)
S(2)-Pt-P(2)	86.39(3)	C(11)-P(1)-Pt	117.71(12)
S(1)-Pt-P(2)	174.40(4)	C(10)-P(2)-Pt	122.51(14)
P(1)-Pt-P(2)	96.19(3)	C(29)-P(2)-Pt	113.01(12)
C(35)-S(1)-Pt	104.85(15)	C(23)-P(2)-Pt	112.35(13)

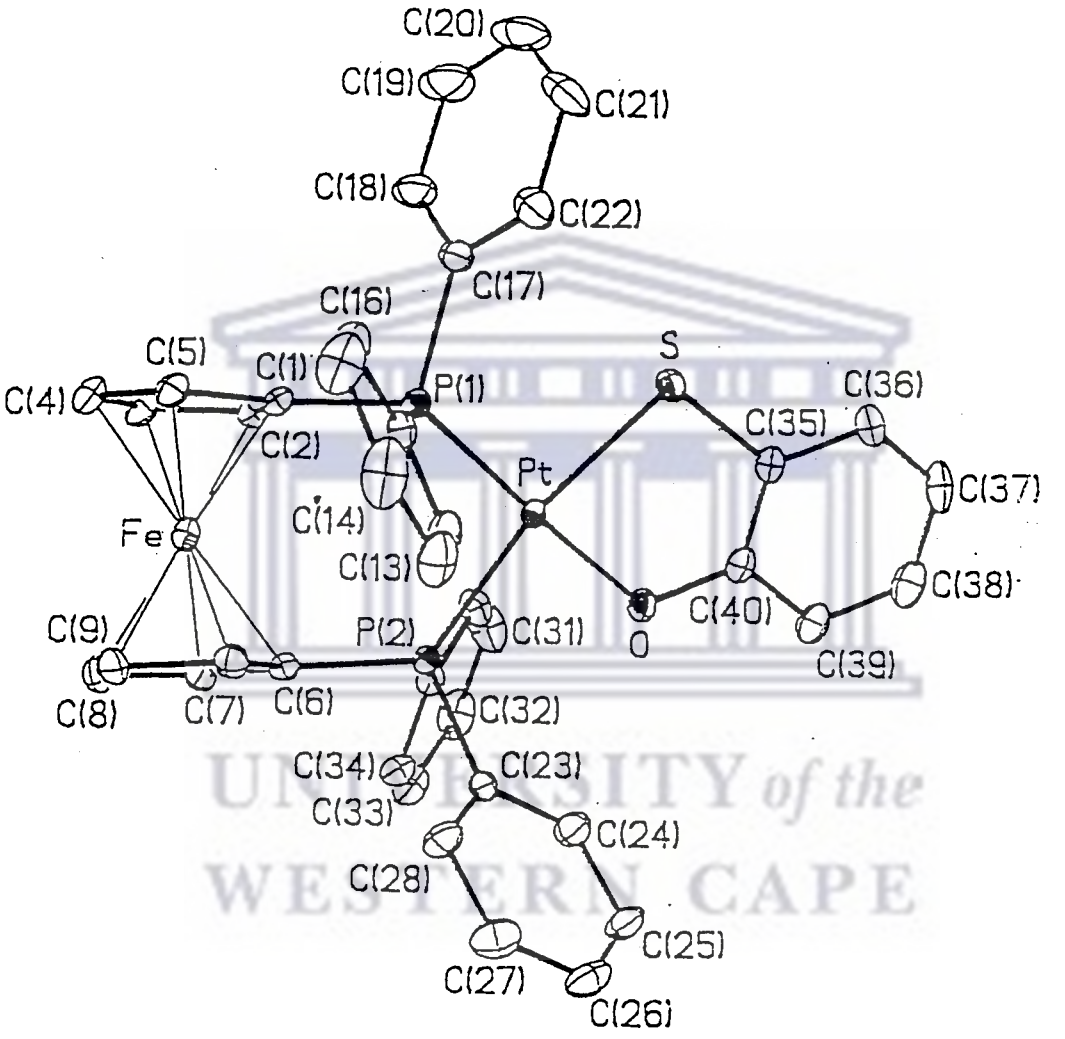

Fig. 14 The ORTEP drawing of **3d**.

Table 14. Selected bond distances and angles of Pt(dppf)(SC_6H_4O-o)

Bond distances (Å)			
Pt-O	2.028(2)	P(1)-C(17)	1.827(4)
Pt-P(1)	2.225(8)	P(2)-C(6)	1.809(3)
Pt-P(2)	2.288(9)	P(2)-C(29)	1.821(3)
Pt-S	2.296(9)	P(2)-C(23)	1.824(3)
P(1)-C(1)	1.813(3)	O-C(40)	1.341(4)
P(1)-C(11)	1.819(3)	S-C(35)	1.760(3)

Bond angles (°)			
O-Pt-P(1)	177.08(7)	P(2)-Pt-S	167.26(3)
O-Pt-P(2)	81.52(7)	C(35)-S-Pt	96.92(12)
P(1)-Pt-P(2)	101.12(3)	C(1)-P(1)-Pt	116.75(11)
O-Pt-S	85.89(7)	C(40)-O-Pt	117.60(2)
P(1)-Pt-S	91.51(3)	C(6)-P(2)-Pt	122.94(11)

4.2.3 The structure of 2g.

X-ray crystallography of **2g** not only gave a quick confirmation of the proposed structure from the ^{1}H NMR spectra, but it also confirmed the failure to get Te insertion into the C-Li bond of $LiSC_6H_4Li$-*o* as expected from the literature.[82a]

The molecular structure of **2g** is shown in Fig. 15 and selected bond distances and angles are presented in Table 15. The Pd atom in **2g** exhibits a square planar geometry with the *cis* angles ranging between 85.78(2)-101.09(2)° and the *trans* angles are 168.45(2) and 170.55(2)°. The presence of two alkyl substituents on the phosphorus atoms results in the expansion of the P-Pd-P angle to 101.09(2)° with a concomitant reduction of the S-Pd-S angle to 87.69(1)°. The corresponding angles in $Pd(dppf)Cl_2$ are 99.07(5)° and 87.80(1)°, while in $Pd(dppf)(SC_6H_4S\text{-}o)$ (**1a**), they are 97.24(3) and 88.34(3)° respectively. In **2g**, atoms Pd, S(1), S(2), and P(2) are planar within 0.07 Å while phosphorus P(1) is displaced 0.570(1) Å out of the plane. The Pd-P distances are slightly different (2.330(6) and 2.346(7) Å), with the Pd-P(1) distance being 0.016(3) Å shorter. The Pd-P bond lengths in **2g** are somewhat longer than the 'normal' Pd-P bond of 2.290(5) Å. The latter value was obtained by averaging of 2422 Pd-P distances in complexes reported in the (CSD)[90]. The Pd-S distances in **2g** (2.388(7) and 2.370(7) Å) are also different with the Pd-S bond *trans* to atom P(2) being 0.018(7) Å longer. Both Pd-S distances in **2g** are longer than the length of the 'typical' Pd-S distances (2.30(3) Å) obtained by averaging 340 Pd-S distances found in the relevant complexes reported in the CSD[90]. The phenyl groups on the sulfur atoms point to the opposite sides of the plane defined by the Pd and two S atoms. The Pd-S-S angles are close to the ideal tetrahedral value of 109.4°. The ferrocene moiety is again quite typical with the rings in a staggered conformation.

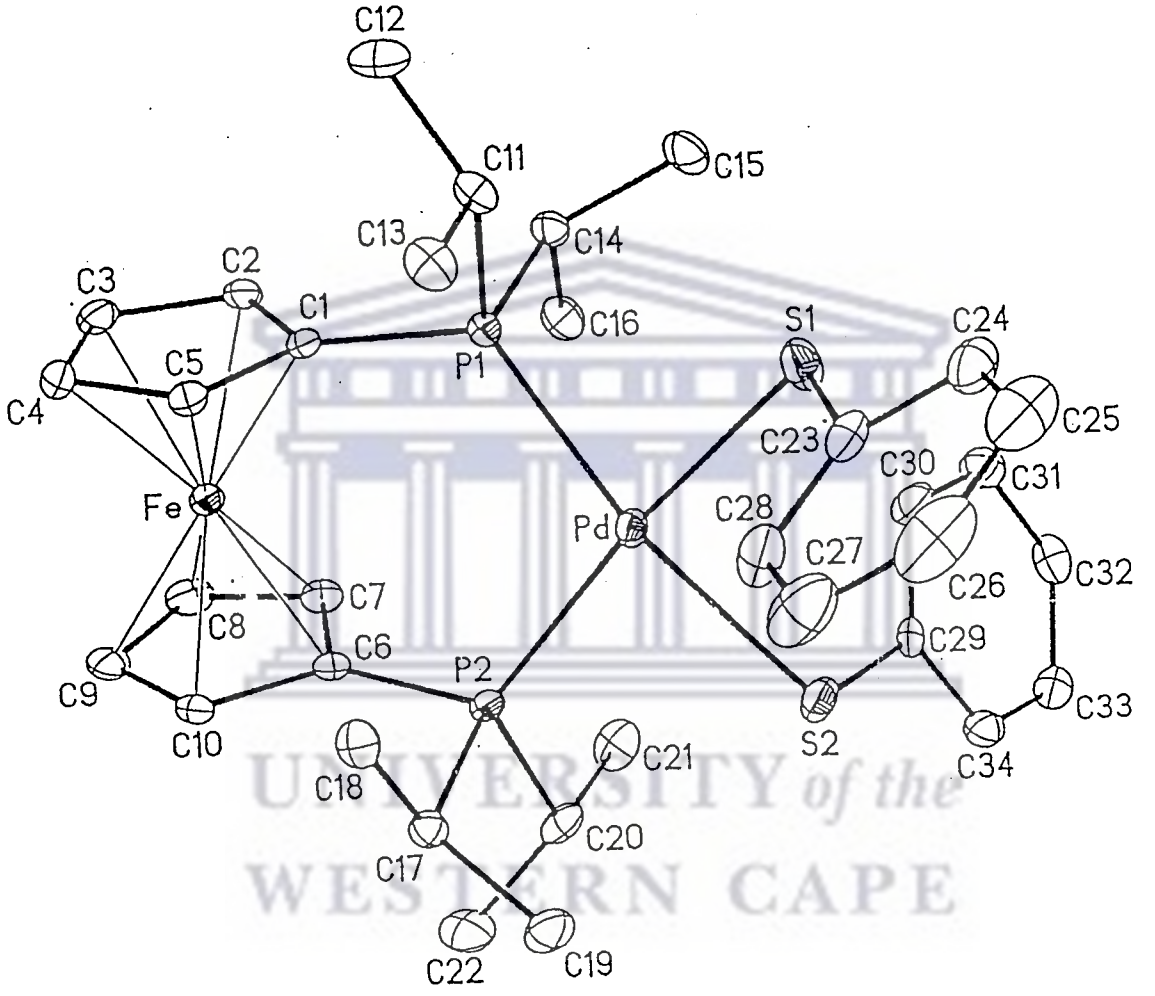

Fig. 15 The ORTEP drawing of **2g**.

Table 15. Selected bond distances and bond angles for Pd(dippf)(SC_6H_5)$_2$

Bond distances (Å)			
Pd-P(1)	2.330(6)	P(1)-C(1)	1.809(2)
Pd-P(2)	2.346(7)	P(1)-C(11)	1.853(2)
Pd-S(2)	2.370(7)	P(1)-C(14)	1.853(2)
Pd-S(1)	2.388(7)	P(2)-C(6)	1.816(2)
S(1)-C(23)	1.757(3)	P(2)-C(20)	1.855(2)
S(2)-C(29)	1.770(2)	P(2)-C(17)	1.858(2)

Bond angles (°)			
P(1)-Pd-P(2)	101.09(2)	S(2)-Pd-S(1)	87.69(3)
P(1)-Pd-S(2)	168.45(2)	C(23)-S(1)-Pd	107.19(9)
P(2)-Pd-S(2)	86.56(2)	C(29)-S(2)-Pd	103.26(8)
P(1)-Pd-S(1)	85.78(2)	C(1)-P(1)-Pd	123.45(8)
P(2)-Pd-S(1)	170.55(2)	C(6)-P(2)-Pd	122.46(7)

CHAPTER 5

ELECTROCHEMISTRY

Electrochemical studies of Pd(dppf), Pd(dippf) and Pt(dppf) aryldithiolato and mixed aryldichalcogenide complexes.

Cyclic voltammetry (CV) is perhaps the most versatile electroanalytical technique for the study of electroactive species. Its versatility combined with ease of measurement has resulted in extensive use of cyclic voltammetry in the fields of electrochemistry, inorganic chemistry, and biochemistry.[95] Cyclic voltammetry is often the first experiment performed in an electrochemical study of a compound. The effectiveness of CV results from its capability for the rapid observation of redox behaviour over a wide potential range. The resulting voltammogram is analogous to a conventional spectrum in that it conveys information as a function of an energy scan. For a redox activity to be reversible, three conditions must be met, namely: (i) the peak currents should be the same irrespective of the scan rate; i.e. $i_c / i_a \approx 1$ (where i_a is the anodic current and i_c is the cathodic current); (ii) the peak potentials should not vary with scan rate. (iii) the difference between the oxidation and reduction peak potentials should be approximately 60 mV.

In this project cyclic voltammetry was used to investigate the electrochemical behaviour of the complexes synthesised, cycling between –1000 and 1600 mV. Since in this study ferrocene was used an internal standard, the reversibility of the complexes was referenced to ferrocene as it is known to give a reversible redox couple that involves the transfer of one electron. There are two main centres of redox activity that were observed in the

cyclic voltammetry of all the complexes. The first redox activities were quasi-reversible peaks with less positive potentials between 400 and 1100 mV (Table 16). The second redox activities were more positive potentials between 800 and 1400 mV (Fig. 17). The former redox activity is ligand-based as reported for the analogous nickel(II) complexes of the general formula Ni(dppe)($SC_6H_3H_3RE$-*o*) (E = S, O, Se; R = H, Me).[27] Other ligand-based redox activity for nickel complexes have been reported by Bowmaker *et al.* for M(dppe)($S_2C_2Ph_2$) (M = Ni, Pd, Pt) and Ni(dppe)(SC_6H_3MeS-*o*)[96]. In contrast to the redox behaviour of the nickel complexes, both Pd and Pt complexes displayed cathodic peaks, signifying that some stabilisation of the oxidised species is provided by M(dppf) (M = Pd, Pt) and Pd(dippf) fragments that allow the oxidised species to pick up electrons. Further evidence of the ligand-based redox activity is obtained from the cyclic voltammograms of M(dppf)Cl_2 (M = Pd, Pt) and Pd(dippf)Cl_2 (Fig. 16) that showed only one redox activity in the region 800-1100 mV assigned to the dppf and dippf ligands. From the voltammograms, it can be observed that the redox activity of the complexes ranged from quasi-reversibility to irreversibility. The second redox activity was the irreversible oxidation of dppf or dippf. Irreversible ferrocene-based redox behaviour when dppf is bound to a metal is exemplified by Pd(dppf)B_3H_7[97].

In complexes containing homoleptic sulfur ligands (**1a-c**, **2a-c** and **3a-c**) the ease of oxidation of the ligand was **b** > **a** > **c** (Fig. 17). This conforms to the effect of either an electron releasing group (**b**) or an electron withdrawing group (**c**) on the ligand. The trend is in line with a ligand-based oxidation as any direct substitution on the ligands would affect the electron density. In particular, the oxidation potentials of the complexes **2b**, **2a**

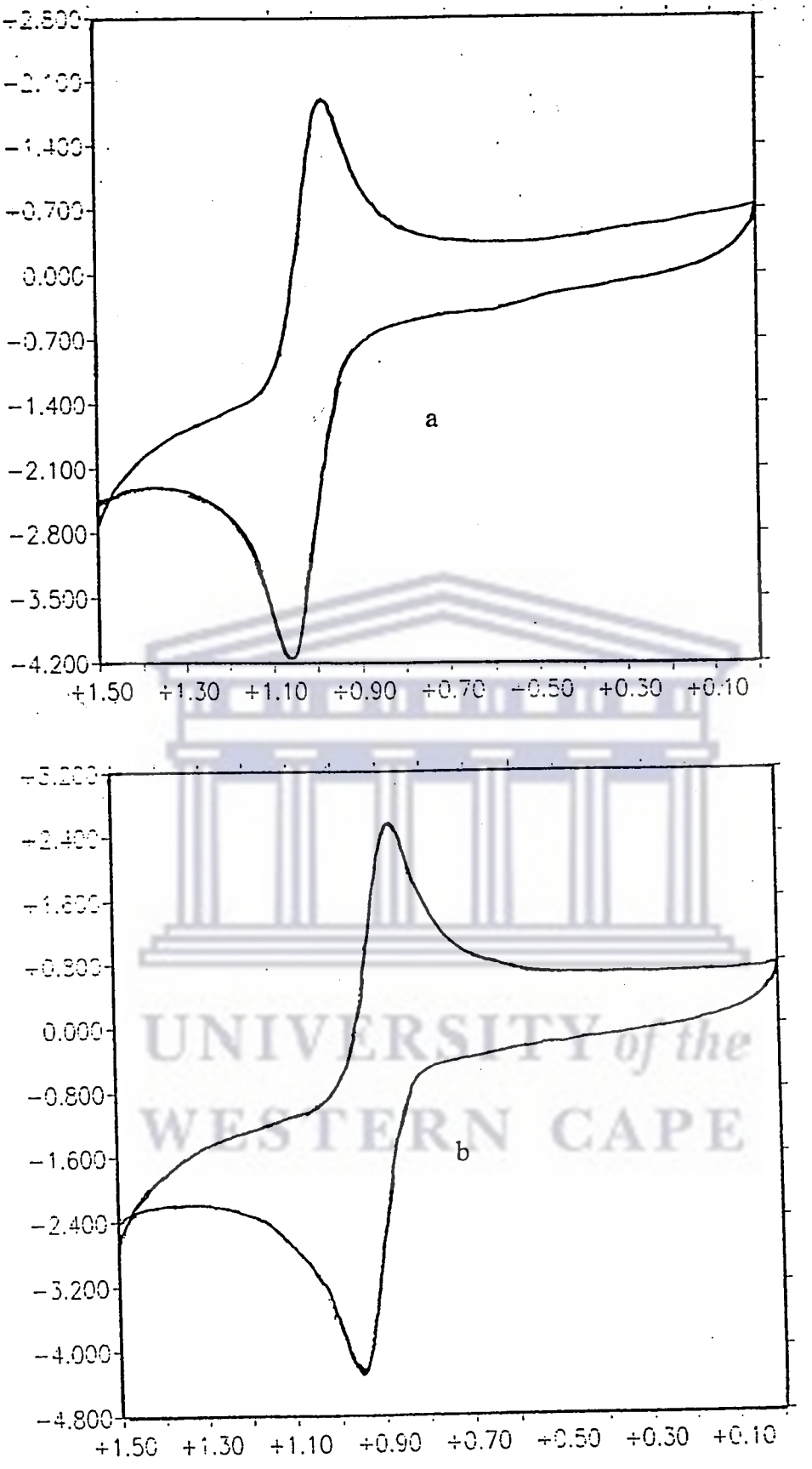

Fig.16 Cyclic voltammograms of $Pd(dppf)Cl_2$ (a) and $Pd(dippf)Cl_2$ (b).

and **2c** were found to be 665, 730 and 881 mV respectively for the ligand. The representative voltammograms of compounds **3a**, **3b**, **3c** and **3e** are shown in Fig. 17 to illustrate the effect of the substituents on the oxidation potentials of the ligand. Table 16 gives the electrochemical data for all the complexes studied.

The mixed aryldichalcogenide metal complexes had oxygen and sulfur atoms bound to the metals. Where there was a simple oxygen atom involved, as in **1d, 2d** and **3d**, the anodic peaks were at lower potentials than the peaks for the homoleptic sulfur compounds. However, for the complexes featuring a carbonyl functional group (**1e-f, 2e-f** and **3e-f**), anodic peaks were as high as those found in the **c** series (i.e. **1c**, **2c** and **3c**). The high values for the anodic peaks of the carbonyl-containing ligands are due to the electron-withdrawing effect of the carbonyl, which makes oxidation difficult. It is worth noting that the pyridine-based metal complexes (**1f**, **2f** and **3f**) displayed broad single oxidation peaks. A rotating disc experiment revealed two separate oxidation processes at the observed peak values, implying that the voltammograms were overlapping oxidation peaks of the thiolato ligands and the one associated with either dppf or dippf. The overlapping might be due to the nitrogen atom in the pyridine withdrawing electrons from the aryldithiolato ligand, thus making it difficult to oxidise. As a result of this, the ligand redox activity merges with the one associated with either the dppf or dippf. The complexes containing pyridine-based ligands were found to be quasi-reversible compared to the others. This could be determined from the current ratios and the change in potential. In particular, for **1f** $\Delta E = 69$ mV and $i_c/i_a = 0.88$. The values are very close to the $\Delta E = 60$ mV and $i_c/i_a = 1$, needed for a complete reversible redox activity.

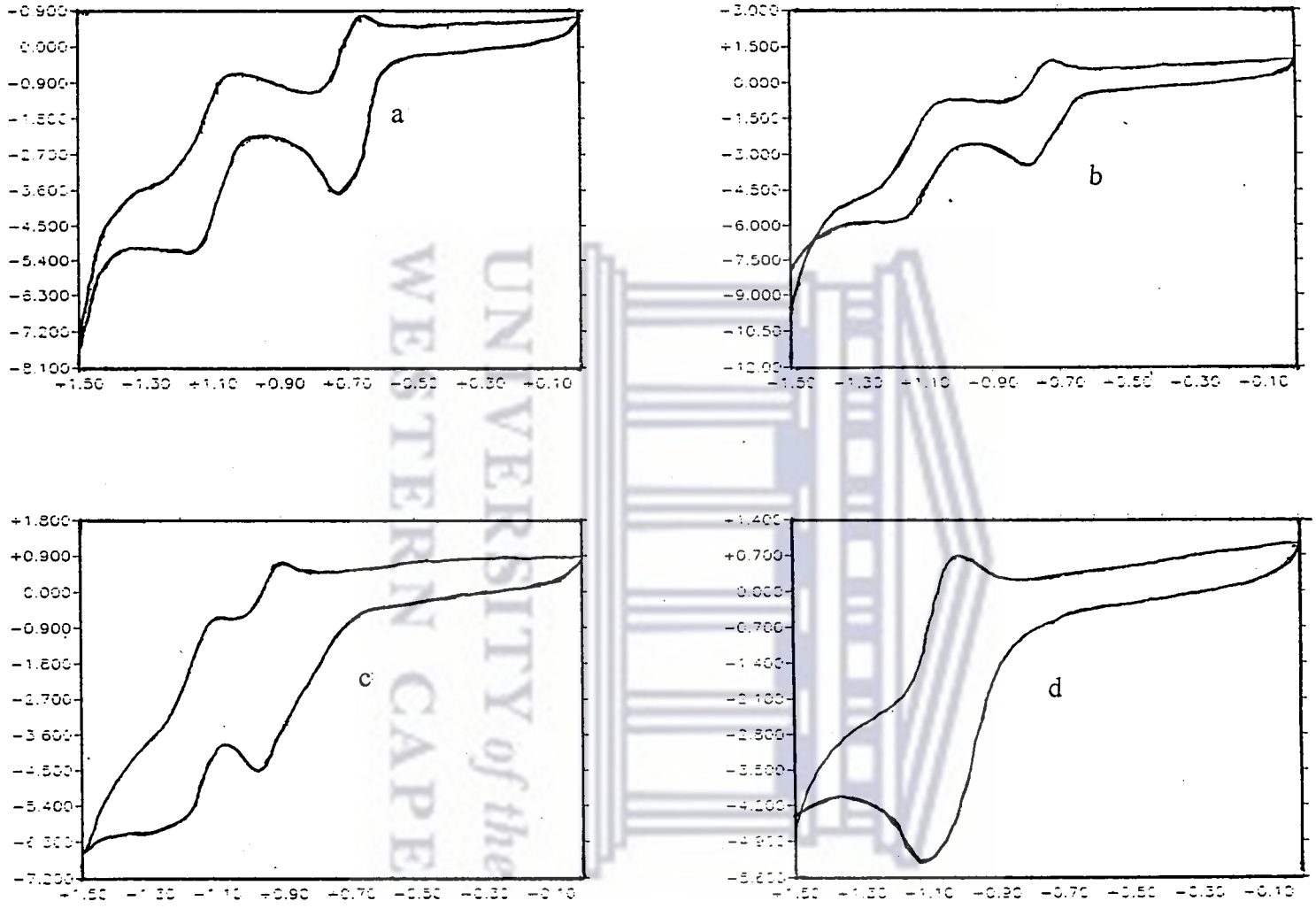

Fig. 17 Cyclic voltammograms of **3b** (a), **3a** (b), **3c** (c) and **3f** (d).

The second redox activity is associated with dppf and dippf ligands. Although dppf is known to oxidise irreversibly, when complexed to a metal (e.g. Pd, Pt) it gives a quasi-reversible redox couple. This has been established for $M(dppf)Cl_2$ (M = Pd, Pt) and $Pd(dippf)Cl_2$ (Fig. 16). The redox activity of the dppf or dippf in the complexes did not follow a well-defined trend. Complexes containing the dppf where found to have less reversible redox behaviour compared to the ones containing the dippf ligand. This could be deduced from Table 16 where the current ratios for the dppf complexes are close to 0.5. Unlike the aryldithiolato ligand potentials that had a close effect with the substituent, the phosphines had no such effect and thus difficult to rationalise peak values. The dppf and dippf ligand peaks are observed after the ligands have been oxidised (which can cause decomposition etc.). Thus, these peaks only represent the state of the complexes after the ligands have been destroyed. An attempt to postulate possible structures of the oxidised species failed as the complexes did not follow a well-defined trend with respect to oxidation. In general, the dippf complexes were easier to oxidise compared to the dppf complexes due to the better electron donating ability of dippf. The Pd complexes have lower oxidation potentials than the analogues Pt complexes.

Table 16: Electrochemical data of Pd(dppf), Pd(dippf) and Pt(dppf) complexes.

Complex	Oxidation peaks for arylthilato ligand (mV)	ΔE for arylthiolato ligand (mV)	i_c/i_a for arylthiolato ligand	Oxidation peaks for diphosphino ligand (mV)	ΔE for diphosphino ligand (mV)	i_c/i_a for diphosphino ligand
1a	718	80	0.35	1113	68	0.69
1b	663	134	0.40	1110	226	0.58
1c	934	64	0.33	1315	219	0.72
1d	495, 765	66	0.38	1225	179	0.68
1e	978	66	0.36	1172	121	0.28
1f	-	69	0.88	1122	86	0.64
1g	523	115	0.49	1159	142	0.78
2a	730	87	0.76	1080	129	0.93
2b	665	84	0.68	1134	201	0.52
2c	881	75	0.72	1233	158	0.78

2d	470, 709	83	0.71	900, 998	79	0.65
2e	508, 784	87	0.93	955	74	0.92
2f	-	80	0.92	1034	83	0.61
2g	820	97	0.87	1127	114	0.81
3a	792	70	0.60	1258	202	0.61
3b	686	64	0.40	1275	117	0.69
3c	965	66	0.41	1227	155	0.62
3d	593	76	0.61	1193	216	0.46
3e	1012	62	0.39	1207	142	0.52
3f	-	68	0.63	1102	79	0.75
3g	570	88	0.82	1165	72	0.83
$Pd(dppf)Cl_2$	-	-	-	106	65	0.86
$Pd(dippf)Cl_2$	-	-	-	952	69	0.92
$Pt(dppf)Cl_2$	-	-	-	114	62	0.75

CHAPTER 6

REACTIONS

Reactions of the complexes with dimethylacetylenedicarboxylate (DMAD) and sulfur dioxide (SO_2).

This chapter describes the reactions of the Pd and Pt aryldichalcogenide complexes with acetylenes and sulfur dioxide. The reactions were performed to test the nucleophilicity of the metal aryldichalcogenide complexes that were prepared. In general the sulfur atoms of metal thiolato complexes serve as nucleophiles.[17-18] Preliminary results of these reactions are presented in this chapter.

6.1 Reactions of M(dppf) (M = Pd, Pt) and Pd(dippf) aryldichalcogenide complexes with dimethylacetylene dicarboxylate (DMAD).

Solutions of the compounds **1a-b, 1d, 2a-b and 2d** and DMAD (1:50 mole ratio) in CH_2Cl_2/toluene (1:1) were refluxed, typically for 48 h, to yield the products in Scheme 7.

The reaction was very slow at room temperature and could take up to 10 days to complete but proceeded more rapidly at higher temperatures. The compounds were isolated as a mixture of two dominant products, the cyclotrimerisation product, hexamethylbenzene hexacarboxylate (HMBC) and the cyclodimerisation product, tetramethylcyclobuta-1,3-dienetetracarboxylate (TMCTC). This is in contrast to the results obtained from reactions of Ni(dppe) thiolates with DMAD[27] where HMBC was the only product isolated. Of all the compounds tested only Pd(dppf)(SC_6H_4S-*o*) gave HMBC as the dominant product.

The HMBC was identified by its white colour, elemental analysis, mass spectrometry and NMR spectroscopy. On the other hand complexes **1b, 1d, 2a, 2b and 2d** gave the four-

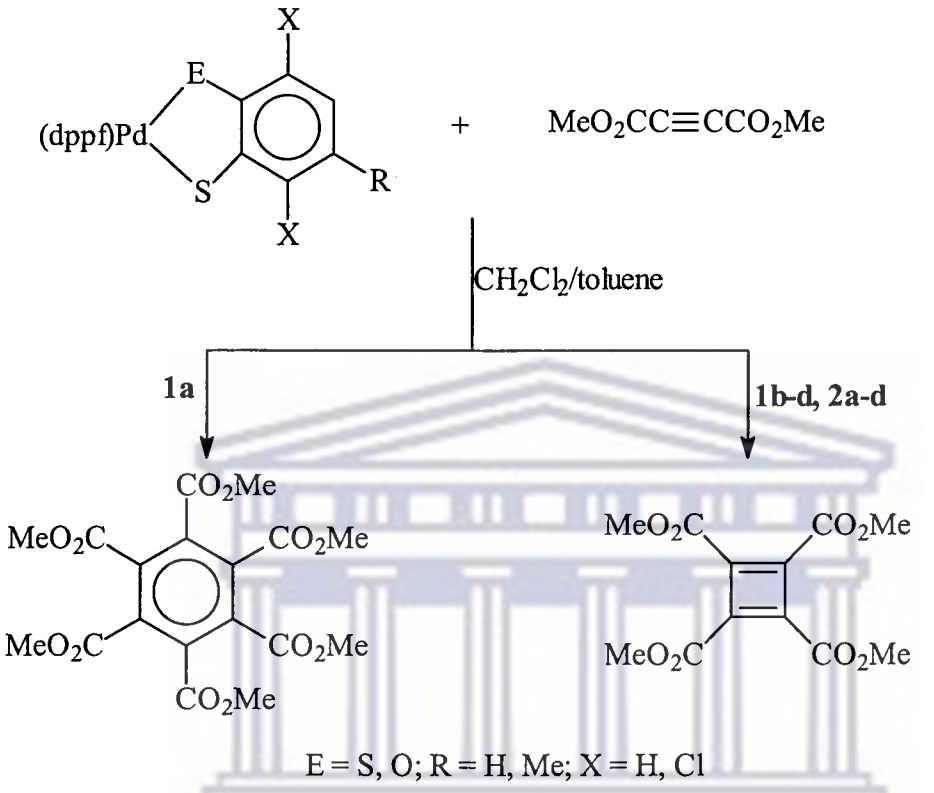

Scheme 7. Reactions of complexes with DMAD.

Table 17. Percentage conversion of DMAD by Pd(dppf) and Pd(dippf) aryldichalcogenide complexes.

Complex	Amount of DMAD used (mmol)	%Yield of HMBC	%Yield of TMCTC
1a	4.07	28	8
1b	4.07	11	32
1d	4.07	9	25

2a	4.07	14	22
2b	4.07	16	29
2d	4.07	11	18

membered cyclised product, TMCTC as the dominant product. The TMCTC is an oil. The ^{1}H NMR spectrum of HMBC (Fig. 18a) had singlet peak at 3.88 ppm, which is characteristic of the methyl protons of HMBC. Methyl protons of HMBC are more downfield relative to the normal region of methyl protons. The electron-withdrawing effect of the carboxylato groups causes a downfield shift of methyl protons.

The $^{13}C\{^{1}H\}$ NMR spectrum of HMBC (Fig. 18b) shows three peaks for the three different carbon atoms of the compound. The most upfield peak at 53.48 ppm was assigned to the shielded methyl carbon. The peak at 133.89 ppm is in the aromatic region and is due to the benzene carbons, all of which are equivalent and was observed as only one peak. The appearance of a peak in the aromatic region strongly suggested the cyclisation of DMAD. The peak which appears most downfield at 165.12 ppm is due to the carbonyl carbon.

The electron impact mass spectrometry (EI-MS) of HMBC (Fig. 19a) showed the molecular ion peak at m/z = 426 with an intensity of 12%. The parent peak of the compound was m/z = 395 which corresponds to the loss of OMe from the molecular ion. The mass spectrum thus served as evidence that the DMAD cyclisation product was HMBC. In a study by Darkwa and co-workers[27] HMBC is found to lose OMe as the first

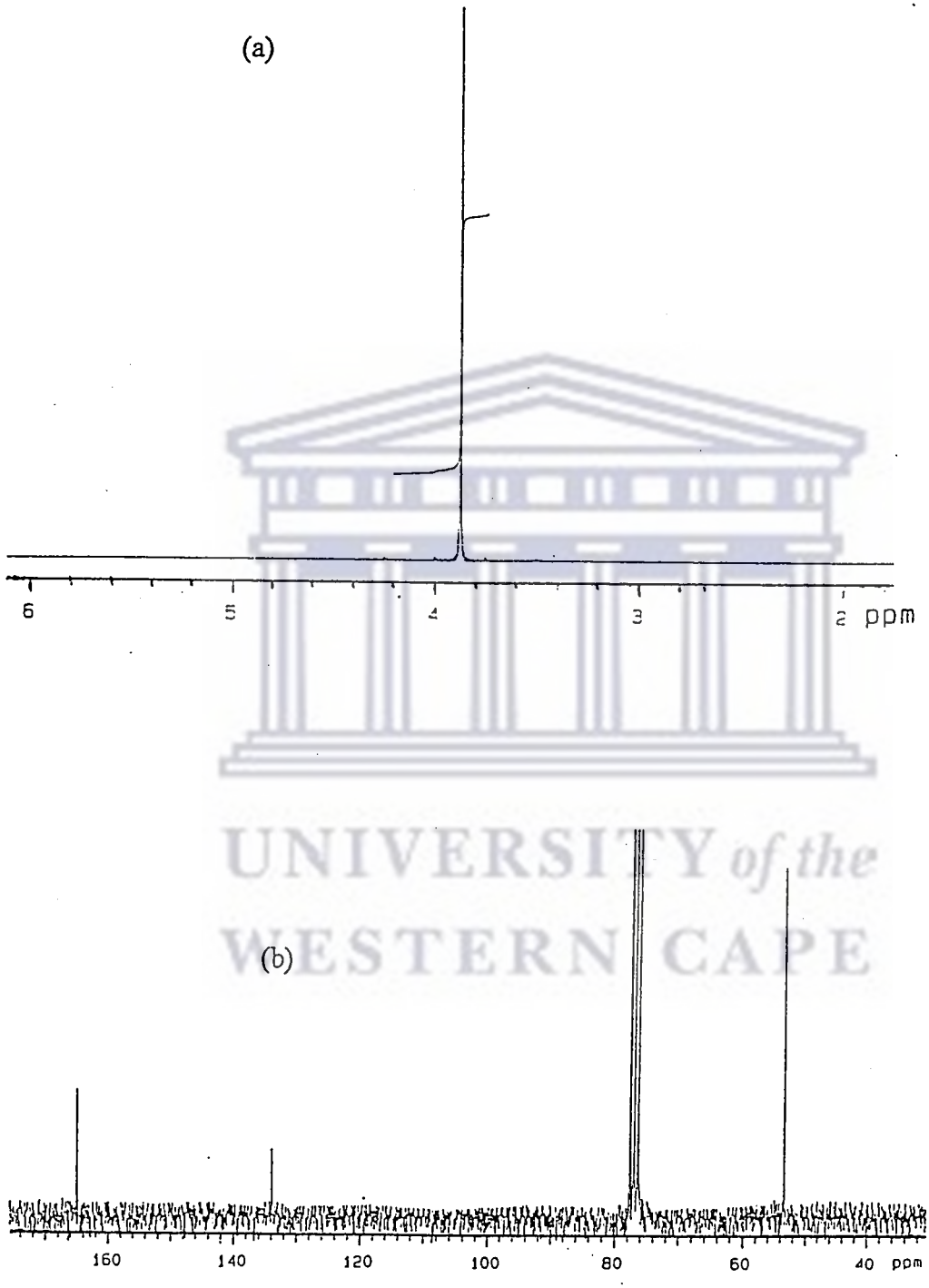

Fig. 18 ^{1}H NMR spectrum (a) and $^{13}C\{^{1}H\}$ NMR spectrum (b) of HMBC.

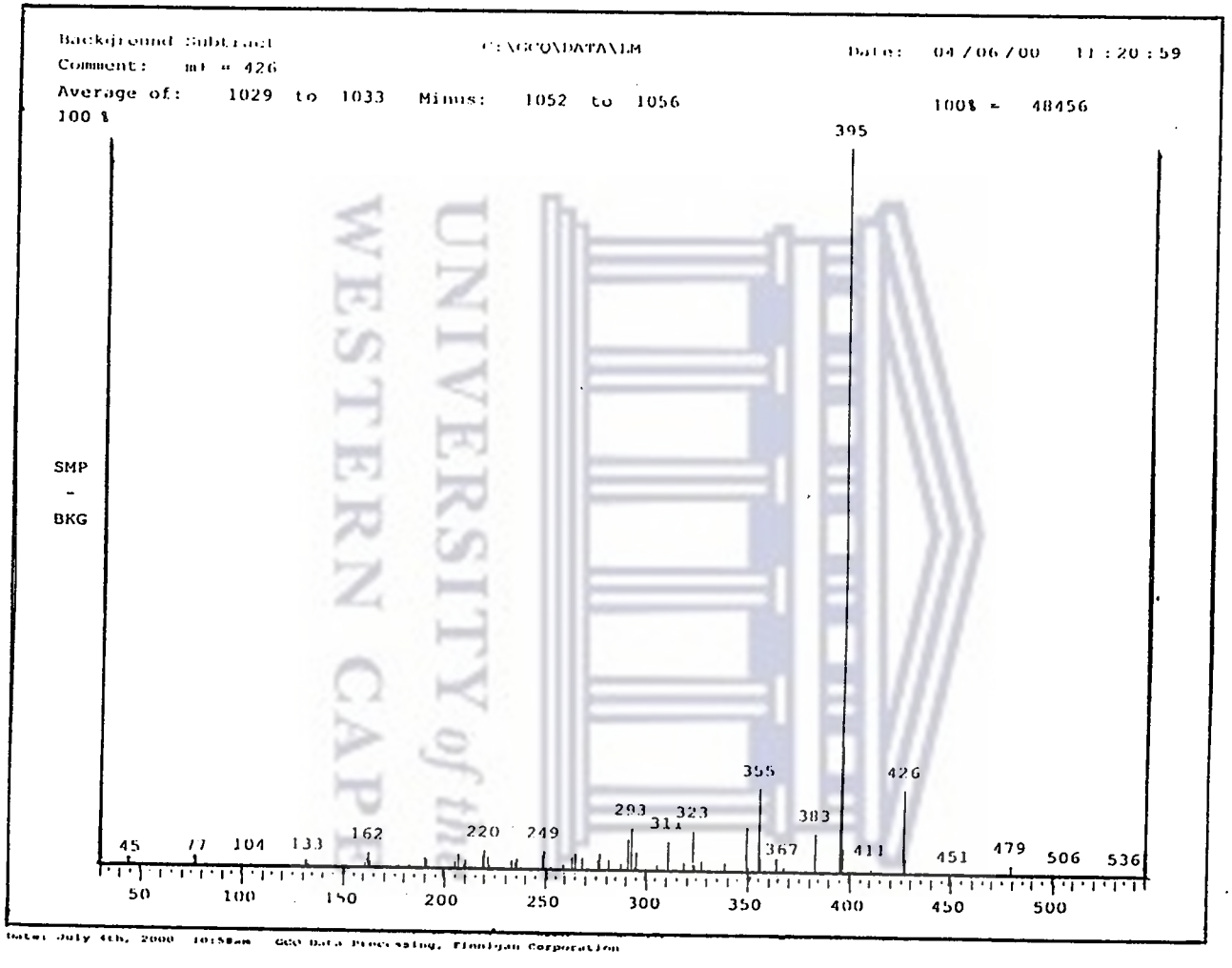

Fig. 19a EI-Mass Spectrum of HMBC.

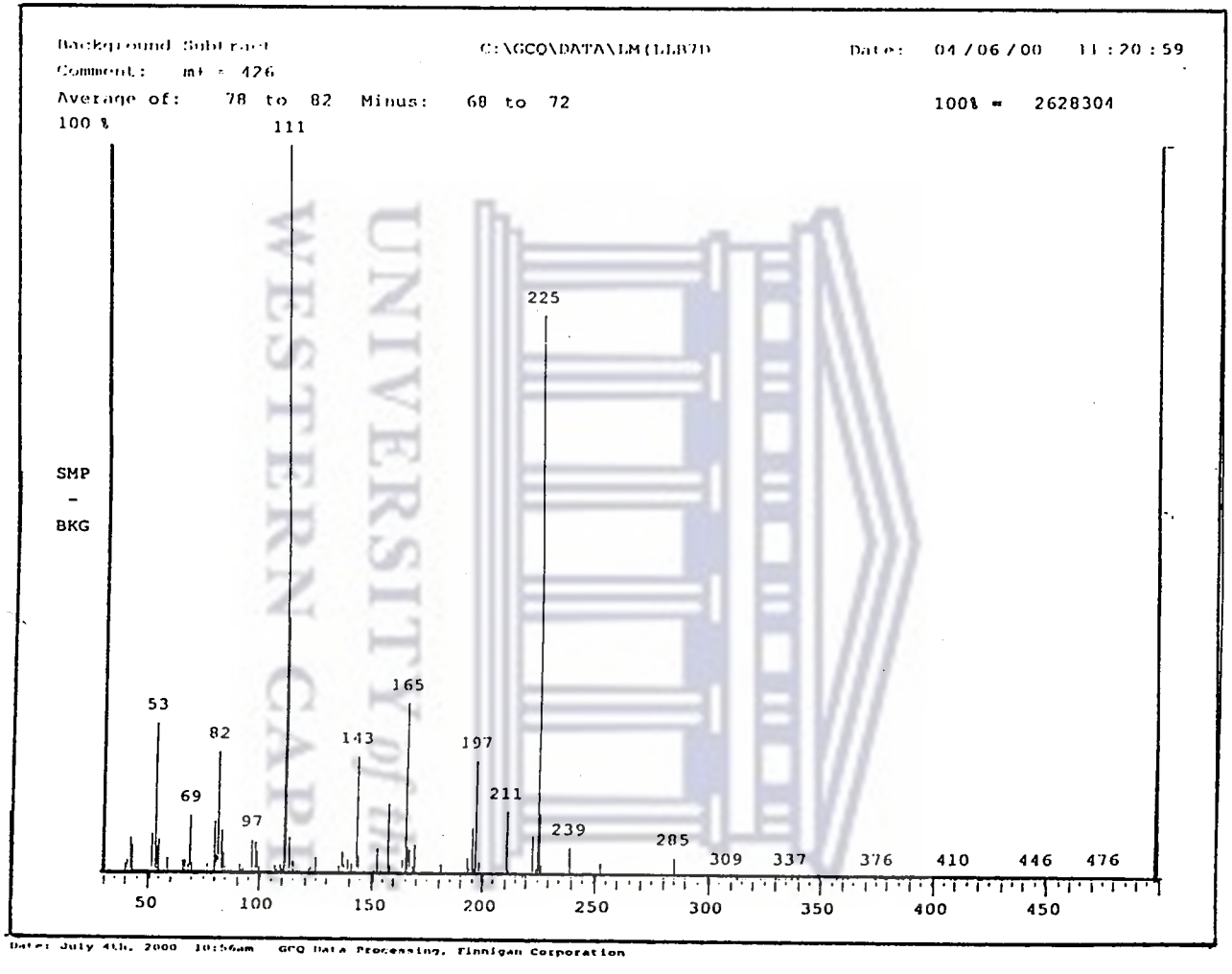

Fig. 19b EI-Mass Spectrum of TMCTC.

step in the fragmentation pattern. The ^{1}H and $^{13}C\{^{1}H\}$ NMR spectra of TMCTC were found to be similar to that of HMBC. This is not surprising when one considers the structures of the two compounds. The only difference between TMCTC and HMBC was observed in the elemental analysis and mass spectra of the two compounds.The elemental analysis of TMCTC was found to be in good agreement with the calculated percentages of the atoms. The EI-MS of TMCTC (Fig. 19b) showed a molecular ion peak at m/z = 285 (4%). The peak at m/z = 225 (78%) shows the loss of OMe from the molecular ion. Other peaks in the spectrum include the parent ion at m/z = 111 and could not be assigned.

One of the proposed mechanisms from the literature is depicted in Scheme 8.[98] This would involve the initial loss of the dithiolato ligand and the subsequent binding of DMAD and its transformation as in Scheme 8. However, there is no evidence of this initial dissociation occurring in our reactions.

In order to probe how this cyclisation takes place, we performed the reaction in dark; first to investigate the effect of light and secondly to see if the initial product formed could be isolated. Initial step in acetylene cyclisation involves coordination of DMAD to the sulphur atoms of the dithiolato ligands (Fig. 20). The figure shows the ^{1}H NMR spectrum of Pd(dippf)(SC_6H_4S-*o*) before and after reaction with DMAD. In Fig. 20b, a peak around 3.8 ppm was due to the methyl protons of the bound acetylene. The protons of aryldithiolato ligand shifted downfield relative to the ones in the unreacted complex. The

shift of these proton peaks suggests that the initial step in acetylene cyclisation involve the coordination of DMAD to the two sulfur atoms.

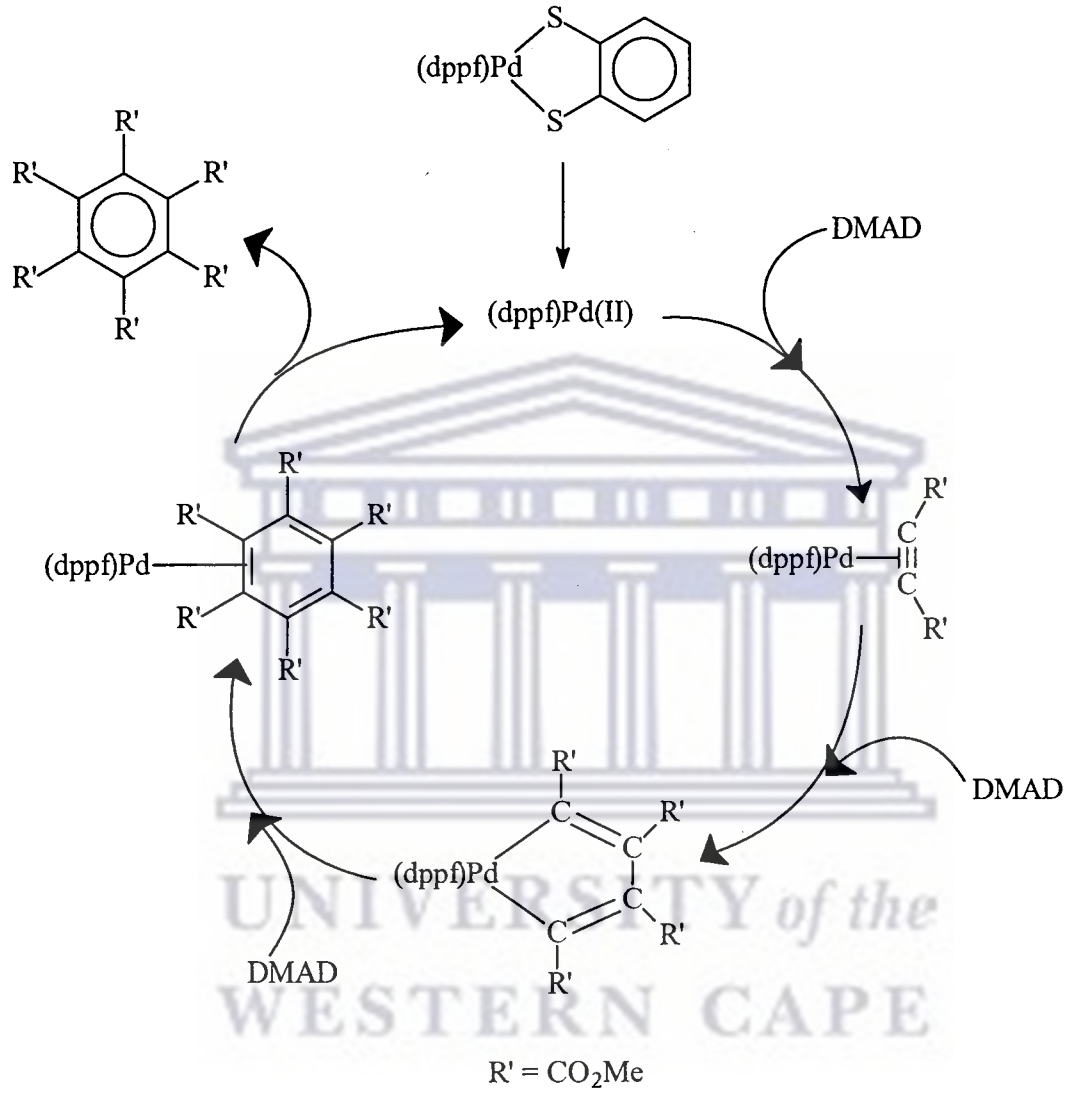

Scheme 8. The cyclisation pathway of DMAD to form HMBC.

Because of the electron-withdrawing groups attached to the two sulfur atoms, the aryldithiolato protons are deshielded and hence lie downfield. The figure suggests a different pathway of acetylene cyclisation from that postulated in Scheme 8 and the structure of the initial product formed after the coordination of the first acetylene is as

shown in Scheme 9. This gives the evidence of Pd(dippf)(SC_6H_4S-*o*) behaving as a nucleophile. It is suggested that further work needs to be done to elucidate the mechanism of cyclisation.

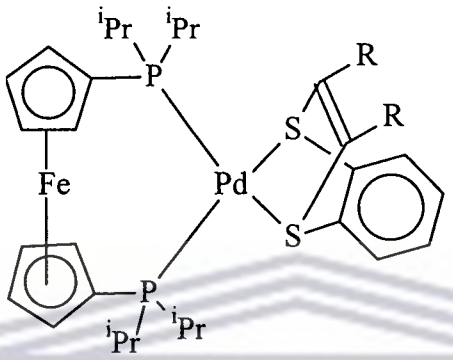

Scheme 9. Initial step in acetylene cyclooligomerisation.

A control experiment was setup by refluxing DMAD in CH_2Cl_2/toluene (1:1) for 48 h. This was performed in order to confirm the efficiency and selectivity of the complexes to effect the cyclodi- and trimerisation processes. However a mixture of products were observed in the GC-MS. Even the TMCTC and HMBC identified in the GC-MS were in quantities of less than 5%. This observation suggests that the complexes are efficient and also selective in DMAD reactions. When phenylacetylene was used in place of DMAD, no reaction was observed even after increasing the catalyst concentration and the acetylene could be recovered in near quantitative amounts. This suggests that the bulkier and less electrophilic alkynes could not be activated by the complexes. The observations also suggest that the cyclotrimerisation and cyclodimerisation processes might involve the attack of the metal complex by the alkyne as proposed by Mao *et al.*[99] and recently by Darkwa *et al.*[27]

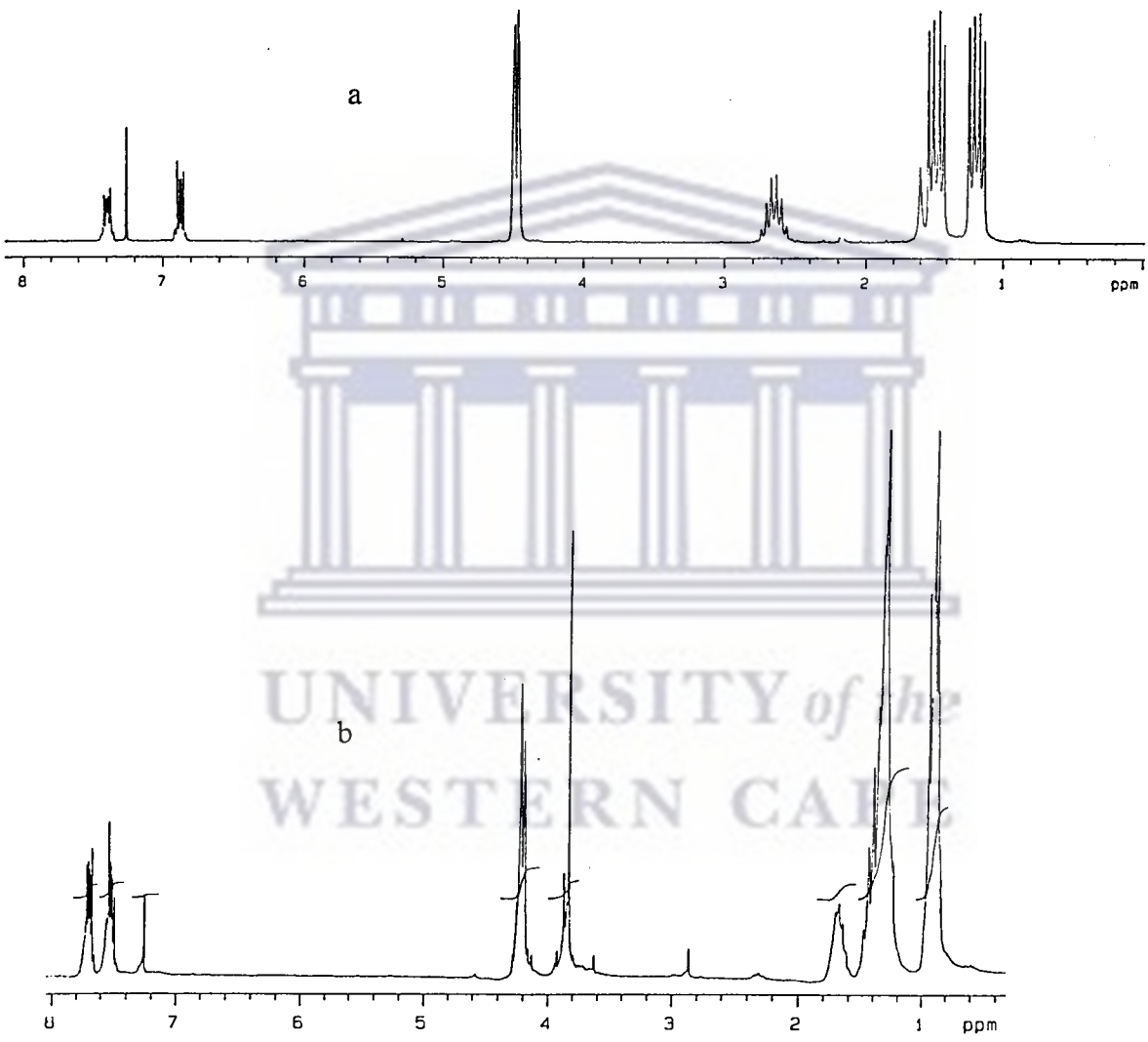

Fig. 20 ^{1}H NMR of **2a** before (a) and after (b) reaction with DMAD in the dark.

6.2 Reactions of Pd and Pt aryldithiolato complexes with sulfur dioxide (SO_2).

Reactions of M(dppf)(SC_6H_3RS-*o*) and Pd(dippf)(SC_6H_3RS-*o*) (M = Pd, Pt; R = H, Me) with SO_2 were performed in NMR tubes and monitored by ^1H NMR spectroscopy. This was used in combination with the UV-vis spectroscopy where the complexes were dissolved in CH_2Cl_2. To monitor the SO_2 reaction, ^1H NMR spectra of the complexes were run in $CDCl_3$. Sulfur dioxide was then bubbled through the solution for about 3 minutes and the ^1H NMR spectrum re-run. The reaction of the complexes with SO_2 was indicated by the colour changes that occurred when the gas was bubbled through the solutions. The colour change was more pronounced in the platinum complexes as all of them were initially yellow in solution but changed to deep orange when the SO_2 gas was bubbled through. For the palladium analogues of the complexes, the initial orange colour changed only slightly. Reactions of SO_2 with $Cp_2Cr_2S_5$ (Cp = η^5-C_5H_5) causes colour changes from blue to deep red.[37c]

Of all the complexes tested, only the dithiolato complexes containing the ligands SC_6H_3RS (R = H, Me) (i.e. **1a-b, 2a-b** and **3a-b**) were found to react with SO_2. The dithiolato complexes **1c**, **2c** and **3c** and the mixed aryldichalcogenide complexes did not react with SO_2. This was evident from both the UV-Vis (Fig. 22) and ^1H NMR spectra where there was no perturbation of the original spectra without SO_2. Attempts to isolate the complexes from SO_2 saturated CH_2Cl_2 solutions were unsuccessful primarily due to the loss of SO_2 on precipitation. This was observed from the colour change of the SO_2 adducts from the deep orange to the original colour of the complexes without SO_2. The SO_2 was also easily desorbed on a rotary evaporator.

The cyclopentadienyl region in the ^{1}H NMR spectra of the dithiolato complexes without SO_2 shows only two peaks. However the SO_2 adducts generally showed three peaks as exemplified by the ^{1}H NMR spectrum of **1b** shown in Fig. 21. There are two possible ways in which the SO_2 can bind to the metal complexes. The first is the binding of SO_2 to the metal, as observed for the square planar nickel complexes Ni(dppe)(1,2-SC_6H_4S-*o*) and Ni(dppe)(SC_6H_3MeS-*o*) (dppe = 1,2-bis(diphenylphosphino)ethane.[18d] The second option is the SO_2 binding to the ligand similar to that observed in $Pt(PPh_3)(CH_3)I.SO_2$.[36]

In the ^{1}H NMR spectra of the SO_2 adduct, the hydrogen atoms nearest to the sulfur atom of the dithiolato ligands are shifted upfield relative to the unreacted dithiolate complexes. This is in contrast to the spectrum observed for the SO_2 adduct of (bme-daco)Ni (bme-daco = N,N'bis(mercaptoethyl)-1,5-diazacyclooctane),[18a] where the proton spectrum shows little perturbation of the nearest protons by the bound SO_2 group. The ^{1}H NMR spectra of the SO_2 adduct suggests that electron density is drawn from the perihydrogens of the dithiolato ligands. This could mean that the SO_2 is bound to the two sulfur atoms of the dithiolate ligands. Such binding would be similar to that reported by Sadler and co-workers for [Au(SC_6H_3MeS-*o*)$_2$][n-Bu_4N].[18b] If the SO_2 was bound to the two sulfur atoms, it will have less effect on the cyclopentadienyl protons. Furthermore we expected only two cyclopentadienyl peaks because the electronic environments of the cyclopentadienyl protons would be similar to that observed in the unreacted complexes.

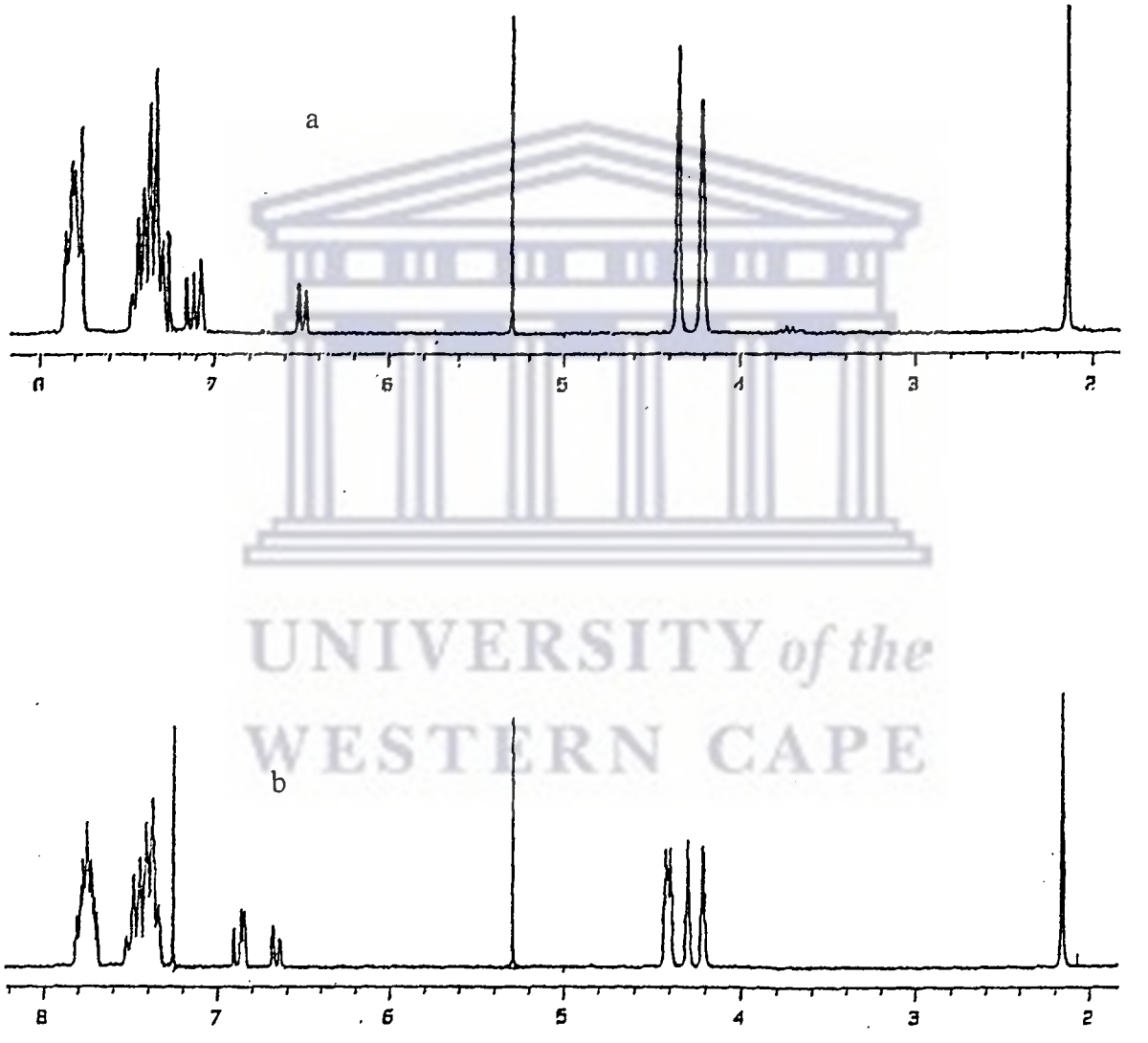

Fig. 21 ^{1}H NMR spectrum of **1b** before (a) and after (b) bubbling SO_2

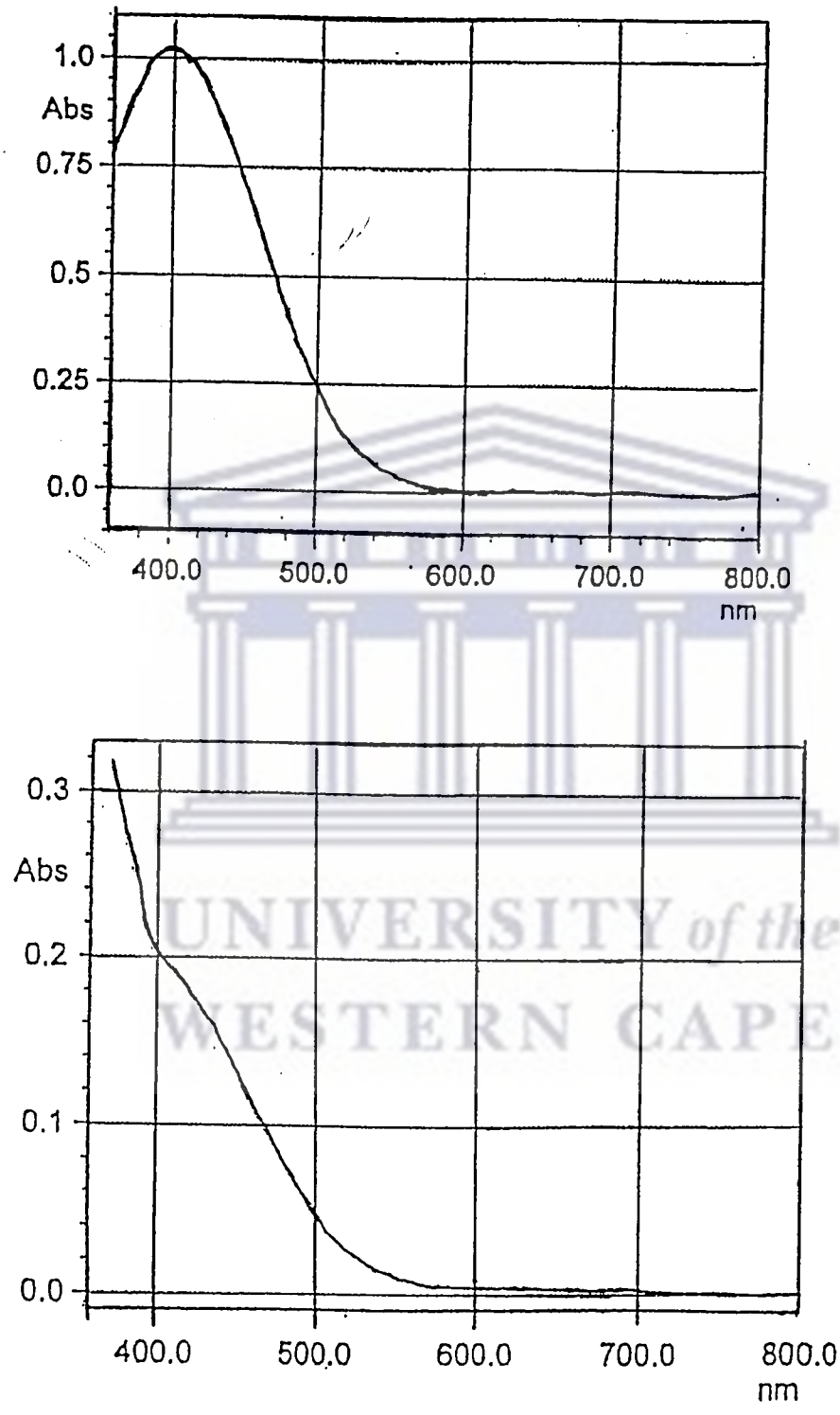

Fig. 22 UV-Vis spectrum of **3b** before (a) and after (b) bubbling SO_2.

This rules out the binding of the SO_2 to the sulfur atoms and suggests that the SO_2 is bound to the metal atom. From the UV-vis spectra of the platinum complexes and their SO_2 adducts, it was clear the non-SO_2 adducts had λ_{max} whereas SO_2 adducts did not. The UV-vis spectra also showed that these spectra are not primarily due to d-d transitions, but have some ligand charge transfer contribution. Based on the UV-vis spectra of the platinum complexes alone, one could conclude that the SO_2 binding is on the ligand since the spectra show ligand pertubation. However from the nickel example from the literature[18d] and results of the palladium complexes where there are d-d transition, it could be infered that the SO_2 is bound to the metal. Thus the overall reaction can be represented as shown in eq. 8. A representative UV-vis spectrum of **3b** is shown in Fig. 22.

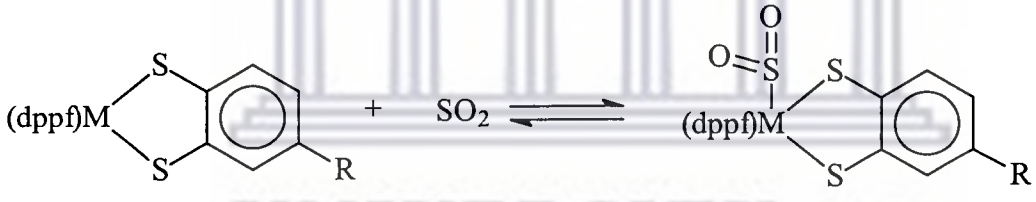

(8)

M = Pd, Pt; R = H, Me

In order to confirm the proposed structures of the SO_2 adduct, attempts were made to obtain crystals but these were unsuccessful. Further work needs to be done to confirm the proposed binding of SO_2, but the facile manner in which the SO_2 desorbs shows the potential of **1a-b**, **2a-b** and **3a-b** as SO_2 scrubbers.

CHAPTER 7

CONCLUSION

The synthesis of complexes of the general formulae M(dppf)(SC_6H_3RE-*o*) and Pd(dippf)(SC_6H_3RE-*o*) (M = Pd, Pt; E = S, O, CO_2) was achieved in moderate to high yields by the reaction of M(dppf)Cl_2 and Pd(dippf)Cl_2 with the appropriate arylthiolato ligands in the presence of triethylamine. The complexes had the same structures in solid state and in solution. This was deduced from spectroscopic data and single crystal X-ray diffraction studies of six of the complexes. All X-ray structures show distorted square planar geometries around the Pd and Pt centres with the phosphorus atoms in a *cis* configuration.

The ^{31}P NMR shifts were dependent on the substituent attached to aryldichalcogenide ligand. The more electron releasing groups on the aryl ring tend to shield the chemical shifts and hence the peaks are observed upfield. The order of ligand donation for the homoleptic dithiolato ligands was SC_6H_3MeS-*o* > SC_6H_4S-*o* > $SC_6H_2Cl_2S$-*o*. The ^{31}P chemical shifts of mixed aryldichalcogenide complexes were found to be dependent on the *trans*-influence of the chalcogens. The more polarisable sulfur atom deshields the chemical shift *trans* to it relative to the less polarisable oxygen atom. In general, Pt(dppf) complexes were found to be more stable than their analogous Pd(II) complexes. This was deduced from mass spectrometry where all the Pt(dppf) complexes showed molecular ion peaks in both EI and FAB mass spectrometry whereas their Pd counterparts showed molecular ion peaks only in the softer FAB mode.

Electrochemical studies show that the redox activity of the complexes ranged from quasi-reversibility to irreversibility with two redox processes, one due to the oxidation of the arylthiolato ligand while the other is due to dppf or dippf ligands. The arylthiolato ligand oxidation peaks were influenced by the substituents attached to aryl ring. Ligands containing electron-releasing groups were easier to oxidise than those containing electron-withdrawing groups. The dippf complexes were easier to oxidise compared to dppf complexes due to the better electron donating ability of the dippf.

Selected compounds reacted with dimethylacetylene dicarboxylate (DMAD) and formed mainly two products, hexamethylbenzene hexacarboxylate (HMBC) and tetramethylcyclobuta-1,3-diene tetracarboxylate (TMCTC). When phenylacetylene was used in place of DMAD, no reaction was observed. This clearly indicated that the palladium complexes did not activate the bulkier and less electrophilic alkyne.

The SO_2 reactions were monitored by UV-visible and ^1H NMR spectroscopy, which suggest that SO_2 reacted reversibly with the complexes. At reduced pressure, the sulfur dioxide adducts readily lost SO_2 to reform the original complexes. Based on spectroscopic data, the SO_2 molecule in the adducts was deduced to be attached to the metal centre. This however needs to be confirmed by X-ray crystallography. Attempts to characterise the SO_2 adducts by X-ray or elemental analysis were unsuccessful as the complexes readily lost the sulfur dioxide molecule.

REFERENCES

1. M. Draganja, T.B. Rauchfuss, *Angew. Chem., Int. Ed. Engl.*, 1985, **24**, 742.
2. (a) J. Darkwa, E.-Y. Osei-Twum, L.A. Litorja, Jr, *Polyhedron*, 1999, **18**, 1115. (b) T.B. Rauchfuss, D.M. Roundhill, *J. Am. Chem. Soc.*, 1975, **77**, 3386.
3. (a) T. Kiss, P. Buglyo, G. Micera, A. Dessi, D. Sanna, *J. Chem. Soc. Dalton Trans.*, 1993, 1849. (b) W. Clegg, N. Duran, K.A. Fraser, P. Conzalez-Duarte, J. Sola, I.C. Taylor, *J. Chem. Soc. Dalton Trans.*, 1993, 3453.
4. (a) T. Gaines, D.M. Roundhill, *Inorg. Chem.* 1974, **13**, 2521. (b) A. Shaver, P.-Y. Plouffe, *Inorg. Chem.*, 1992, **31**, 1823.
5. J. Darkwa, F. Bothata, L.M. Koczon, *J. Organomet. Chem.*, 1993, **455**, 235.
6. R.G. Hayter, F.S. Humiec, *Inorg. Chem.*, 1964, **26**, 807.
7. M. Schmidt, G.G. Hoffman, *J. Organomet. Chem.*, 1977, **124**, C5.
8. (a) M. Capdevila, P. Conzalez-Duarte, C. Foces-Foces, F.H. Cano, M. Martinez-Ripoll, *J. Chem. Soc. Dalton Trans.*, 1990, 1430. (b) M. Capdevila, W. Clegg, P. Conzalez-Duarte, B. Harries, I. Mira, J. Sola, I.C. Taylor, *J. Chem. Soc. Dalton Trans.*, 1992, 2817.
9. T.B. Rauchfuss, J.S. Shu., D.M. Roundhill, *Inorg. Chem.*, 1976, **15**, 2096.
10. J. Darkwa, L.M. Koczon, J.M. Rost, *Synth. React. Inorg. Met.-Org. Chem.*, 1993, **23**, 509.
11. (a) G.J. Kubas, R.R. Ryan, *Inorg. Chem.*, 1984, **23**, 3181. (b) G.J. Kubas, H.J. Wasserman, R.R. Ryan, *Organometallics,* 1985, **4**, 2012. (c) K.A. Kubat-Martin, G.J.

Kubas, R.R. Ryan, *Organometallics*, 1989, **8**, 1910. (d) G.J. Kubas, R.R. Ryan, *Polyhedron*, 1986, **5**, 473.

12. (a) G.J. Kubas, R.R. Ryan, *J. Am. Chem. Soc.*, 1985, **107**, 6138. (b) G.J. Kubas, H.J. Wasserman, R.R. Ryan, *Organometallics*, 1985, **4**, 419.
13. (a) A. Neher, I.-P. Lorenz, *Angew. Chem. Int. Ed. Engl.*, 1989, **28**, 1342. (b) D.H. Farrar, R.R. Gukathasan, *J. Chem. Soc. Dalton Trans.*, 1989, 557.
14. W.A. Schenk, *Angew. Chem. Int. Ed. Engl.*, 1987, **26**, 98.
15. D.M.P. Mingos, R.W.W. Wardle, *J. Chem. Soc. Dalton Trans.*, 1986, 73.
16. (a) A. Shaver, P.-Y. Plouffe, E. Livingstone, *Inorg. Chem.*, 1990, **29**, 1826. (b) A. Shaver, P.-Y. Plouffe, *Inorg. Chem.*, 1992, **31**, 1823.
17. (a) P.G. Eller, G.J. Kubas, *J. Am. Chem. Soc.*, 1977, **99**, 4346. (b) A. Toupadakis, G.J. Kubas, C.J. Burn, *Inorg. Chem.*, 1992, **31**, 3810. (c) D.K. Mills, J.H. Reibenspies, M.Y. Darensbourg, *Inorg. Chem.*, 1990, **29**, 4364. (d) M.Y. Darensbourg, I. Font, D.K. Mills, M. Pala, J.H. Reibenspies, *Inorg. Chem.*, 1992, **31**, 4965.
18. (a) M.Y. Darensbourg, T. Tuntulani, J.H. Reibenspies, *Inorg. Chem.*, 1994, **33**, 611. (b) M.A. Mazid, M.T. Razi, P.J. Saddler, *Inorg. Chem.*, 1981, **20**, 2872. (c) J. Darkwa, R.M. Moutloali, T. Nyokong, *J. Organomet. Chem.*, 1998, **564**, 37. (d) J. Darkwa, *Inorg. Chim. Acta*, 1997, **257**, 137.
19. R.M. Bounomo, I. Font, M.J. Maguire, J.H. Reibenspies, T. Tuntulani, M.Y. Darensbourg, *J. Am. Chem. Soc.*, 1995, **117**, 963.
20. (a) P.G. Eller, R.R. Ryan, D.C. Moody, *Inorg. Chem.*, 1976, **15**, 2442. (b) S.J. LaPlaca, J.A. Ibers, *Inorg. Chem.*, 1966, **5**, 405. (c) K.W. Muir, J.A. Ibers, *Inorg.*

Chem., 1969, **8**, 1921. (d) D.C. Moody, R.R. Ryan, *Inorg. Chem.*, 1976, **15**, 1823. (e) P.G. Eller, G.J. Kubas, R.R. Ryan, *Inorg. Chem.*, 1977, **16**, 2454.

21. (a) L.H. Vogt, Jr, J.L. Katz, S.E. Wiberley, *Inorg. Chem.*, 1965, **4**, 1157. (b) R.R. Ryan, G.J. Kubas, *Inorg. Chem.*, 1978, **17**, 637.
22. (a) M.R. Churchill, K.L. Kalra, *Inorg. Chem.*, 1973, **12**, 1646. (b) M.R. Churchill, K.L. Kalra, *Inorg. Chem.*, 1973, **12**, 1650. (c) S. Otsuka, Y. Tatsuno, M. Miki, T. Aoki, M. Matsumoto, H. Yoshioka, K. Nakatsu, *J. Chem. Soc. Chem. Commun.*, 1973, 445. (d) L.S. Benner, M.M. Olmstead, H. Hope, A.L. Balch, *J. Organomet. Chem.*, 1978, **153**, C31.
23. (a) D.C. Moody, R.R. Ryan, *J. Chem. Soc. Chem. Commun.*, 1976, 503. (b) D.C. Moody, R.R. Ryan, *Inorg. Chem.*, 1977, **16**, 2473. (c) R.D. Wilson, J.A. Ibers, *Inorg. Chem.*, 1978, **17**, 2134.
24. J.W. Moore, H.W. Baird, H.B. Miller, *J. Am. Chem. Soc.*, 1968, **90**, 1358.
25. G.J. Kubas, *Inorg. Chem.*, 1979, **18**, 1.
26. G.J. Kubas, *Inorg. Chem.*, 1979, **18**, 182.
27. M.S. Thomas, J. Darkwa, *Polyhedron*, 1998, **17**, 1811.
28. A. Shaver, P.-Y. Plouffe, D. Liles, E. Singleton, *Inorg. Chem.*, 1992, **31**, 997.
29. P. Conway, S.M. Gariel, A.R. Manning, F.S. Stephens, *Inorg. Chem.*, 1983, **22**, 3714.
30. D.C. Moody, R.R. Ryan, *Inorg. Chem.*, 1979, **18**, 223.
31. (a) G.D. Jarvinen, G.J. Kubas, R.R. Ryan, *J. Chem. Soc. Chem. Commun.*, 1981, **7**, 305. (b) P. Ewing, L.J. Farrugia, *Organometallics*, 1989, **8**, 1665. (c) D.M.P. Mingos, P.Oster, D.J. Sherman, *J. Organomet. Chem.*, 1987, **320**, 257.

32. (a) C.A. Ghilardi, S. Midollini, L. Sacconi, *Inorg. Chem.*, 1977, **16**, 2377. (b) M. Graziani, R. Ros, G. Carturan, *J. Organomet. Chem.*, 1971, **27**, C19. (c) D.M. Barlex, R.D.W. Kemmitt, *J. Chem. Soc. Dalton Trans.*, 1972, **14**, 1436. (d) K.A. Kubat-Martin, G.J. Kubas, R.R. Ryan, *Organometallics Commun.*, 1988, **7**, 1657.

33. D.C. Moody, R.R. Ryan, A.C. Larson, *Inorg. Chem.*, 1979, **18**, 227.

34. G.J. Kubas, R.R. Ryan, V. McCarty, *Inorg. Chem.*, 1980, **19**, 3003.

35. (a) P. Conway, S.M. Grant, A.R. Manning, *J. Chem. Soc. Dalton Trans.*, 1979, 1920. (b) J. Valentine, D. Valentine, Jr, J.P. Collman, *Inorg. Chem.*, 1971, **10**, 219.

36. M.R. Snow, J.A. Ibers, *Inorg. Chem.*, 1973, **12**, 224.

37. (a) P.J. Farmer, T. Solouki, D.K. Mills, T. Soma, D.H. Russell, J.H. Reibenspies, M.Y. Darensbourg, *J. Am. Chem. Soc.*, 1992, **114**, 4601. (b) G.J. Kubas, R.R. Ryan, K.A. Kubat-Martin, *J. Am. Chem. Soc.*, 1989, **111**, 7823.

38. (a) G.C. Thon, P.F. Waters, A.F. Hadermann, *Inorg. Chem.*, 1978, **17**, 1693. (b) A. Shaver, P.-Y. Plouffe, *J. Am. Chem. Soc.*, 1991, **113**, 7780.

39. D.C. Moody, R.R. Ryan, *J. Chem. Soc. Chem. Commun.*, 1980, 1230.

40. P.S. Jarrette, P.J. Sadler, *Inorg. Chem.*, 1991, **30**, 2098.

41. S.J. Berners-Price, P.S. Jarrette, P.J. Sadler, *Inorg. Chem.*, 1987, **26**, 3074.

42. (a) S.J. Berners-Price, P.J. Sadler, *Struct. Bonding*, 1988, **70**, 27. (b) S.J. Berners-Price, M.A. Mazid, P.J. Sadler, *J. Chem. Soc. Dalton Trans.*, 1984, 969.

43. S.E. Sherman, S.J. Lippard, *Chem. Rev.*, 1987, **87**, 1153.

44. C.K. Mirabelli, D.T. Hill, L.F. Faucette, F.L. McCabe, G.R. Girard, D.B. Bryan, B.M. Sutton, J.O. Bartus, S.T. Crooke, R.K. Johnson, *J. Med. Chem.*, 1987, **30**, 2181.

45. A.L. Balch, E.Y. Fung, *Inorg. Chem.*, 1990, **29**, 4764.

46. (a) P.J. Sadler, *Struct. Bonding*, 1976, 171. (b) M.A. Mazid, M.T. Razi, P.J. Sadler, *Inorg. Chem.*, 1981, **20**, 2872.

47. J.H. Enemark, J.A. Ibers, *Inorg. Chem.*, 1968, **7**, 2636.

48. P.S. Jarrett, P.J. Sadler, *J. Inorg. Biochem.*, 1991, **43**, 598.

49. P.S. Jarrett, O.M. Dhubhghaill, P.J. Sadler, *J. Chem. Soc. Dalton Trans.*, 1993, 1863.

50. (a) G.B. Karet, S.L. Castro, K. Folting, J.C. Bollinger, R.A. Heintz, G. Christou, *J. Chem. Soc. Dalton Trans.*, 1998, 67. (b) L.J. McCaffery, W. Henderson, B.K. Nicholson, J.E. Mackay, M.B. Dinger, *J. Chem. Soc. Dalton Trans.*, 1997, 2577. (c) M.B. Dinger, W. Henderson, *J. Organomet. Chem.*, 1998, **560**, 233.

51. W. Henderson, L.J. McCaffery, B.K. Nicholson, *J. Chem. Soc. Dalton Trans.*, 2000, 2753.

52. D.M. Roe, C. Calvo, N. Krishnamachari, P.M. Maitlis, *J. Chem. Soc. Dalton Trans.*, 1975, 125.

53. W. Reppe, O. Schlichting, K. Klager, T. Toepel, *Justus Liebigs Ann. Chem.*, 1948, **561**, 1.

54. M.A. Bennet, E. Wenger, *Organometallics*, 1995, **14**, 1267.

55. G.N. Schrauzer, P. Glockner, S. Eichler, *Angew. Chem.*, 1964, **76**, 28.

56. J.J. Eisch, J.E. Galle, *J. Organomet. Chem.*, 1975, **96**, C23.

57. G.N. Schrauzer, V.P. Mayweg, *J. Am. Chem. Soc.*, 1965, **87**, 1483.

58. C. Bianchini, A. Meli, *J. Organomet. Chem.*, 1982, **236**, C75.

59. Y. Kaneko, N. Suzuki, A. Nishiyama, T. Suzuki, K. Sobe, *Organometallics*, 1998, 17, 4875.

60. J. D. Woollins, *Inorganic Experiments*, VCH Verlagsgesellschat, Weinheim, 1994, p59.

61. J.J. Bishop, A. Davison, M.L. Katcher, D.W. Lichtenberg, R.E. Merill, J.C. Smart, *J. Organomet. Chem.*, 1971, **27**, 241.

62. B. Corain, B. Longato, G. Favero, D. Ajo, U. Russo, F.R. Kreissl. *Inorg. Chim. Acta,* 1989, **159**, 259.

63. Reaction of $PdCl_2$ and dippf under similar conditions as in Ref. **2b** gave near quantitative yield of $Pd(dippf)Cl_2$.

64. H.C. Clark, L.E. Manzer, *J. Organomet. Chem.*, 1973, **59**, 411.

65. P.J. Stang, B. Olenyk, J. Fan, A.M. Arif, *Organometallics*, 1996, **15**, 904.

66. R.H. Blessing, *Acta Cryst.*, 1995, **A51**, 33.

67. G.M. Sheldrick, SHELXTL (version 5.1) *Program Library, Bruker Analytical X-ray Systems*, Madison, WI.

68. G.M. Sheldrick, SADABS, *An Empirical Absorption Correction*, Private Communication to subscribers of the Siemens CCD e-mail list.

69. T. Nyokong, *Polyhedron*, 1993, **12**, 375.

70. K. Nakamoto, *Infrared and Raman spectra of inorganic and coordination compounds*, 4th Edition, 1986, John Wiley and Sons, p380.

71. P. Bhattacharyya, J. Parr, *J. Chem. Soc. Dalton Trans.*, 1998, 3263.

72. S.P. Kaiwar, J.K. Hsu, L.M. Liable-Sands, A.L. Rheingold, R.S. Pilato, *Inorg. Chem.*, 1997, **36**, 4234.

73. T. Hayashi, M. Konishi, Y. Kobori, M. Kumada, T. Higuchi, K. Hirotsu, *J. Am. Chem. Soc.*, 1984, **106**, 158.

74. S. Li, B. Wei, P.M.N. Low, H.K. Lee, T.S.A. Hor, F. Xue, T.C.W. Mak, *J. Chem. Soc. Dalton Trans.*, 1997, 1289.

75. J.M. Brown, P.J. Guiry, *Inorg. Chim. Acta*, 1994, **220**, 249.

76. T. Hayashi, A. Ohno, S. Lu, Y. Matsumoto, E. Fukuyo, K. Yanagi, *J. Am. Chem. Soc.*, 1994, **116**, 4225.

77. R. Knapp, M. Rehahn, *J. Organomet. Chem.*, 1993, **452**, 239.

78. H. Friebolin, *Basic one- and two-dimensional NMR spectroscopy*, 3rd Ed, Wiley VCH Verlag, Weinheim, 1998, p124.

79. P. Bhattacharyya, A.M.Z. Slawin, M.B. Smith, *J. Chem. Soc. Dalton Trans.*, 1998, 2471.

80. C.A. Ghilardi, P. Innocenti, S. Midollini, A. Orlandini, A. Vacca, *J. Chem. Soc. Dalton Trans.*, 1995, 1109.

81. S.O. Grim, R.L. Keiter, W. McFarlane, *Inorg. Chem.*, 1967, **6**, 134.

82. (a) D.M. Giolando, T.B. Rauchfuss, A.L. Rheingold, *Inorg. Chem.*, 1987, **26**, 1638. (b) E. Colacio, G. Guesta, M. Ghazi, M.A. Huertas, J.M. Moreno, A. Navarrete, *Inorg. Chem.*, 1997, **36**, 1652. (c) C.E. Keefer, R.D. Bereman, S.T. Purrington, B.W. Knight, P.D. Boyle, *Inorg. Chem.*, 1999, **38**, 2294.

83. (a) A.F. Williams, *A theoretical Approach to Inorganic Chemistry*, Springer-Verlag, Berlin, Heidelberg, 1979, p235. (b) B.E. Douglas, D.H. McDaniel, J.J. Alexander, *Concepts and Models of Inorganic Chemistry*, 2nd Ed, John Wiley and Sons, Inc, 1983, p374.

84. J.P. Collman, L.S. Hegedus, *Principles and applications of Organotransition metal Chemistry*, Mill Valley, California, 1980, p58.

85. (a) S.Y. Tyree, Jr, K. Knox, *Textbook of Inorganic Chemistry*, MacMillan Co., New York, 1961, p35. (b) F.A. Cotton, *Prog. Inorg. Chem.*, 1962, **4**, p385.

86. E.A.V. Ebsworth, D.W.H. Rankin, S. Cradock, *Struct. Methods in Inorganic Chemistry*, 2nd Ed., Blackwell Scientific, 1987, p58.

87. G. Mann, D. Baranano, J.F. Hartwig, A.L. Reingold, I.A. Guzei, *J. Am. Chem. Soc.*, 1998, **120**, 9207.

88. P. Dierkes, P.W.M.N. van Leeuwen, *J. Chem. Soc. Dalton Trans.*, 1999, 1519.

89. I.A. Guzei, L.L. Maisela, J. Darkwa, *Acta Cryst.*, 2000, **C56**, 465.

90. F.A. Allen, O. Kennard, *Chem. Des. Autom. News*, 1993, **8**, 31.

91. P.R. Pilloni, S.P. Midollini, *J. Organomet. Chem.*, 1987, **6**, 2107.

92. W.L. Steffen, G.J. Palenik, *Inorg. Chem.*, 1976, **15**, 2436.

93. G.Y. Zheng, D.P. Rillema, J.H. Reibenspies, *Inorg. Chem.*, 1999, **38**, 797.

94. Y. Chen, C. Woods, M.W. Perkovic, D.P. Rillema, *J. Chem. Crystallogr.*, 1996, **26**, 527.

95. P. Kissinger, W.R. Heineman, *J. Chem. Edu.*, 1983, **60**, 703.

96. (a) G.A. Bowmaker, P.D.W. Boyd, G.K. Campbell, *Inorg. Chem.*, 1982, **21**, 2403. (b) G.A. Bowmaker, P.D.W. Boyd, G.K. Campbell, *Inorg. Chem.*, 1983, **22**, 1208.

97. C.E. Housecroft, S.M. Owen, P.R. Raithby, B.M. Shaykh, *Organometallics*, 1990, **445**, 163.

98. V.O. Reikhsfel'd, K.L. Markovetskil, *Russian Chem. Rev.*, 1966, **35**, 510.

99. F. Mao, D.M. Schut, D.R. Tyler, *Organometallics*, 1996, **15**, 4770.